Modeling, Designing and Evaluating Fully Dilutable Self Microemulsifying Delivery System for Hydrophobic Pharmaceuticals and Nutraceuticals

by

Mehdi Nouraei

A thesis submitted in conformity with the requirements
for the degree of Doctor of Philosophy

Graduate Department of Chemical Engineering and Applied Chemistry
University of Toronto

Modeling, Designing and Evaluating Fully Dilutable Self Microemulsifying Delivery System for Pharmaceuticals and Nutraceuticals

Mehdi Nouraei

Doctor of Philosophy

Graduate Department of Chemical Engineering and Applied Chemistry
University of Toronto

2017

Abstract

Many newly discovered drugs and nutraceuticals are hydrophobic in nature. When these drugs and nutraceuticals are ingested, their low aqueous solubility limits their ability to dissolve in intestinal fluid and eventually permeate the intestinal membrane to become bioavailable. To overcome this limitation, various delivery systems have been developed to enhance the solubility and absorption of active ingredients. Lipid-based delivery systems (LBDS) such as microemulsions (μE) and self-microemulsifying delivery systems (SMEDS) are among the most advanced systems. However, there are multiple technological challenges in the design and applications of SMEDS.

Using lecithin as the main surfactant and hydrophilic and lipophilic linkers as co-surfactants, a platform was developed to produce food-grade, fully dilutable microemulsions containing hydrophobic solutes. The in vitro and in vivo experiments showed a high solubilization capacity for hydrophobic solutes. For ibuprofen, used as model solute a significant improvement in absorption and bioavailability was observed. The results also showed a shorter absorption time and a longer drug circulation time when ibuprofen was formulated in fully dilutable system.

The main tool used to design the fully dilutable SMEDS was the Hydrophilic-Lipophilic – Difference (HLD) framework. HLD was used to predict the phase inversion point of surfactant-oil-water (SOW) systems as a function of formulation composition. The HLD was further coupled with Net-Average-Curvature (NAC) model to predict the minimum surfactant required to produce fully dilutable systems. The same tool was also used to characterize the effect of the solute on the formulation and design reformulation strategies to maintain the fully dilutable path.

To explore the potential for controlled release with SMEDS, the idea of integrating the concepts of SMEDS and organogels was explored. This novel self-dispersing organogel provides 1-4 days release, which is a substantial improvement over the instantaneous release obtained with SMEDS alone.

Acknowledgments

I would like to thank my supervisors Dr. Edgar Acosta and Dr. Levente Diosady for their support, guidance and thoughtful feedback during this research project. Their continuous support, guidance, and encouragement were instrumental in this project and my professional development.

I am eternally grateful to my advisory committee members (Dr. Yu Ling Cheng and Dr. Rao) as well as Dr. Ping Lee. I also would like to thank the help of Dr. Chereen Collymore and the lab technicians at the Division of Comparative Medicine (DCM) laboratories at the Faculty of Medicine for their contribution on *in vivo* studies.

I am eternally grateful to Endang Susilawati at Biozone labs - Chemical Engineering Department- and Dan Mathers at Analest labs- Chemistry Department- Bih King at Food Engineering lab and Sal Boccia at Scanning Electron Microscopy lab - Material Science Department - for facilitating analytical experiments.

I like to also extend my appreciation to all my research fellows in the Laboratory of Colloid and Formulation Engineering for their collaboration and providing me with lots of support whenever needed.

I also extend my gratitude to Natural Science and Engineering Research Council of Canada (NSERC) and The Connaught Fund for their financial support.

My wife - Shahrzad - and my daughter- Nikta - deserve special thanks for being part of my experience and their encouragement throughout my graduate programs.

Table of Contents

List of Tables

List of Figures

Chapter 1. Thesis Overview

1.1. Introduction

The majority of newly-discovered drugs show low bioavailability due to poor aqueous solubility [1]. Similarly, many nutraceuticals and health-promoting bioactive compounds such as fat-soluble vitamins (A, D, E, K) and vitamin-like compounds (tocopherols, CoQ-10, curcumin) have limited bioavailability due to the same issues [2–5]. To promote the solubility and the absorption of hydrophobic active ingredients, necessitates the development of delivery systems to (artificially) increase the active concentration in the intestinal fluid to enhance the dissolution and absorption of the active ingredients at an optimum rate.

An ideal drug delivery system is designed and formulated such that it encloses the active ingredient and releases it in a bioavailable state at the site of interest, preferably at a controlled rate. Numerous types of delivery systems have been developed, of which lipid-based delivery systems (LBDS) present promising strategies to increase the solubility and the bioavailability of poorly soluble active ingredients [6,7]. LBDS are composed of a variety of oils and oil-like ingredients, emulsifiers and sometimes water. LBDS can be classified into three categories: liquids, solids and gels. The liquid LBDS include emulsions, liposomes, nanoemulsions, microemulsions (μE) and self-(micro) emulsifying delivery systems (SEDS/SMEDS). The solid LBDS include solid lipid nanoparticles (SLN), and solid SMEDS. Gel-based LBDS include organogels that consist of an oil and gelator(s). Microemulsions, unlike their name, are neither emulsion nor micron sized. A microemulsion system is a thermodynamically stable self-assembled, transparent/translucent, optically homogeneous (but microscopically heterogeneous) colloidal system containing oil and aqueous phases, stabilized by an interfacial film of amphiphilic molecules [8–12]. Self-dispersing LBDS such as self-emulsifying and self-microemulsifying delivery systems (SEDS/SMEDS) are isotropic mixtures of oil, surfactant/cosurfactant that spontaneously form nanoemulsions/microemulsions

upon mild agitation in an aqueous solvent [13] and influence the bioavailability of drugs. For example, comparative clinical studies have shown that the bioavailability of Cyclosporine A in SEDS is twice that of the emulsified formulation. [14,15]. SMEDS may concisely be defined as a concentrated microemulsion or latent μE [16] and numerous studies have reported an improvement in the bioavailability of lipophilic drugs when incorporated in SMEDS [7,15,17–21]. The loaded SMEDS form μE droplets with a small size (5-100 nm) that facilitates the intestinal absorption via different mechanisms. In conventional emulsions, energy is needed to break down the oil droplets and to create new surfaces. However, due to the high surface energy, the droplets tend to coalescence. On the other hand, self-microemulsification is a thermodynamically-favoured process that occurs spontaneously. Since SMEDS are water-free system with close-to-zero water activity, it is more likely that their shelf life is longer compared to o/w microemulsion. Despite their effectiveness in increasing the solubility of poorly soluble solutes, there are numerous challenges in designing and formulating SMEDS that limits their wide-spread use [22].

1.2. Challenges and objectives

Understanding phase transition during the dilution of SMEDS is of critical importance. In a surfactant-oil-water (S-O-W) ternary phase diagram, any point inside the triangle is a mixture of water, oil, and surfactant with a specific composition. Any point on the line connecting vertices S (surfactant) and O (oil) contain of surfactant and oil only. This mixture could be a SMEDS, provided that when diluted with water, forms a single phase μE. We define dilution line as any line drawn from vertex W to a point on the SO line directly (the red arrow in Figure 1-1). Any point on this line, has a constant ratio of oil and surfactant, regardless of water content. For example, the formulations presented by red line shown in Figure 1-1 has 60% surfactant and 40% oil.

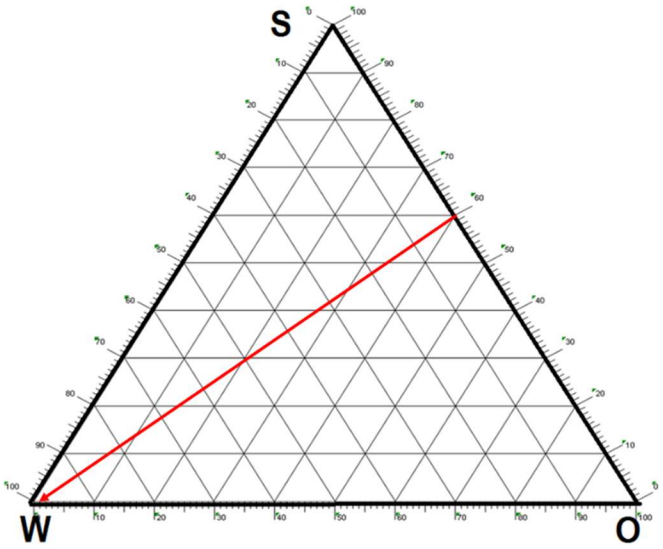

Figure 1-1:Ternary phase diagram and dilution line. (W, O and S stand for water, oil and surfactant)

There are a wide range of surfactants available to formulate µEs but only a limited number of combinations of surfactants leads to a fully dilutable SMEDS formulation. Due to regulatory constraints, developing food-grade SMEDS formulations is more complex since there is only a limited number of biocompatible food-grade surfactants and oils are available that may produce a fully water-dilutable system. Ionic surfactants have excellent solubilization capacity, but they tend to be irritant and are not food grade. Non-ionic and zwitter ionic surfactants are less toxic and -depending on the molecular structure and pH- could be biocompatible. The ternary phase diagrams of numerous surfactant/oil/water systems (SOW) presented in the literature show that full dilutabilty is a major concern. There are two types of phase behaviour observed during the dilution of SEDS/SMEDS: S-type and U-type [23]. In the former, the water-in-oil (W/O) to oil-in-water(O/W) microemulsion transformation involves passing through various multiphase systems and undergo phase separation during dilution. Therefore, they are not fully dilutable. In U-type uEs, the W/O→O/W evolution is continuous and progressive, passing through a bicontinuous (BC) state

(W/O→BC→O/W). This single-phase system is an unsaturated microemulsion with no excess phases.

There is a widespread misuse of the SMEDS concept in the literature. After oral administration, the delivery system experiences extensive dilution and therefore being fully dilutable is a requirement for SMEDS [24]. However, a great number of the formulations introduced in the literature are partially dilutable, as shown in Figure 1-2 as an example.

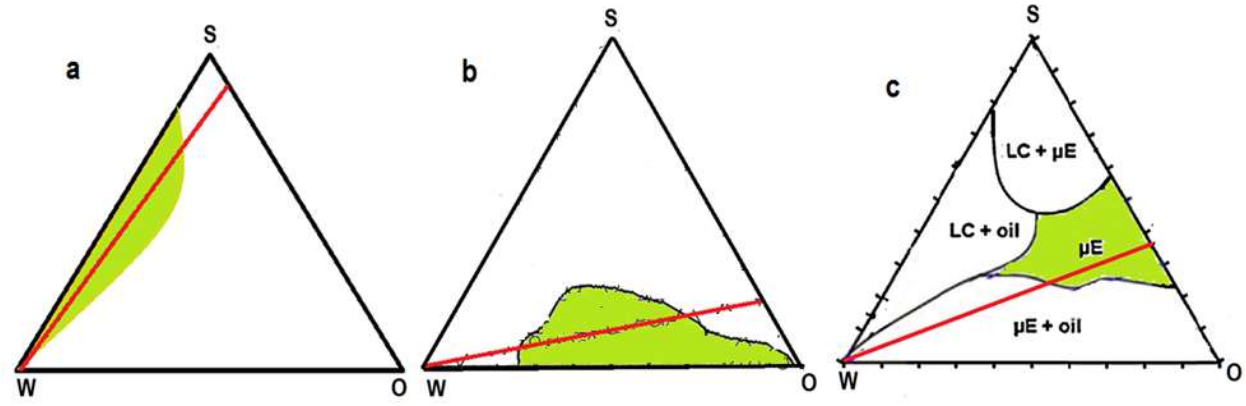

Figure 1-2: The ternary phase diagrams for SEDS/SMEDS formulations that are not fully dilutable. The green area represents the region in which microemulsion is formed and the red line shows a dilution line. The a, b, and c graphs adopted and modified from [25], [26] and [27], respectively

The group of Garti were one of the pioneers in developing U-type formulations (Figure 1-3). In their first generation of food grade fully dilutable microemulsions, however, they used a mixture of water-propylene glycol (PG) as diluting media. In the second generation, hexanol was used as cosolvent to formulate a pharma-grade SMEDS to enhance the bioavailability of diclofenac.

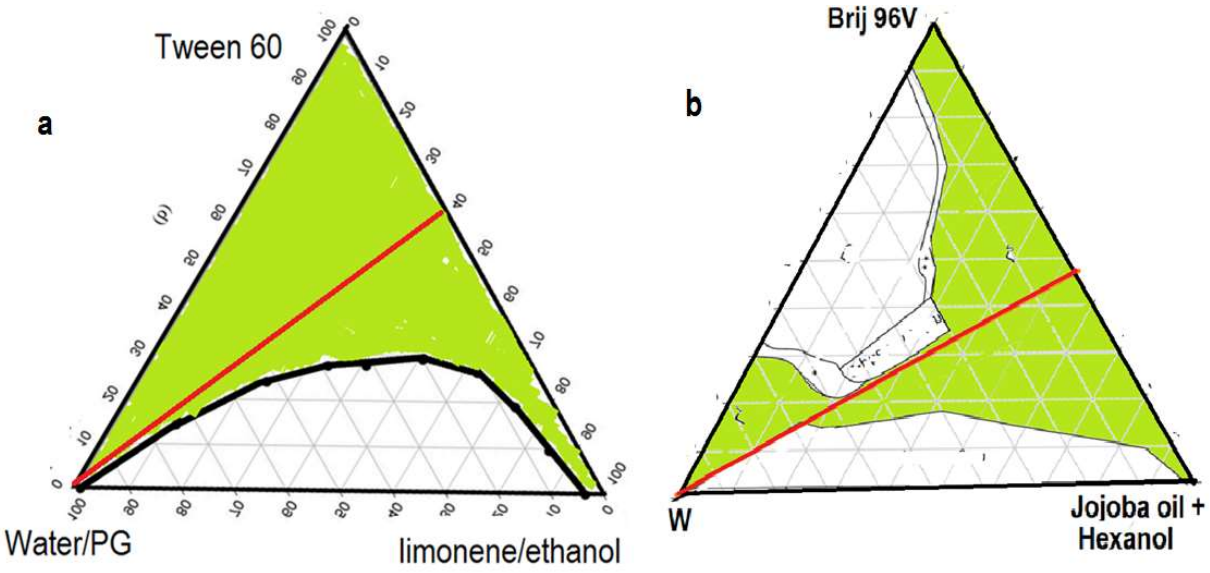

Figure 1-3. The ternary phase diagrams for fully dilutable microemulsions adopted from [28,29] (a) and [30] (b)

As shown in

Table 1-1, currently PEGylated compounds are dominantly used as the main surfactants, However, they may irritate the gastrointestinal (GI) mucosa or may form secondary products due to auto-oxidation [31]. This can affect the chemical stability of the formulation.

Table 1-1: The commonly used surfactants/cosurfactants for formulating LBDS

Trade Name	Chemical / USP NF Name
Cremophor® EL, RH40, RH60	Polyoxyl glycerides of hydrogenated Castrol oil
Capryol 90	Propylene glycol monocaprylate
Captex 355	Glyceryl Tricaprylate/Tricaprate
DK ester SS	Sucrose ester of fatty acid
Emulsifier OP	Alkylphenol polyoxyethylene ether
Gelucire 44/14	Lauroyl Polyoxyl-32 glycerides
Labrafac PG	Propylene glycol dicaprolate/dicaprate
Labrafil M 1944 CS	Oleoyl polyoxyl-6 glycerides
Labrafil M 2125 CS	Linoleoyl Polyoxyl-6 glycerides
Labrasol	Caprylocaproyl Polyoxyl-8 glycerides
Lauroglycol 90	propylene glycol monolaurate
Lauroglycol-FCC	Propyleneglycol caprylate
Lutrol-E400	Polyethylene glycol 400
Mirj 45	PEG-8 stearate
Mirj 52	PEG-40 stearate
Myvacet 9-45	Acetic acid ester of mono/di-glyceride
Solutol® HS15	PEG-15 hydroxy stearate
Tagat TO	Polyoxyethylene glyceryl trioleate
Transcutol-HP	Diethylene glycol monoethyl ether
Tween 20	Polyoxyethylene-20 sorbitan monolaurate
Tween 80	Polyoxyethylene (20) sorbitan monooleate

It is also well known that a single surfactant does not lead to a dilutable microemulsion and a combination of surfactants, cosurfactants and cosolvents (alcohols) is required. Alcohol-free lecithin-based formulations are preferred. Lecithin, has a generally recognized as safe (GRAS) status, but tends to form liquid crystals and gels and cannot form microemulsions by itself. Most pharmaceutical formulations, such as Neoral®, use alkyl-polyethylene glycol surfactants that although are very good at promoting the solubilization of hydrophobic component, their resistance to biodegradation causes an imbalance of lipids in the system and do not form part of the

chylomicron/lipoprotein transport of lipids [32] . However, even for cancer treatment, there are calls for the replacement of alkyl-polyethylene glycol surfactants, and more specifically, the replacement of cremophor, which is the main surfactant used in most SEDS and SMEDS formulations [33]. This situation has prevented the broad use of SEDS and SMEDS for other non-life-threatening conditions, or for the delivery of micronutrients and nutraceuticals. In the area of nutraceutical delivery, it is shown that LBDS effectively increase the absorption of fat-soluble vitamins via oral, transdermal or intravenous administration [2]. Currently, the only μE-based commercial formulation (Nutralease®) uses a combination of an aqueous co-solvent, a surfactant, and an alcohol co-surfactant, in addition to the oil and the nutraceutical. The Nutralease® approach is a significant improvement, but it requires a substantial amount of either water or water-cosolvent. This means that the formulation of Nutralease® has to be delivered in the form of a liquid product, which limits its range of applicability and the amount of active.

Table 1-2 summarizes the literature on nutraceutical SEDDS/SMEDS systems. Having reviewed these works, one can conclude that SEDDS/SMEDS have high solubilization capacity of lipophilic micronutrients and a relatively small dose of them can readily provide a large portion of the recommended daily intake. However, in terms of the chemical structure of the excipients, the common feature of all developed systems is the use of PEG-based compounds as surfactant/cosurfactant. Furthermore, the ternary phase diagram of most of these systems shows that they are not fully dilutable as shown in Figure 1-2.

Table 1-2: Formulated SEDDS/SMEDS for improving the bioavailability of nutraceuticals

Type	Expedients	Load	Increase in absorption	Ref.
Curcumin				
SMEDS	Ethyl oleate, Emulsifier OP , Cremophor, PEG	2.1 %	3.86 folds	[25]
SMEDS	Isopropyl myristate, Ethanol, Cremophor	5.0 %	12.73 folds	[34]
SMEDS	Labrasol, Cremophor EL, Labrafac PG, Capryol	4.4 %	14 folds	[35]
SEDDS	Labrasol, Vit. E TPGS, PEG 400	6.7 %	35.8 folds	[36]
S-	Labrasol, Lauroglycol FCC, Transcutol HP	4.6 %	NA	[37]
CO-Q10				
SEDS	Labrasol , Myvacet 9-45, lauroglycol	5.6 %	2 fold	[38]
SEDS	Medium-chain triglycerides, DK ester SS,	5 %	21.7 fold	[39]
SEDS	Labrasol, Labrafil M 1944/ M 2125,	6 %	2.4 fold	[40]
SEDS	Labrasol , Lauroglycol FCC, Transcutol P	0.8-1.6%	4.5 fold	[26]
Carotenoids				
SMEDS	Orange oil, Capmul, Tween 20, Labrasol, PEG	140.8 lg/ml	NA	[41]
SMEDS	Labrasol, Phosal 53 MCT	4 %	11.8 fold	[42]
Vitamins (A, D, E, K)				
SMEDS	Ethyl oleate, Tween 80, PEG 400	3 %	1.45 fold	[43]
SEDS	Soybean oil, Cremophor EL, Capmul MCM	25 %	1.5-2 fold	[44,45]
SEDS	Cremophor EL, labrasol, Captex 355, Ethanol	1-50 mM	2 fold	[46]
SEDS	Soy oil, Tween 80, Labrasol, Tocomin 50%		2–3 fold	[47]
Flavonoids				
SEDS	Labrafil M 1944CS, Cremophor EL, Transcutol	4.4 %	1.5 fold	[48]
Terpenoid (Oleanolic acid)				
SMEDS	Ethyl Oleate, Cremophor EL, Ethanol	1%	5.1 fold	[49]

As an alternative to traditional PEGylated surfactants and alcohol cosolvents, the lecithin linker approach has been proposed. Previous works had shown that linker-based lecithin microemulsions have desirable phase behaviour and excellent solubilization capacity for a wide variety of oils and can replace cosurfactants/cosolvents in microemulsion formulations [27,50–52]. In these systems soy lecithin is used as the main surfactant accompanied by a glycerol monooleate as a lipophilic "linker" (LL) and C8/C10 polyglycerols as a hydrophilic linker (HL). Lipophilic linkers can be considered as a lipophilic component somewhere in between a co-surfactant and an oil co-solvent and HL is a hydrophilic component in between a hydrophilic cosurfactant and a water co-solvent (Figure 1-4).

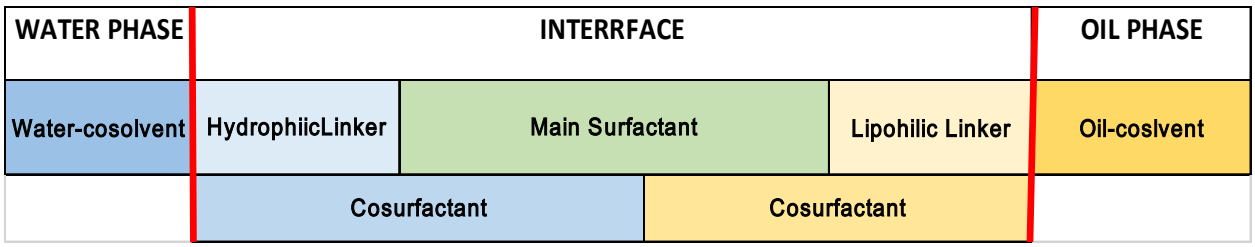

Figure 1-4: The lipophilic-hydrophilic spectrum of components at the interface

The presence of lecithin brings the two linkers together into a "self-assembled" surfactant at the interface. Because all the components of this "trio" are either already part of the lipid cycle (lecithin and glycerol monooleate) or can be easily enzymatically hydrolyzed (C8/C10 polyglycerol), they are not expected to disrupt the lipid metabolic pathways in the same way that alkyl polyethylene glycols do.

Table 1-3 shows the lecithin linker delivery systems that have been developed in the past. Lecithin linker μE system for lidocaine [53–55], produce twice the transdermal flux obtained with water. When lecithin linker was formulated as a the SEDS system [27], the in vitro permeability study revealed that stable emulsions with drop sizes of 150–300 nm produce large and irreversible permeation of b-carotene to sheep intestine. Although the results were promising in terms of absorption and

penetration in this first-generation lecithin linker systems, they failed to reduce the droplet size to below 100 nm and did not exhibit full dilutability, a requirement for an effective delivery system[27].

Table 1-3: The lecithin liker delivery systems

Type	**µE** [53–55]	**SEDS** [27]		**µE-based gel** [56]
Physical state	Liquid	Liquid		Gel
Administration Route	Transdermal	Oral		Ophthalmic, Transdermal
Application	Cosmetic/ Pharma	Pharma	Nutra	Pharma
Active ingredient	Lidocaine	β-Sitosterol	Ω-3 FA, Vit. A, E, β-Carotene	Lidocaine, Dexamethasone
Oil	Isopropyl Myristate	Ethyl Caprate	Fish oil, Ω-3 esters	Isopropyl Myristate
Lipophilic Linker	Sorbitan mono-oleate	Sorbitan mono-oleate	Glyceryl mono-oleate	Sorbitan mono-oleate
Hydrophilic Linker	Caprylic Acid / Sodium Caprylate	Decaglyceryl caprylate& PEG-6-capric glycerides	Polyglyceryl-6- caprylate	Decaglyceryl caprylate/caprate & PEG-6- capric glycerides
Surfactant	**Lecithin**			

In the early stages of this work, one of the goals was to adapt the lecithin-linker formulations to include iron as the active ingredient for food fortification applications. However, the iron compounds that are currently used for iron fortification are water-soluble, including ferrous sulphate and ferrous pyruvate. SMEDS, including lecithin-linker formulas, are lipid-based formulas and the loaded active ingredients should be oil-soluble if one wants to produce a single-phase system and not a suspension. Iron fatty acids salts were considered as suitable candidates. However, due to long tails of ferric palmitate (MW= 825.1) and ferric oleate (MW=900.3), the net Fe content is as low as 6.8% and 6.2%, respectively. Having loaded it to SMEDS formulation (e.g. at 5%) this would have resulted in a final iron content of ~0.3% in the SMEDS.

To increase the loading capacity, it was explored the use of medium chain fatty acids iron salts such as ferrous caprylate (MW= 342.2) with an iron content of ~16.4%. By interacting sodium caprylate with ferrous sulfate and ferric chloride, shorter chain fatty acid salts were synthesized and characterized. However, loading this compound to the SMEDS formulation was a challenging task. It was observed that these compounds can function as organogelator themselves. This behavior depends on type of the oil as is shown in Appendix B. Due to low loading capacity of this approach for iron, it was decided to work on oil-soluble active ingredients that could be formulated at concentrations that can match recommended daily intake for nutraceuticals or the recommended dose for pharmaceuticals. This work concentrated on ibuprofen as model oil-soluble active pharmaceutical ingredient, and beta-carotene as model nutraceutical.

Considering the above discussion, the first objective of this work was exploring the design of a fully dilutable self-microemulsifying lecithin linker platform to be used as a delivery system. In addition to the physical characterization of the system, the biological performance of the system was also considered via animal models. In addition to pharmacokinetic studies with ibuprofen-loaded SMEDS, the work also explored the potential (side) effects of long-term consumption of lecithin linker SMEDS loaded with beta-carotene. This study can facilitate the approval process by regulatory bodies to assure the safety of the formulation. While numerous reports in the literature have proven SMEDS enhance solubilization and improve the bioavailability of poorly soluble bioactive compounds, there is a shortage of data on the safety of the formulation, particularly when it is consumed for a long period of time.

Another challenge in designing a fully dilutable SMEDS is lacking a predictive model for SOW systems. Currently, the routine practice for examining the phase behaviour of the excipients in SMEDS formulation is trial and error [57] which normally involves constructing various ternary

phase diagrams. This approach is resource intensive and there is a shortage of comprehensive models to design and predict the phase behaviour of self-micro-emulsifying systems. The traditional model-like approaches such as hydrophilic-lipophilic balance (HLB), Critical Micelle Concentration (CMC), Critical Packing Parameter (CPP) and phase inversion temperature (PIT), Windsor R are either not quantitative, or difficult to implement practically, or only partially explain the outcome of a formulation [58]. The latest advance in surfactant theory has come from the HLD and HLD-NAC frameworks [59–64]. HLD is an equation that correlates the formulation variables (oil polarity, surfactant hydrophilicity) and field variables (temperature and salinity) with phase behaviour. For a non-ionic surfactant system, the equation is [65]:

$$\boldsymbol{HLD = b * (S) - k * EACN + Cc + c_T(T - 25) + f(A)} \qquad \textbf{1-1}$$

Where "S" is the electrolyte concentration (g NaCl/100 ml), "EACN" is the equivalent alkane carbon number; "Cc" is the characteristic curvature of the surfactant, "T" is the temperature of the system (˚C), "f (A)" is a function of alcohol or cosolvents concentration. Finally, K, c_T, and b are empirical constants for a given system. A hydrophilic (or lipophilic) system has a negative (or positive) HLD values and generates O/W (or W/O) microemulsions with excess oil (or water). When HLD approaches zero, a bicontinuous microemulsion is formed.

HLD-NAC (hydrophilic-lipophilic difference- net average curvature) connects the HLD equation of state to the NAC model and is a powerful approach to predict and characterize the phase behaviour of SOW systems. Previous work has demonstrated that HLD-NAC can effectively quantify and predict the characteristics of μEs phase behaviour, such as interfacial tension, solubilization capacity, stability, viscosity, morphology and droplet size [66–69]. However, the model has not been applied for complex SMEDS formulations, in particular for linker-based ones.

When designing a SMEDS, the critical questions the formulator needs to answer are:

- What kind of oil/ surfactant to choose to solubilize the active ingredient without drug precipitation?
- What is the optimum oil to surfactant ratio that can be diluted infinitely without phase separation?
- What is the optimum ratio of components within the surfactant mixture (surfactant, cosurfactant, cosolvents, or linkers) to avoid phase separation upon dilution?

Knowing these values assist to predict the overall map of the ternary phase diagram and dilution profile of the SMEDS. Therefore, another objective of this work is examining the application of the HLD-NAC model as a framework for rational formulation design for SMEDS and understanding the thermodynamics and characteristics of SMEDS phase behaviour. This study provides the tools for the engineering of SMEDS formulations for drug/nutraceutical delivery applications.

Another challenge in using SMEDS for drug delivery is the unexpected interactions of the loaded active ingredient and the SMEDS excipients. The reports in the literature show that physicochemical properties of loaded and unloaded dilutions are different [70] . While an unloaded SMEDS may be fully dilutable, the incorporation of the active ingredient can alter the phase behaviour. Restoring the formulation to its fully dilutable feature could be challenging and require time-consuming reformulation. The deviation in dilution profile after the addition of the active ingredient occurs due to change in the HLD of the system. Since the initial approach for developing lecithin linker platform was based on the HLD approach, it was hypothesized that the HLD framework may assist in quantifying the change in hydrophilicity of the system and restore the formulation.

Liquid μE systems, including the SMEDS formulations, generally show a burst release profile due to their self-emulsifying properties [28]. One approach to modifying the release profile is transforming the physical state of a delivery vehicle from liquid to solid or semisolid forms. Solidification can stabilize lipid colloidal systems [71] and has recently gained attention and is it becoming a trend in designing LBDS. Over the last decade, the potential of organogels as potential drug delivery systems has been investigated. Compared to other lipid-based drug delivery systems, the use of organogels as delivery vehicles is a relatively new approach, in particular, gels made with low molecular weight gelators (LMWG) such as phytosterols (β-sitosterol and γ-oryzanol). By now only a limited number of organogels have been investigated as drug delivery systems. They include μE based-gels, alanine-based in situ forming organogels, and 12-Hydroxy Stearic Acid (HSA) organogels for transdermal, parenteral and oral delivery systems, respectively [8],[28]. Difficulty finding food and pharmaceutical grade materials limits the application of organogels. A full review of organogel applications in cosmetics, pharmaceutics and foods can be found somewhere else [74]. β-sitosterol and γ-oryzanol are two phytosterols with health-promoting properties that can be used as food grade organogelator. Organogels made with β-sitosterol+γ-oryzanol show unique properties such as thermo-reversibility and high active payload. A recent study has suggested that these organogels can be considered as a controlled-release drug delivery system [75].

It would be an appealing approach to have an integrated system of SMEDS, and organogels. It was hypothesized that integrating the concept of SMEDS and organogels can combine the advantages of both delivery systems such as self-dispersion, ease of production, sub-micron particle size with the extended release profile organogels. Dilution of conventional organogels (made with only oil and gelators) does not result in stable nano-dispersions, and a surfactant-rich environment is

required to produce a stable dispersion. Previous work has overcome this issue by adding surfactants to an aqueous phase to facilitate and stabilize the dispersion or by sonicating/applying high shear. In this study, we implemented another approach: adding gelator to the surfactant-rich SMEDS formulation to make an organogel. In this novel food-grade SMEDS-based organogel, the SMEDS formulation functions as the oil phase (solvent for gelators), and β-sitosterol+ γ-oryzanol are the gelators. We hypothesize that this system, upon exposure to aqueous media, self-disperses -without applying high shear- and therefore it can be called a "self microemulsifying organogel delivery system". The objective is to produce a controlled release SMEDs through a self-dispersing organogel.

The table below schematically summarizes the challenges identified in this work. These challenges could be classified into two main groups: The (pre)formulation challenges and the application challenges. The corresponding chapters in Table 1-4 presents the answers, or advances, obtained in this work.

Table 1-4: Common challenges in design and application of SMEDS along with the proposed approaches

Challenges/ Gaps	Corresponding Objective	Corresponding Chapter
Formulation Challenges		
Lack of Biocompatible surfactants	Developing Lecithin linker systems	Chapter 2
Phase separation during dilution	Developing Lecithin linker systems	Chapter 2
Lack of predicting model for phase behaviour	Extending the HLD-NAC model to SMEDS	Chapter 2
Quantifying SMEDS-Active interactions	Applying HLD framework	Chapter 3
Performance Challenges		
Lack of Pharmacokinetic data on lecithin linker SMEDS	Conducting In vivo dose response	Chapter 3
Immediate Release	Developing controlled release SMEDS	Chapter 4
Lack of Toxicity data	Long-term pathology/histology study	Appendix A

1.3. References

1. McClements, D. J., Decker, E. a & Weiss, J. Emulsion-based delivery systems for lipophilic bioactive components. *J. food Sci.* **72,** R109-24 (2007).

2. Gonnet, M., Lethuaut, L. & Boury, F. New trends in encapsulation of liposoluble vitamins. *J. Control. Release* **146,** 276–290 (2010).

3. Trautwein, E. A., Demonty, I. & Ras, R. T. Plant Sterols - A Dietary Approach For Effective Blood Lipid Lowering As Part Of A Heart Healthy Diet. *Curr. Top. Nutraceut. R.* **8,** 137–148 (2010).

4. Tyagi, S., Singh, G., Sharma, A. & Aggarwal, G. Phytochemicals as candidates therapeutics: an overview. *Intl J Pharm. Sci. Rev. Res.* **3,** 53–55 (2010).

5. Rochfort, S. & Panozzo, J. Phytochemicals for health, the role of pulses. *J. Agri. food Chem.* **55,** 7981–94 (2007).

6. *Nanocarrier Technologies : Frontiers of Nanotherapy*. *Drug Delivery* **180,** (Springer, 2006).

7. Hauss, D. J. Oral lipid-based formulations. *Adv. Drug Deliv. Rev.* **59,** 667–76 (2007).

8. Shah, D. O., Bagwe, R.P., Kanicky, J.R., Palla, B.J., Patanjali, P.K. Improved drug delivery using microemulsions: Rationale, recent progress, and new horizons. *Crit. Rev. Ther. Drug Carrier Syst.* **18,** 77–140 (2001).

9. Garti, N. & Yuli-Amar, L. Micro- and nano-emulsions for delivery of functional food ingredients. in *Delivery and controlled release of bioactives in foods and nutraceuticals* (ed. Garti, N.) 149–184 (Woodhead Publishing Limited, 2008).

10. Paul, B. K. & Moulik, S. P. Uses and applications of microemulsions. *Cur. Sci.* **80,** 990–1001 (2001).

11. Lawrence Jayne, W. W. Nanoparticulates As Drug Carriers. in *Nanoparticulates As Drug Carriers* (ed. Torchilin, V. P.) 129–131 (Imperial College Press, 2006).

12. Flanagan, J. & Singh, H. Recent advances in delivery of food-derived bioactives and drugs using microemulsios. in *Nanocarrier Technologies: frontiers of nanotherapy* (ed. Mozafari, M. R.) 95–111 (Springer Netherlands, 2006).

13. McClements, D. J. & Li, Y. Structured emulsion-based delivery systems: controlling the digestion and release of lipophilic food components. *Adv. Colloid Interface Sci.* **159,** 213–28 (2010).

14. Choc, M. G. Bioavailability and pharmacokinetics of cyclosporine formulations: Neoral vs Sandimmune. *Int. J. Dermatol.* **36 Suppl 1,** 1–6 (1997).

15. Fatouros, D. G., Karpf, D. M., Nielsen, F. S. & Mullertz, A. Clinical studies with oral lipid based formulations of poorly soluble compounds. *Ther. Clin. Risk Manag.* **3,** 591–604 (2007).

16. McClements, D. J. Nanoemulsions versus microemulsions: terminology, differences, and similarities. *Soft Matter* **8,** 1719 (2012).

17. Balakrishnan, P., Lee, B.-J., Oh, D. H., Kim, J. O. & Hong, M. J. Enhanced oral bioavailability of dexibuprofen by a novel solid self-emulsifying drug delivery system. *Eur. J. Pharm. Biopharm.* **72,** 539–45 (2009).

18. O'Driscoll, C. M. Lipid-based formulations for intestinal lymphatic delivery. *Eur. J. Pharm. Sci.* **15,** 405–15 (2002).

19. Porter, C. J. H., Trevaskis, N. L. & Charman, W. N. Lipids and lipid-based formulations: optimizing the oral delivery of lipophilic drugs. *Nat. Rev. Drug. Discov.* **6,** 231–48 (2007).

20. Porter, C. J. & Charman, W. N. In vitro assessment of oral lipid based formulations. *Adv. Drug Deliv. Rev.* **50 Suppl 1,** S127-47 (2001).

21. Talegaonkar, S., Azeem, A. & Ahmad, F. J. Microemulsions: a novel approach to enhanced drug delivery. *Recent Pat. Drug Deliv. Formul.* **2,** 238–57 (2008).

22. Dokania, S. & Joshi, A. K. Self-microemulsifying drug delivery system (SMEDDS) - challenges and road ahead. *Drug Deliv. Inf. Healthc.* **22,** 1521–464 (2015).

23. Djekic, L. & Primorac, M. Microemulsion Systems Application in Delivery of Poorly Soluble Drugs. in *Colloids in Drug Delivery* (ed. Fanum, M.) 245–270 (CRC Press, 2010).

24. Lakkis, J. *Encapsulation and controlled release technologies in food systems*. (2007).

25. Cui, J. *et al.* Enhancement of oral absorption of curcumin by self-microemulsifying drug delivery systems. *Int. J. Pharm.* **371,** 148–155 (2009).

26. Akhter, M. H., Ahmad, A., Ali, J. & Mohan, G. Formulation and development of CoQ10-loaded s-SNEDDS for enhancement of oral bioavailability. *J. Pharm. Innov.* **9,** 121–131 (2014).

27. Chu, J. *et al.* Lecithin-linker formulations for self-emulsifying delivery of nutraceuticals. *Int. J. Pharm.* **471,** 92–102 (2014).

28. Garti, N., Avrahami, M. & Aserin, A. Improved solubilization of Celecoxib in U-type nonionic microemulsions and their structural transitions with progressive aqueous dilution. *J. Colloid Interface Sci.* **299,** 352–65 (2006).

29. Spernath, A., Yaghmur, A., Aserin, A., Hoffman, R. E. & Garti, N. Food-grade microemulsions based on nonionic emulsifiers: media to enhance lycopene solubilization. *J. Agri. food Chem.* **50,** 6917–22 (2002).

30. Shevachman, M., Garti, N., Shani, A. & Sintov, A. C. Enhanced percutaneous permeability of diclofenac using a new U-type dilutable microemulsion. *Drug Dev. Ind. Pharm.* **34,** 403–12 (2008).

31. Hauss, D. J. Oral lipid-based formulations. *Adv. Drug Deliv. Rev.* **59,** 667–676 (2007).

32. Torcello-Gómez, A. *et al.* Investigating the effect of surfactants on lipase interfacial behaviour in the presence of bile salts. *Food Hydrocoll.* **25,** 809–816 (2011).

33. Gelderblom, H. & Verweij, J. Cremophor EL, the drawbacks and advantages of vehicle selection for drug formulation. *Eur. J. Cancer* **37,** 1590–1598 (2001).

34. Wu, X., Xu, J., Huang, X. & Wen, C. Self-microemulsifying drug delivery system improves curcumin dissolution and bioavailability. *Drug Dev. Ind. Pharm.* **37,** 15–23 (2011).

35. Setthacheewakul, S. & Mahattanadul, S. Development and evaluation of self-microemulsifying liquid and pellet formulations of curcumin, and absorption studies in rats. *Eur. J. Pharm. Biopharm.* **76,** 475–85 (2010).

36. Pawar, Y. B. *et al.* Novel lipid based oral formulation of curcumin: Development and optimization by design of experiments approach. *Int. J. Pharm.* **436,** 617–623 (2012).

37. Yan, Y.-D. *et al.* Enhanced oral bioavailability of curcumin via a solid lipid-based self-emulsifying drug delivery system using a spray-drying technique. *Biol. Pharm. Bull.* **34,** 1179–86 (2011).

38. Kommuru, T. R., Gurley, B., Khan, M. a & Reddy, I. K. Self-emulsifying drug delivery systems (SEDDS) of coenzyme Q10: formulation development and bioavailability assessment. *Int. J. Pharm.* **212,** 233–46 (2001).

39. Onoue, S. *et al.* Self-nanoemulsifying particles of coenzyme Q10 with improved nutraceutical potential. *PharmaNutrition* **3,** 153–159 (2015).

40. Balakrishnan, P. *et al.* Enhanced oral bioavailability of Coenzyme Q10 by self-emulsifying drug delivery systems. *Int. J. Pharm.* **374,** 66–72 (2009).

41. Peng, C. *et al.* Design of microemulsion system suitable for the oral delivery of poorly aqueous soluble beta-carotene. *Pharm. Dev. Technol.* **0,** 1–7 (2017).

42. Shanmugam, S. *et al.* Solid self-nanoemulsifying drug delivery system (S-SNEDDS) containing phosphatidylcholine for enhanced bioavailability of highly lipophilic bioactive carotenoid lutein. *Eur. J. Pharm. Biopharm.* **79,** 250–257 (2011).

43. Liu, Y. & JiamgXiaoye. Prescription Design and Bioavailability Assessment of Self-Microemulsifying System of Vitamin AD. *Lat. Am. J. Pharm.* **34,** 36.44 (2014).

44. Taha a, I. & Al-Saidan, S. Preparation and in vitro characterization of self-nanoemulsified drug delivery system (SNEDDS) of all-trans-retinol acetate. *Int. J. Pharm.* **285,** (2004).

45. Taha, E., Ghorab, D. & Zaghloul, A. A. Bioavailability assessment of vitamin A self-nanoemulsified drug delivery systems in rats: A comparative study. *Med. Princ. Pract.* **16,** 355–359 (2007).

46. Alqahtani, S., Alayoubi, A., Nazzal, S., Sylvester, P. W. & Kaddoumi, A. Enhanced solubility and oral bioavailability of gama-tocotrienol using a self-emulsifying drug delivery system (SEDDS). *Lipids* **49,** 819–829 (2014).

47. Yap, S. P. & Yuen, K. H. Influence of lipolysis and droplet size on tocotrienol absorption from self-emulsifying formulations. *Int. J. Pharm.* **281,** 67–78 (2004).

48. Li, W. *et al.* Self-nanoemulsifying drug delivery system of persimmon leaf extract: Optimization and bioavailability studies. *Int. J. Pharm.* **420,** 161–171 (2011).

49. Yang, R., Huang, X., Dou, J., Zhai, G. & Lequn, S. Self-microemulsifying drug delivery system for improved oral bioavailability of oleanolic acid: Design and evaluation. *Int. J. Nanomedicine* **8,** 2917–2926 (2013).

50. Salager, J.-L., Graciaa, A. & Lachaise, J. Improving solubilization in microemulsions with additives. Part III: Lipophilic linker optimization. *J. Surfactants Deterg.* **1,** 403–406 (1998).

51. Sabatini, D. A., Acosta, E. & Harwell, J. H. Linker molecules in surfactant mixtures. *Curr. Opin. Colloid Interface Sci.* **8,** 316–326 (2003).

52. He, C.-X., He, Z.-G. & Gao, J.-Q. Microemulsions as drug delivery systems to improve the solubility and the bioavailability of poorly water-soluble drugs. *Expert opin. drug Deliv.* **7,** 445–60 (2010).

53. Yuan, J. S., Ansari, M., Samaan, M. & Acosta, E. J. Linker-based lecithin microemulsions for transdermal delivery of lidocaine. *Int. J. Pharm.* **349,** 130–43 (2008).

54. Yuan, J. S. *et al.* Effect of surfactant concentration on transdermal lidocaine delivery with linker microemulsions. *Int. J. Pharm.* **392,** 274–84 (2010).

55. Yuan, J. S. & Acosta, E. J. Extended release of lidocaine from linker-based lecithin microemulsions. *Int. J. Pharm.* **368,** 63–71 (2009).

56. Xuan, X.-Y., Cheng, Y.-L. & Acosta, E. Lecithin-linker microemulsion gelatin gels for extended drug delivery. *Pharmaceutics* **4,** 104–29 (2012).

57. Gao, P. Design and Development of Self-Emulsifying Lipid Formulations for Improving Oral Bioavailability of Poorly Water-Soluble and Lipophilic Drugs. in *Formulating Poorly Water Soluble Drugs* (eds. Williams III, R. O., Watts, A. B. & Miller, D. A.) **3,** 243–266 (Springer New York, 2012).

58. Troncoso, A. B. & Acosta, E. Van der Waals free energy model for solubilization of oil in micelles. *Soft Matter* **11,** 516–531 (2015).

59. Nagarajan, R. & Ruckenstein, E. Molecular Theory of Microemulsions. *Langmuir* **16,** 6400–6415 (2000).

60. Nardello, V., Chailloux, N., Poprawski, J., Salager, J.-L. & Aubry, J.-M. HLD concept as a tool for the characterization of cosmetic hydrocarbon oils. *Polym. Int.* **52,** 602–609 (2003).

61. Rondon-Gonzalez, M., Madariaga, L. & SallagerJean-Louis. Emulsion Catastrophic Inversion from Abnormal to Normal Morphology. 8. Effect of Formulation on the Inversion Produced by Continuous Stirring. *Ind. Eng. Chem. Res* **48,** 2913–2919 (2009).

62. Salager, J. L. *et al.* The emergence of formulation engineering in emulsion making?transferring know-how from research laboratory to plant. *Polym. Int.* **52,** 471–478 (2003).

63. Thakur, R. K., Villette, C., Aubry, J. M. & Delaplace, G. Dynamic emulsification and catastrophic phase inversion of lecithin-based emulsions. *Colloids Surf., A* **315,** 285–293 (2008).

64. Acosta, E. J. Modeling and Formulation of Microemulsios: The net Average Curvature Model and the Combined Linker Effect, Dissertation. (University of Oklahoma, 2004).

65. Kiran, S. K. & Acosta, E. J. HLD–NAC and the Formation and Stability of Emulsions Near the Phase Inversion Point. *Ind. Eng. Chem. Res.* **54,** 6467–6479 (2015).

66. Kiran, S. K., Acosta, E. J. & Moran, K. Evaluating the hydrophilic-lipophilic nature of asphaltenic oils and naphthenic amphiphiles using microemulsion models. *J. Colloid Interface Sci.* **336,** 304–13 (2009).

67. Kiran, S. K. & Acosta, E. J. Predicting the Morphology and Viscosity of Microemulsions Using the HLD-NAC Model. *Ind. Eng. Chem. Res* **49,** 3424–3432 (2010).

68. Kiran, S. K. & Acosta, E. J. Development of Thermodynamic Correlation to Predict Microemulsion Morphology and Viscosity. 1–6 (2008).

69. Castellino, V., Cheng, Y.-L. & Acosta, E. The hydrophobicity of silicone-based oils and surfactants and their use in reactive microemulsions. *J. Colloid Interface Sci* **353,** 196–205 (2011).

70. Pestana, K. C. *et al.* Oil-in-water lecithin-based microemulsions as a potential delivery system for amphotericin B. *Colloids Surfaces B Biointerfaces* **66,** 253–259 (2008).

71. Tan, A., Rao, S. & Prestidge, C. a. Transforming lipid-based oral drug delivery systems into solid dosage forms: an overview of solid carriers, physicochemical properties, and biopharmaceutical performance. *Pharm. Res.* **30,** 2993–3017 (2013).

72. Sahoo, S. *et al.* Organogels: Properties and Applications in Drug Delivery. *Des. Monomers Polym.* **14,** 95–108 (2011).

73. Murdan, S. Organogels in drug delivery. *Expert Opin. Drug Deliv.* **2,** 489–505 (2005).

74. Balasubramanian, R., Sughir, A. & Damodar, G. Oleogel: A promising base for transdermal formulations. *Asian J. Pharm.* **6,** 1 (2012).

75. Chung, O. Sterol-Based Organogel Drug Delivery Systems, MASc. thesis. (University of Toronto, 2012).

76. You, X. *et al.* Optimizing surfactant content to improve oral bioavailability of ibuprofen in microemulsions : Just enough or more than enough ? *Int. J. Pharm.* **471,** 276–284 (2014).

77. Xing, Q. *et al.* Microemulsions containing long-chain oil ethyl oleate improve the oral bioavailability of piroxicam by increasing drug solubility and lymphatic transportation simultaneously. *Int. J. Pharm.* **511,** 709–718 (2016).

78. Chan, J. Extracting Lipid and Carotenoids from Microalgae with Lecithin- Linker Microemulsions. (University of Toronto, 2012).

79. Tchakalova, V. & Fieber, W. Classification of fragrances and fragrance mixtures based on interfacial solubilization. *J. Surfactants Deterg.* **15,** 167–177 (2012).

Chapter 2. Predicting Solubilization Features of Ternary Phase Diagrams of Fully Dilutable Lecithin Linker Microemulsions

This chapter is derived from the following published manuscript:

M. Nouraei and E. J. Acosta, “Predicting solubilization features of ternary phase diagrams of fully dilutable lecithin linker microemulsions,” J. Colloid Interface Sci., vol. 495, pp. 178–190, 2017.

2.1. Abstract

Fully dilutable microemulsions (μEs), used to design self-microemulsifying delivery system (SMEDS), are formulated as concentrate solutions containing oil and surfactants, without water. As water is added to dilute these systems, various μEs are produced (water-swollen reverse micelles, bicontinuous systems, and oil-swollen micelles), without the onset of phase separation. Currently, the formulation dilutable μEs follows a trial and error approach that has had a limited success. The objective of this work is to introduce the use of the hydrophilic-lipophilic-difference (HLD) and net-average-curvature (NAC) frameworks to predict the solubilization features of ternary phase diagrams of lecithin-linker μEs and the use of these predictions to guide the formulation of dilutable μEs. To this end, the characteristic curvatures (Cc) of soybean lecithin (surfactant), sorbitol monooleate (lipophilic linker) and polyglycerol caprylate (hydrophilic linker) and the equivalent alkane carbon number (EACN) of ethyl caprate (oil) were obtained via phase scans with reference surfactant-oil systems. These parameters were then used to calculate the HLD of lecithin-linkers-ethyl caprate microemulsions. The calculated HLDs were able to predict the phase transitions observed in the phase scans. The NAC was then used to fit and predict phase volumes obtained from salinity phase scans, and to predict the solubilization features of ternary phase diagrams of the lecithin-linker formulations. The HLD-NAC predictions were reasonably accurate and indicated that the largest region for dilutable μEs was obtained with slightly negative HLD values. The NAC framework also predicted and explained, the changes in microemulsions properties along dilution lines.

2.2. Introduction

Fully dilutable microemulsions (μEs) have been a subject of research because of the role that aqueous dilution plays in oilfield chemistries, drug delivery and other applications [1,2,3,4,5].The most common use of dilutable μEs is as self-micro emulsifying delivery systems (SMEDS), where a drug is dissolved in the oil + surfactant "pre-concentrate" to be diluted by body fluids [6]. SMEDS may concisely be defined as concentrated μEs or latent μEs [7]. A microemulsion system can be defined as a thermodynamically stable, transparent/translucent dispersion of an aqueous and/or oil phase, stabilized by an interfacial film of surfactants [8,9,10,11,12].

The first challenge in formulating dilutable μEs has been the choice of safe and effective surfactants and oils. Linker-based lecithin μEs have been shown to have a desirable phase behaviour and excellent solubilization capacity, and to be non-toxic [13,14,15,16]. In a lecithin-linker formulation, there are three surface active components, namely the lecithin surfactant, the lipophilic and the hydrophilic linkers. The lipophilic linker is a surface-active species that segregate near the surfactant tails, increasing the lipophilic interactions between the surfactant (lecithin) and the oil [13]. The hydrophilic linker is a short chain surfactant-like molecule that co-adsorbs with the surfactant at the oil/water interface, increasing the interfacial area [13,14]. The choice of oil, linkers, lecithin, and their concentrations are among the decisions the formulator needs to make. This multi-variable problem is similar for other μE formulations, which can require the evaluation of thousands of combinations to find a fully dilutable system.

Currently, the development of fully dilutable μEs requires the use of a trial and error approach [17]. There is a shortage of models to design, formulate and predict the phase behaviour of surfactant-oil-water systems (SOW) such as dilutable μEs. Indicators, such as the hydrophilic-lipophilic

balance (HLB), critical micelle concentration (CMC), critical packing parameter (CPP), interaction energy ratio (Windsor's R ratio) and phase inversion temperature (PIT), have only served as guidelines [18]. Thermodynamic models have been explored to predict the phase behaviour, including Helfrich's membrane-free energy approach, however, the lack of model parameters have hindered further practical applications of those approaches [19,20,21,22]. Statistical and data mining models have attracted the interest in the pharmaceutical industry for predicting phase boundaries of ternary phase diagrams (TPDs), however, these models require gathering experimental data for similar systems to train the model [23,24].

Perhaps the most effective method to predict the phase behaviour of μEs is through the hydrophilic-lipophilic-difference (HLD) framework [25,26]. The HLD is a semi-empirical correlation that indicates the combination of variables that leads to an "optimal formulation" in a phase behaviour scan. A phase behaviour scan consists of a series of test tubes containing equal volumes of oil and aqueous phases, typically with a constant total surfactant concentration of less than 10.0% by volume, where one formulation variable is gradually changed. The optimal formulation (HLD=0) corresponds to the system where the μE contains equal amounts of oil and water solubilized in the system, with (Winsor Type III) or without (Winsor Type IV) excess aqueous and oil phases. For negative HLDs (Winsor Type I), the surfactant partitions in the aqueous phase, coexisting with an excess oil phase. For positive HLDs (Winsor Type II), the surfactant partitions in the oil phase, coexisting with an excess aqueous phase. The equations of the HLD framework are [25,26,27]:

For ionic surfactants $$HLD = \ln(S) - k \cdot EACN + Cc - \alpha_T \cdot (T-25) \quad \textbf{(2-1)}$$

For nonionic surfactants $$HLD = b \cdot S - k \cdot EACN + Cc + c_T \cdot (T-25) \quad \textbf{(2-2)}$$

where "*S*" is the electrolyte concentration (g NaCl/100 ml), "*EACN*" is the equivalent alkane carbon number; "*Cc*" is the characteristic curvature of the surfactant, "*T*" is the temperature of the system (˚C). Finally, k, α_T, b, c_T are empirical constants for a given surfactant.

The HLD alone has been used to assess trends in formulation properties, including the shape of TPDs. Figure 2-1 shows the sign of HLD and the corresponding shape of the TPD [25].

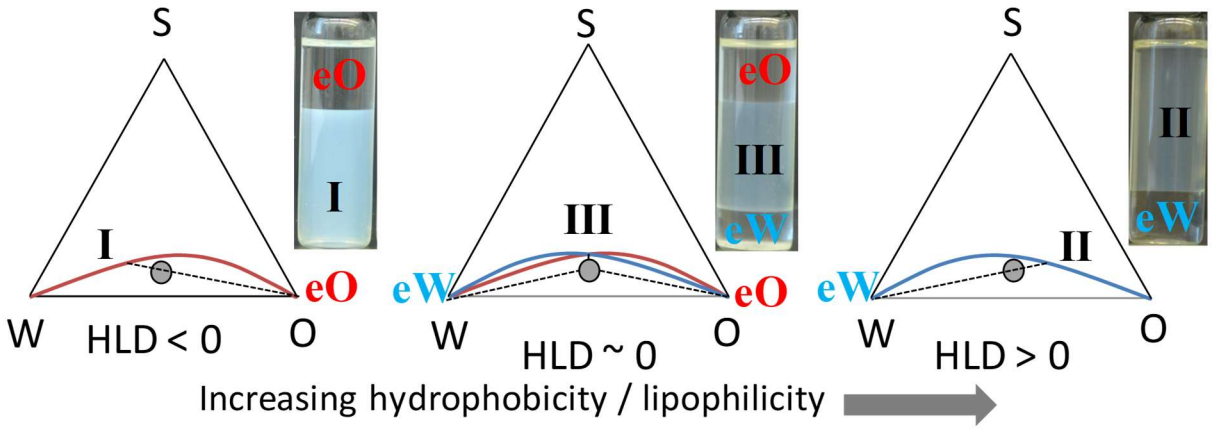

Figure 2-1: HLD and its connection with ternary phase diagram (TPD). I, II, III are Winsor Type I, II and III μEs. eO and eW are the excess oil and aqueous phases. S, O, W correspond to pure surfactant, oil and water, respectively. The circle in the triangle represents the initial composition (volume fraction, based on total volume) of a system with the appearance of the test tubes shown next to each triangle. The dotted line represents a tie line(s) passing through that composition.

The schematics in Figure 2-1 represent only a guideline. The objective of this work is to use the HLD framework to predict the solubilization features of the TPDs for dilutable lecithin-linker systems in the 2 or 3 phase regions obtained near the base of the triangle.

The value of HLD can be used to predict the solubilization capacity of a μE system via the net-average curvature (NAC) model [28,29]. The NAC framework uses a mathematical description of the solubilization of oil and water where any μE is represented by two coexisting states, one where oil is solubilized as spheres of radius R_o in a continuous aqueous media, and a second one where water

is solubilized as spheres of radius R_w in a continuous oil phase. The radius of solubilization of the dispersed phase (R_{disp}) in the continuous phase is calculated as [28]:

$$\mathbf{R_{disp} = 3 \cdot V_{disp} / A_S} \qquad \mathbf{2\text{-}3}$$

where V_{disp} is the volume of the dispersed phase (oil or water) solubilized in the continuous phase, and A_S is the interfacial area provided by the adsorption of the surfactant, calculated as [28]:

$$\mathbf{A_S = \Sigma n_{S,i} \cdot a_{S,i}} \qquad \mathbf{2\text{-}4}$$

where $n_{S,i}$ and $a_{S,i}$ are the number of molecules of surfactant "i" adsorbed at the oil-water interface, and the area per molecule of that surfactant species "i".

Using the solubilization radii for oil and water, the NAC model proceeds to define the net (H_n) and average (H_{avg}) curvature, as follows [28,30, 27,31] :

$$\mathbf{H_n = (1/R_o - 1/R_w)} \qquad \mathbf{2\text{-}5}$$

$$\mathbf{H_{avg} = (1/2) \cdot (1/R_o + 1/R_w)} \qquad \mathbf{2\text{-}6}$$

Kiran and Acosta interpreted the net curvature as the area-averaged curvature of the interface, and the average curvature as the surface to volume ratio of real μE drops [32]. Using that information, the actual size and shape of real microemulsion drops can be predicted. The connection between the NAC framework and HLD is through the concept of net curvature. The HLD was found to represent the net curvature of the system, normalized by the length of the surfactant tail (L):

$$\mathbf{HLD = - L \cdot H_n} \qquad \mathbf{2\text{-}7}$$

With respect to the average curvature, it has been shown that the Type I-III-II phase transition can be predicted if one considers that the inverse of the average curvature, which grows as one approaches HLD = 0, cannot exceed the characteristic length (ξ) of the μE:

$$\mathbf{1/H_{avg} < \xi = 6 \cdot \phi_O \cdot \phi_W \cdot V_m / A_S} \qquad \mathbf{2\text{-}8}$$

where ϕ_O and ϕ_W are the volume fractions of oil and water in the μE, and V_m is the μE volume.

While the HLD-NAC has been shown to effectively quantify and predict the characteristics of μEs phase behaviour, there has been limited use of the framework for lecithin-linker μEs and its use in the design of dilutable μEs and self-microemulsifying delivery systems (SMEDS) [29]. The first part of this work concentrates on the measurement of Cc values for lecithin and linkers, the use of these values to predict the HLD of lecithin-linker salinity phase scans, and the use of HLD-NAC to fit/predict the solubilization capacity of lecithin-linker phase scans.

The use of the HLD framework to predict solubilization features of ternary phase diagrams (TPDs) has been attempted before. The first attempt was introduced by our group (unpublished) and programmed as a demo app by Abbott to illustrate the connection between HLD and TPDs [33]. At that time, the only information disclosed was that the method assumed constant solubilization up until the catastrophic inversion line. That method was later used by Jin et al. to produce ternary phase diagrams for systems relevant to enhanced oil recovery [34,35]. As indicated by Jin et al., and by the group of Johns, the discontinue nature of the methodology produces deviations at high surfactant concentrations. To address this discontinuity, Khorsandi and Johns adapted an alternative method of finding the phase boundaries after noting that the loci of saturated bicontinuous μEs (SBM), defined by the characteristic length (ξ), generated a continuous phase boundary curve [36,37,38]. To this end, a critical characteristic length was introduced to match the two-phase region using two fitting constants, C1 and C2, determined after fitting one set of tie-line data.

During the second part of this article, we will discuss the reasons behind the assumption of constant solubilization for TPD and use HLD-NAC drop shape calculations to establish discontinuity threshold in TPDs. We will also introduce a revised method for predicting TPD solubilization boundaries by revisiting the concept of the continuous phase in concentrated surfactant solutions.

This will lead to a surfactant continuum HLD-NAC model that will be used to predict continuous solubilization boundaries of TPDs of lecithin-linker microemulsions, which will be compared with experimental boundaries. Conductivity, hydrodynamic radius and viscosity measurements were used to characterize dilution lines of fully dilutable μEs obtained with these phase diagrams. The results show that the HLD parameters obtained in the first part of the work can predict the observed phase behaviour and that the surfactant continuum HLD-NAC model can be used to predict the solubilization features of ternary phase diagrams, including the existence of a formulation space for fully dilutable lecithin μEs.

2.3. Materials and Methods

2.3.1. Materials

Ethyl decanoate (≥98.0%) was purchased from Sigma - Aldrich (ON, Canada) and was used as the oil phase in the lecithin-linker formulation. L-alpha-lecithin, granular (from soybean oil) obtained from Acros Organics (NJ, USA). Polyglyceryl-6 Caprylate (Dermofeel® G6CY, 100% active) was donated by Kinetik Technologies (Morris, NJ, USA) and was used as a hydrophilic linker. Glycerol monooleate (GMO or Peceol®) was donated by Gattefossé Canada (Etobicoke, ON, Canada) and was used as a lipophilic linker.

Glacial acetic acid (ACS, ≥99.7%) was purchased from Fisher Scientific (Markham, ON, Canada). Sodium chloride (>99.0%), and sodium hydroxide (ACS reagent grade) were purchased from Bioshop® (Burlington, ON, Canada). Sodium taurocholate hydrate (≥97.0%), cyclohexane (ACS reagent, ≥99.5%), decahydronaphthalene (cis + trans, reagent grade 98.0%), sodium dihexyl sulfosuccinate (SDHS, 80% in H_2O), dodecane, (≥90.0%), hexadecane (≥99.0%) were purchased from Sigma Aldrich (Oakville, ON, Canada). Hexanes, HPLC grade was purchased from Caledon

Laboratories (Georgetown, ON, Canada). Octyl-decyl penta-ethylene glycol ($C_{8-10}E5$, Dehydol® OD5, 100% active) was a gift from BASF (Wyandotte, MI, USA) and was used as a reference surfactant to find the Cc of lecithin and linkers. The composition of the fed state simulated intestinal fluid is listed below. This is a slightly modified version of the USP formulation reported by Marques [39] except that the pH was adjusted to 6.8:

Table 2-1. Composition of fed state simulated intestinal fluid (FeSSIF)

	mM
NaOH	101.0
NaCl	203.2
Acetic Acid	144.1
Sodium taurocholate	15.0
Lecithin	3.8
pH	Adjusted to 6.8

2.3.2. Methods

Phase (salinity) scans.

A series of surfactant solutions of increasing salinity (0, 5, 10, 15 … 30 g NaCl/100 mL) with equal volumes of aqueous and oil phases were prepared. The total surfactant concentration was 10.0 wt% unless otherwise stated. Further adjustments to the salinity scans were introduced (change in salinity step), if needed, to obtain the Type I-III-II transition.

To obtain the Cc of lecithin and linkers, a Type I-III-II transition is necessary to identify the optimal formulation where HLD~0. For most surfactants, including lecithin and linkers, it is not possible to obtain this transition with the surfactant alone. Instead, mixtures of a reference surfactant, that undergoes the transition, and the test surfactant are used[27,40]. For each combination of reference ($C_{8-10}E5$) and test surfactant, salinity scans were conducted. These scans produced a series of optimal salinities (S*, the salinity to obtain optimal μEs) for different molar fractions of

the test surfactant (Y_{test}, on the basis of total moles of test + reference surfactant). As the surfactant formulations are primarily nonionic, the HLD expression for nonionic surfactants (Eq. 2-2) was used to interpret the salinity scans for mixtures of $C_{8-10}E5$ and lecithin and linkers. Zarate-Muños et al. provide a direct expression[40]:

$$\mathbf{Cc_{test} = Cc_{ref} - b\cdot(S^*_{mix}-S^*_{ref})/Y_{test}} \qquad \mathbf{2\text{-}9}$$

where Cc_{test} is the characteristic curvature of the test surfactant (lecithin or linkers), and Cc_{ref} is the corresponding value for the reference surfactant, $C_{8-10}E5$. Cc and "b" for the HLD of $C_{8-10}E5$ formulations (Eq. 2-2) have been found to be -0.96 and 0.12 (for NaCl), respectively[40].

The EACN for ethyl caprate, the oil used in the lecithin-linker formulations, was obtained through a phase scan using only the anionic surfactant SDHS, and ethyl caprate as oil, without cosurfactants, and at room temperature. Using Eq. 2-1 at the optimal formulation (HLD =0):

$$\boldsymbol{EACN = (ln(S^*) + Cc)/k} \qquad \mathbf{2\text{-}10}$$

where Cc_{SDHS}= -0.92, and k_{SDHS} = 0.17[40].

Unless otherwise specified, all the phase scans were conducted at room temperature (T =24±1°C, taken as 25°C for calculation purposes). The optimal formulations in each case were determined by indicating the salinity of the test tube (interpolating if necessary) where equal volumes of the aqueous and the oil phase were solubilized, determined via image analysis of photographs of the phase scans.

2.3.2.1 Lecithin-linkers phase (salinity) scans.

Phase scans were conducted with mixtures of lecithin (surfactant), Peceol (lipophilic linker), and polyglycerol caprylate (hydrophilic linker) using ethyl caparate as the oil phase and an aqueous phase with increasing salinity. To decide the ratio of hydrophilic and lipophilic linkers to lecithin

for the phase scan, it was important to consider that, in addition to increasing the lipophilic and hydrophilic interactions, another reason for adding lipophilic and hydrophilic linkers is to break down the structure of liquid crystal phases produced by the phospholipids in lecithin. Acosta et al. used lipophilic linker/lecithin mass ratio of 1:1, Chu et al. used a ratio close to 2:1, and Yuan et al. used ratios of 3:1 [14,15,16]. These previous studies used sorbitan monooleate as a lipophilic linker. In the case of Peceol (a mixture of glycerol mono and di- oleates), a phase diagram by Mouri et al. also suggests the use of Peceol/lecithin weight ratios of 1:1 or larger [41]. A series of preliminary phase behaviour were conducted with mixtures of Peceol, polyglycerol caprylate, lecithin and water (data not shown). It was confirmed that Peceol/lecithin ratio of 1:1 or higher was required to avoid undesirable gel phases. Furthermore, it was observed that the more polyglycerol caprylate in the formulation, the smaller the liquid crystal region in the ternary phase diagram. Hydrophilic linkers (polyglycerol caprylate in this case) are known to reduce the interfacial rigidity of surfactants adsorbed at the oil/water interface [13]. Based on these observations, three systems were considered: (a) 10-10-80, (b) 15-15-70, and (c) 20-20-60. The first number represents the lecithin weight percent in the mixture with the linkers, the second and third numbers represent the percent of Peceol and polyglycerol caprylate, respectively. Systems with 50.0% or less of polyglycerol caprylate produced stable emulsions and gels.

To prepare the phase scans, 3 ml of the saline solution containing the required salt, 3 ml of ethyl decanoate (oil) and 0.67 g of lecithin+ linkers (density 1.0 g/ml) were vortex-mixed in 2-dram vials at room temperature. The phases were left to equilibrate at room temperature for two weeks before recording the phase volumes.

2.3.3. **Lecithin-linkers pseudo-ternary phase diagram (TPD)**

Stock solutions containing 10.0, 20.0… 90.0 w/w% of ethyl decanoate and the balance in lecithin-linker mixtures were prepared. For each stock solution, dilution lines were prepared to contain 5.0, 10.0…90.0, 95.0 and 99.0 v/v% of fed-state simulated intestinal fluid (FeSSIF). The resulting dilutions were vortex-mixed in 2-dram glass vials until thorough mixing was achieved. Each ternary phase diagram consisted of at least 108 formulation points plus additional points used to refine the phase boundaries. Sample phase behaviour was noted after two weeks. Transparent single phase samples were identified as μEs when (a) an otherwise clear or translucent phase scattered a red (650nm) laser beam, (b) the sample did not separate upon centrifugation, (c) the sample did not display gel-like behavior (the liquid flows immediately after turning the vial upside down), (d) the vial did not show birefringence when observing the vial through two polarized light filters positioned at 90°. Liquid crystal phases were identified when birefringence was observed. The observed phases were plotted on a pseudo-ternary phase diagram, with the three axes representing FeSSIF, oil and the lecithin-linker mixture.

Electrical Conductivity measurement:

The conductivity of single phase μEs was measured using a VWR conductivity meter (MODEL 4175) equipped with a conductivity microelectrode (Microelectrodes Inc., Bedford, NH, USA).

2.3.3.1 Viscosity

A Carri-Med CSL2 Rheometer (TA Instruments, New Castle, DE, USA) was used to measure the viscosity of SMEDS dilutions (microemulsion). A 4cm parallel-plate geometry with 60 μm gap was used. The temperature was controlled via Peltier Plate to 25°C. The measurements were

conducted in flow mode, with shear rates ranging from 0.1-100 1/s. Over this range the formulas showed a Newtonian profile, hence the average reading was used as the viscosity of the sample.

2.3.3.2 Particle size determination

Brookhaven (Holtsville, NY, USA) BI90 PLUS Particle Size Analyser was used to measure the average droplet size. Four ml of diluted SMEDS were poured into clear cuvettes and placed in the sample chamber. The temperature was set at 25 °C. The scattering angle was 90˚. Laser wavelength was 635 nm and viscosity of the dispersion was set to that obtained above. The mean of five measurements for each dilution was reported.

2.3.3.3 Surface tension

To determine the surface area per unit of a molecule of polyglycerol caprylate the surface tension isotherm was obtained for this surfactant using a KSV Sigma 701 (Espoo, Finland) tensiometer equipped with a Wilhelmy plate (wetting depth 6 mm, thickness 0.1 mm and plate width 10.6mm). The test was conducted at room temperature polyglycerol caprylate concentrations ranging from 10^{-6} to 10^{-2} M. The Gibbs adsorption isotherm for nonionic surfactants was used to calculate the area per molecule using surface tension values below the CMC, as reported elsewhere [42].

2.4. Results and Discussion

2.4.1. HLD parameters for lecithin-linker formulations.

Figure 2-2 presents the optimal salinities of mixtures of the test surfactant (lecithin or linkers) and the reference surfactant $C_{8-10}E5$, as a function of the molar fraction of the test surfactant in the mixture with $C_{8-10}E5$ (Y_{test}). Dodecane was used as the oil phase to determine the Cc of lecithin

(Figure 2-2a), decalin was used to determine the Cc of Peceol (Figure 2-2b), and cyclohexane was used to determine the Cc of polyglycerol caprylate (Figure 2-2c). As predicted by Eq. 2-9, the plots in Figure 2-2 produce straight lines. The slope of the trend lines in Figure 2-2 is equivalent to the term $(S^*_{mix}-S^*_{ref})/Y_{test}$ in Eq. 2-9. Table 2-2 presents a summary of the values of Cc obtained using Eq. 2-9 and the values of the slopes of Figure 2-2.

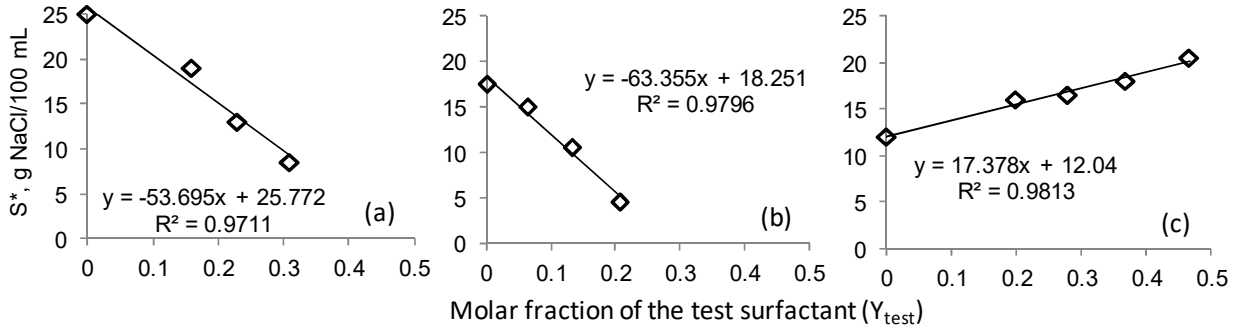

Figure 2-2. Optimal salinities (S*) obtained after conducting phase scans (oil:aqueous phase volume ratio 1:1, 10 wt% total surfactant in aqueous phase, varying salinity, keeping the molar fraction of test surfactant Y_{test}, in mixture with the reference surfactant, constant) in mixtures of reference surfactant $C_{8\text{-}10}E5$ with (a) lecithin using dodecane as oil (b) Peceol using decalin as the oil phase, and (c) polyglycerol caprylate using cyclohexane as the oil phase.

Table 2-2: HLD parameters for lecithin-linker microemulsions.

	Lecithin	**Peceol**	**Polyglycerol caprylate**
MW (g/mol)	750[14]	452[a]	593[b]
Area per molecule, a_s (Å^2/molecule)	90[c]	0[d]	65[e]
Characteristic curvature, Cc	5.5	6.6	-3.0

Notes: (a) Estimated from reported composition [41]. (b) Based on the nominal $C_{26}H_{57}O_{14}$ structure. (c) reported by Acosta et al. [14]. (d) Negligible for lipophilic linkers, according to neutron scattering studies [29]. (e) calculated from the surface tension isotherm (data not shown).

The characteristic curvature of lecithin (Cc=5.5) in Table 2-2 is higher than the value Cc=4 reported by the 30-day challenge consortium[43]. These values are comparable considering that the error associated with the measurement of Cc through the mixed-reference system can be as high

as 25.0% of the value of the calculated Cc [40], and the fact that soybean "lecithin" is a by-product fraction from processing soybeans, thus subject to variability in its composition.

The characteristic curvatures of Peceol and polyglycerol caprylate in Table 2-2 cannot be compared to other values in the literature as it is the first time these values are measured. A Cc value of +6.6, for Peceol, is one of the most positive values reported thus far, and reflects the more lipophilic nature of this linker. The Cc=-3.0 value obtained for the hydrophilic linker, polyglycerol caprylate is consistent with the Cc values reported for other hydrophilic linkers[27].

The EACN of ethyl caprate was determined via a salinity phase scan using the anionic surfactant sodium dihexyl sulfosuccinate (SDHS), following Zarate et al[40]. The value of EACN can be obtained directly from the salinity at optimal formulation (S* = 6.0 g NaCl/100 ml for this system, where the solubilization capacity of oil and water match, at a level of 2 ml/g SDHS), and Eq. 2-10. Following this procedure, $EACN_{ethyl\ caprylate}$ was calculated as 5.1.

2.4.2. HLD-NAC predictions for lecithin-linker phase scans.

The procedures to calculate solubilization capacities and phase volumes via HLD-NAC can be found elsewhere [28,29,30,37]. The calculations proceed in three parts, for negative HLDs the solubilization of oil was approximated to R_o = -L/HLD, for positive HLDs the solubilization of water is R_w = L/HLD. For near zero HLDs, then Eq. 2-5 through 2-8 are combined:

$$\mathbf{R_o = 1/(1/\xi - HLD/2L)} \qquad \mathbf{2\text{-}11}$$

$$\mathbf{R_w = 1/(1/\xi + HLD/2L)} \qquad \mathbf{2\text{-}12}$$

For the lecithin-linker system, we do not know the value of length parameter L. The value of L can be fitted using solubilization data[28]. In this case, the lecithin-linker salinity phase scan conducted with the 15-15-70 system was used to fit the value of L.

Eq. 2-2 is used to calculate the HLD for each test tube of the lecithin-linker salinity scan; $HLD=0.12\cdot(S)-0.16\cdot 5.1+(x_{lecthin}\cdot(5.5)+x_{Peceol}\cdot(6.6)+x_{polygly.cap.}\cdot(-3.0))$, where S is the salinity (g NaCl/100 ml) and x_i is the molar fraction of the surfactant + linker mixture. The temperature was neglected because the scan was at~ 24°C. No cosolvent was used.

Using HLD-NAC values of R_o and/or R_w, and the interfacial area, A_S, the volume of the dispersed phase (oil or water) solubilized can be calculated using Eq. 2-3. The interfacial area A_S was calculated using Eq.2-4, the surfactant area (a_S) from Table 2-2, and the moles of surfactant added into the system. For the 15-15-70 formulation, L and ξ were fitted to minimize the error between the HLD-NAC calculated and experimental phase volumes [28,36]. Figure 2-3 shows this fit.

.

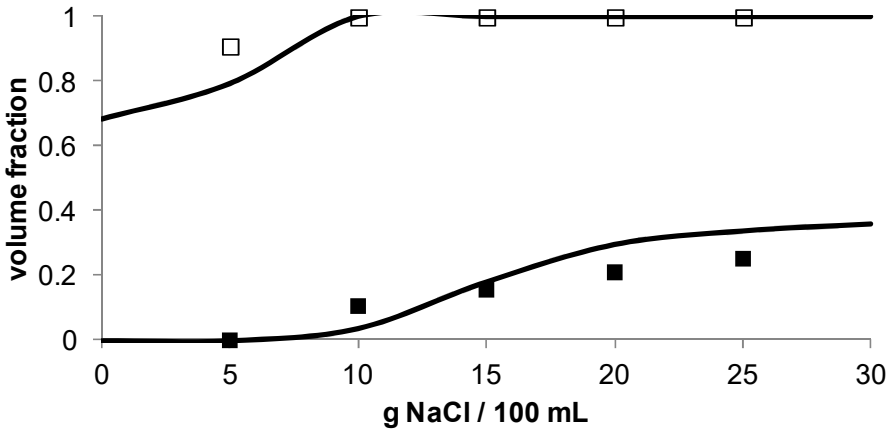

Figure 2-3. Relative phase volumes obtained for the salinity scan (ethyl caprate: saline volume ratio 1:1, 10 v/v% lecithin+linkers in the system, varying salinity) of the system with a mass ratio of 15 lecithin : 15 peceol : 70 polyglycerol caprylate (15-15-70). The solid line represents HLD-NAC phase volumes obtained after fitting Eq. 2-11 and 2-12 using L= 90Å and ξ = 230 Å.

The phase transition observed in Figure 2-3 (between 5 and 15 g NaCl/100 ml), was fully predicted by the HLD. The values of L and ξ used in the NAC framework were fitted to minimize the error between the experimental and NAC-predicted phase volumes. The value of ξ = 230 Å is consistent

with values reported for lecithin-linker systems[14]. The value of L= 90Å cannot be compared to other values because it is the first time that the HLD is properly calculated for lecithin-linker systems, but it is substantially larger than values reported for other surfactants[29]. The large value of L indicates that lecithin is highly effective at solubilizing oil and water in the microemulsion. A large value of L could also mean that there is a significant amount of palisade layer solubilization, which was not considered in the calculation of R_o and R_w [28].

Using the fitted values of L and ξ, complete HLD-NAC predictions of phase scans were produced for systems 10-10-80 and 20-20-60. Figure 2-4 summarizes these predictions. The fully-predicted phase volumes presented in Figure 2-4 are, for the most part, consistent with the experimental observations. The largest deviations are observed with the 10-10-80 formulation where the I-III transition was predicted to occur at 15 g NaCl/100 ml by the HLD-NAC, whereas the actual transition occurred at 20 g NaCl/100 ml. In HLD units, this represents a deviation of $b \cdot |S_{\text{I-III exp}} - S_{\text{I-III act}}| \sim 0.6$ units. This deviation is within the magnitude of deviations expected for the Cc of the test surfactant. Even with the deviation observed, the HLD and HLD-NAC predictions produce a close estimation of the real phase behaviour.

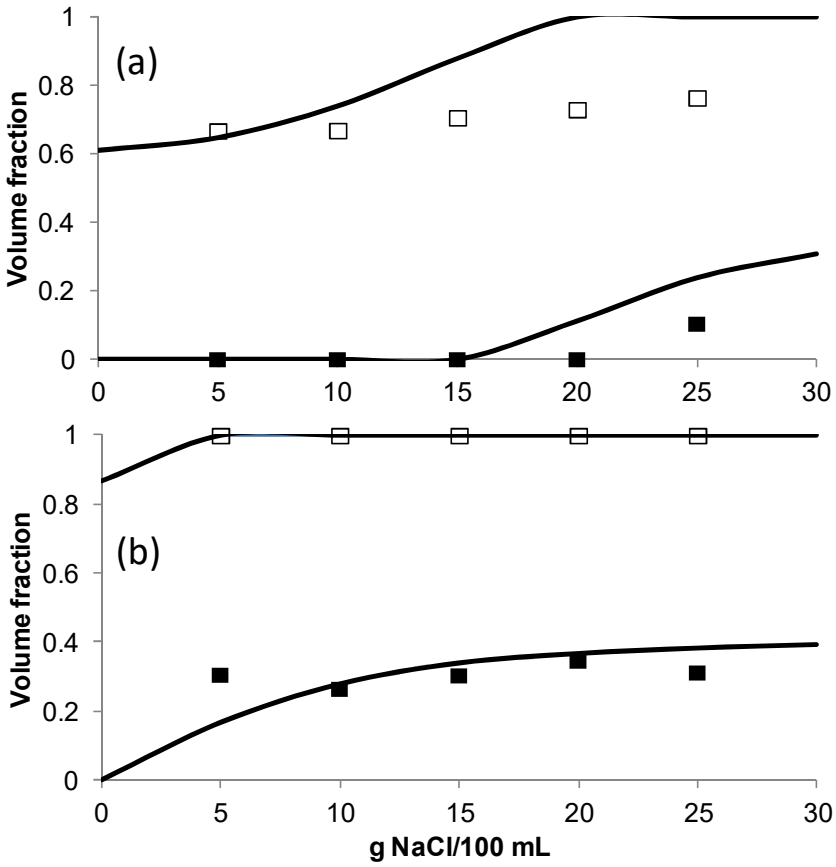

Figure 2-4. Relative phase volumes obtained for the salinity scans (same conditions of Figure 2-3) for the systems with mass ratio of 10-10-80 (a) and 20-20-60 (b). The solid lines represent predicted HLD-NAC phase volumes obtained using L= 90Å and ξ = 230 Å in Eq. 2-11 and 2-12.

2.4.3. HLD-NAC predictions of solubilization features of ternary phase diagrams.

There are two fundamental issues with the HLD concept, the first is that HLD was developed for oil/water ratios close to 1, and the second is that the surfactant concentration is not considered. The HLD-NAC, on the other hand, is influenced by the surfactant concentration and oil/water ratio via the calculations of R_o and R_w (Eq. 2-3). In the case of near-zero HLDs, the values of Ro and Rw are calculated using the net and average curvature (Eq. 2-11 and 2-12). However, for negative

HLDs, Eq. 2-12 produces large or even negative values of R_w, and for positive HLDs, Eq. 2-11 produces large values or even negative values of R_o. What this means is that for negative HLDs, not close to zero, water is a continuous phase, and the value of R_w can be assumed to be large enough where $1/R_w \sim 0$, and simply, $R_o = -L/HLD$. Similarly, for positive HLDs, not close to zero, oil is a continuous environment and R_o is assumed to be large enough such that $1/Ro \sim 0$, and Rw = L/HLD. These two extreme assumptions will be valid for as long as the surfactant concentration in the continuous phase is low enough to for its volume to be negligible in relation to the volume of the continuous phase.

For extreme oil to water ratios, the HLD-predicted continuous phase may be in conflict with water or oil availability. If the water content is too small, a water-continuous environment (predicted by a negative HLD) is not physically possible. In that case, the net and average curvatures (Eq. 2-5 and 2-6), independent of HLD, can be used to shed light on the issue. Kiran and Acosta introduced the physical interpretations of the net and average curvatures[32]:

$$\mathbf{H_n/2 = [2/(L_d + 2R_d)] + [(L_d/R_d)/(2L_d + 4R_d)]} \qquad \mathbf{2\text{-}13}$$

$$\mathbf{H_{avg} = (6L_d + 12R_d)/(9L_d \cdot R_d + 12R_d^2)} \qquad \mathbf{2\text{-}14}$$

where L_d is the length of the cylindrical portion, and R_d is the radius of the oil-swollen micelle. For a given combination of surfactant, oil, and water in a single phase system, the values of R_o and R_w can be calculated using Eq. 2-3. Using Eq. 2-5 and 2-6 one obtains H_n and H_{avg}. Then, Eq. 2-13 and 2-14 are used to calculate L_d and R_d for oil-swollen micelles or water-swollen reverse micelles.

When oil is the discontinuous phase, R_o is calculated using Eq. 2-3. For the radius of the continuous phase (R_{ws} in this case), we added the volume of water and surfactant as they are the continuous phase. This was important because otherwise Eq. 2-13 and 2-14 produced nonsensical predictions of L_d and R_d at high surfactant concentrations. Previous works on HLD-NAC, up to this point, have neglected the surfactant volume and its contribution to the net and average curvature terms; producing relatively accurate predictions because they considered systems where the surfactant concentration is low enough to neglect its volume [27,28,29,32]. Khorsandi and Johns realized this limitation and introduced the notion that half of the surfactant volume as contributing to the dispersed phase volume, and a half to the continuous phase volume [37].

In this work, we consider that the volume of the surfactant is part of the continuous phase. Using this assumption, the values of R_d and L_d were calculated using Eq. 2-13 and 2-14. A similar procedure can be used when water is the discontinuous phase.

Figure 2-5 presents the ratios of L_d/R_d as a function of the fraction of a dispersed oil phase. According to Figure 2-5, the length of the μE droplets tends to approach infinity when the volume fraction of the dispersed phase approaches 12.5 v/v%. This substantial increase in length coincides with the formation of bicontinuous systems[32]. This means that when the water content in the system is less than 12.5%, even if the HLD is negative then there is not enough water to form a water-continuous system as water has to be in the form of discontinued drops.

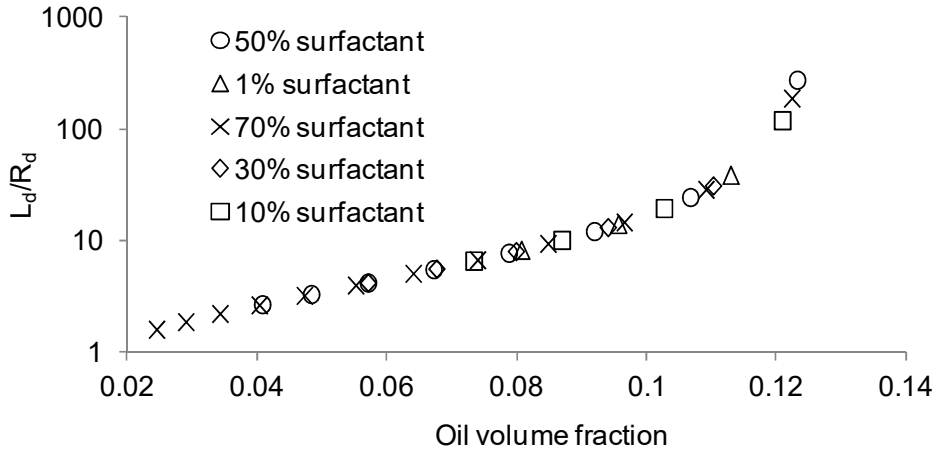

Figure 2-5. Length to radius ratio of oil-swollen micelles, from Eq. 2-13 and 2-14, using H_n and H_{avg} from Eq. 2-5 and 2-6, R_o from Eq. 2-3 and $R_{ws} = 3(V_s/A_S)/\phi_{s\_ws}$. V_s/A_S is the surfactant volume to interfacial area ratio; ϕ_{s_ws} is the surfactant volume fraction in water + surfactant continuum. Vs/As=17Å, but other Vs/As values produce the same curve. The surfactant concentration is in volume percentage. The same curve can be produced with water as dispersed phase.

The items described earlier help us construct a predicted ternary phase diagram, at least its solubilization features. The ternary diagram of interest is that produced with the lecithin-linker mixtures discussed earlier, ethyl caprate as oil, and FeSSIF as the aqueous phase. FeSSIF contains sodium chloride, but it also contains sodium acetate and sodium taurocholate (Table 2-1). The total sodium content in FeSSIF is 219 mM. If that sodium only came from sodium chloride, this would represent the equivalent salinity (S) =1.3 g NaCl/100 ml.

For the system 15-15-70, (Cc = -0.30, S=1.3, EACN =5.1) the HLD is -0.96 (Eq. 2-2), and using the dilute surfactant assumption, R_o = -L/HLD = 94 Å. The oil/surfactant volume ratio for solubilization is (Vo/Vs) = (Ro/3)/(V_s/A_S). For the 15-15-70 system, V_s/A_S = 17.6 Å. The minimum surfactant volume fraction for solubilization (Φ_{Smin}) can be calculated as:

$$\Phi_{Smin} = 1/(1+Vo/Vs) \qquad 2\text{-}15$$

For the 15-15-70 system, the Φ_{Smin} for a fully dilutable μE is 36.0% of the surfactants (lecithin+linkers) in SMEDS (oil+lecithin+linker). According to the simplified HLD-NAC method to estimate the 2-phase boundary, a constant solubilization line is drawn from the FeSSIF vertex to Φ_{Smin} on the oil+surfactant side. The boundary ends at the water discontinuity line (12.5% water) because beyond that point water exist in water-swollen reverse micelles. Any system below the boundary is assumed to produce a μE on the constant solubility line and a pure excess oil phase, as illustrated by the tie lines in Figure 2-6. This simple method uses the dilute surfactant assumption, introduced in Abbott's apps, and used by Jin et al., except that their solubilization line ended at the catastrophic inversion point [33,34,35].

Considering the surfactant volume (V_s) as part of the continuum, the solubilization radius of the continuum (for negative HLD) is $R_{ws} = 3(V_w+V_s)/A_s = 3\cdot(V_s/A_s)/\phi_{s\_ws}$, where ϕ_{s_ws} is the surfactant volume fraction in the water + surfactant continuum. Considering H_n and its relation to HLD (Eq. 2-5 and 2-7), $1/R_{o\_ws}=1/R_{ws}$ - HLD/L, where R_{o_ws} is the oil solubilization radius in a water + surfactant continuum. To produce the phase boundary one would set a value of ϕ_{s_ws}, then R_{o_ws} = - HLD/L+$3\cdot(V_s/A_s)/\phi_{s\_ws}$, and then use R_{o_ws} to find $\phi_{s\_os} =1/[1+(R_{o\_ws}/3)/(V_s/A_S)]$, where ϕ_{s_os} is surfactant volume fraction in the oil + surfactant axis. A point in the TPD is located using ϕ_{s_ws}, ϕ_{s_os}, as illustrated in Figure 2-6. For positive HLDs, the procedure is similar only that the continuum is the oil + surfactant mixture. For systems with HLD close to zero, R_o and R_w are calculated using Eq. 2-11 and 2-12, and then corrected for surfactant continuity (radii R_{o_ws} and R_{w_os}) using the net curvature: $1/R_{o\_ws} -1/R_{w\_ws} = 1/R_o-1/R_w$, and $1/R_{o\_os} -1/R_{w\_os} = 1/R_o-1/R_w$. Figure 2-6 presents the predicted solubilization boundaries using the simple method (H_n and $1/R_w\sim$ 0), and the method including surfactant continuum (H_n and R_{ws}).

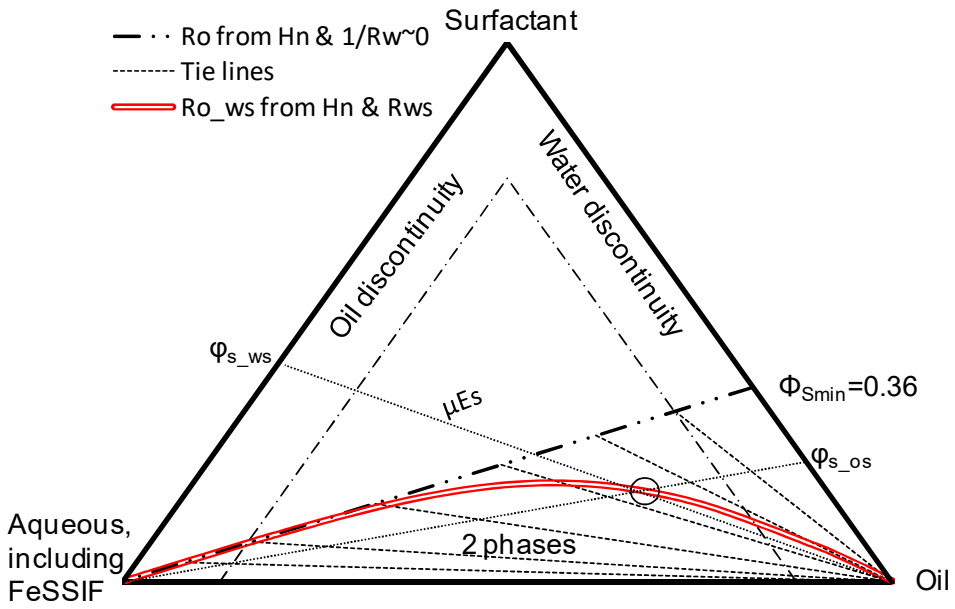

Figure 2-6. Volume-base ternary phase diagram (TPD) for the system 15-15-70 lecithin-Peceol-polyglycerol caprylate, predicted using the simple (R_o) and surfactant continuum (R_{o_ws}) HLD-NAC methods. The "μE" label represent single phase microemulsion regions.

To compare the accuracy of the simple and the surfactant continuum methods, Figure 2-7a presents the phase diagram obtained experimentally for the system 15-15-70. One notes that at the bottom of Figure 2-7a there is a 2-phase region of μEs coexisting with an excess oil phase. This feature was fully predicted by the simple and surfactant continuum HLD-NAC methods. However, the surfactant continuum reproduces the overall shape of the 2-phase region and the top of the 2-phase region. The simple and the surfactant continuum methods converge for $\phi_{s\_ws}<0.20$, which is when the low concentration assumption of the simple method is valid. Furthermore, a tangent to the 2-phase region reveals that a Φ_{Smin} of 37.0% in a mixture with the oil is required to guarantee a fully dilutable formulation. This threshold is consistent with the predicted value of 36.0% in Figure

2-6, and illustrated by the dashed lines in Figure 2-7a also includes pictures of preconcentrate vials of lecithin-linker + ethyl caprate systems diluted with FeSSIF. One aspect that is not predicted by the HLD-NAC is the presence of liquid crystal phases, which can be found experimentally as illustrated in Figure 2-7a. A region of liquid crystal (LC) is observed in the region close to the surfactant + water side of the triangle. A large portion of this LC region seems to be dominated by a Lamellar (L_α) phase as samples from this region display a luminous Maltese cross pattern when the vial is observed under polarized light microscopy. The appearance of L_α phases is common for lecithin-based formulations [44,45].

To avoid potential issues when passing through liquid crystals (viscous or gel-like phases), it is best to use the space between the bottom 2-phase region and the liquid crystal region to design fully-dilutable μEs. Figure 2-7b presents the vials obtained via dilution of a preconcentrate containing 50.0 v/v% of the lecithin+linker mixture and 50.0 v/v% oil. As illustrated in Figure 2-7b, there is no phase separation obtained throughout this dilution process, but it is clear that large changes in drop size are obtained near 70.0 to 80.0% FeSSIF as evidenced by the increase in light scattering obtained in these vials.

A similar procedure to that used for the system 15-15-70 (Figure 2-6) was used for the system 10-10-80, which also has a negative HLD (HLD= -1.85). For the system 20-20-60, the HLD was -0.05. In that case, Eq. 2-11 and 2-12 were solved for R_o and R_w, and the simple and surfactant continuum methods were used as described earlier. Figure 2-8 presents an overlay of the HLD-NAC predictions on top of the experimental phase diagrams obtained with the systems 10-10-80 and 20-20-60.

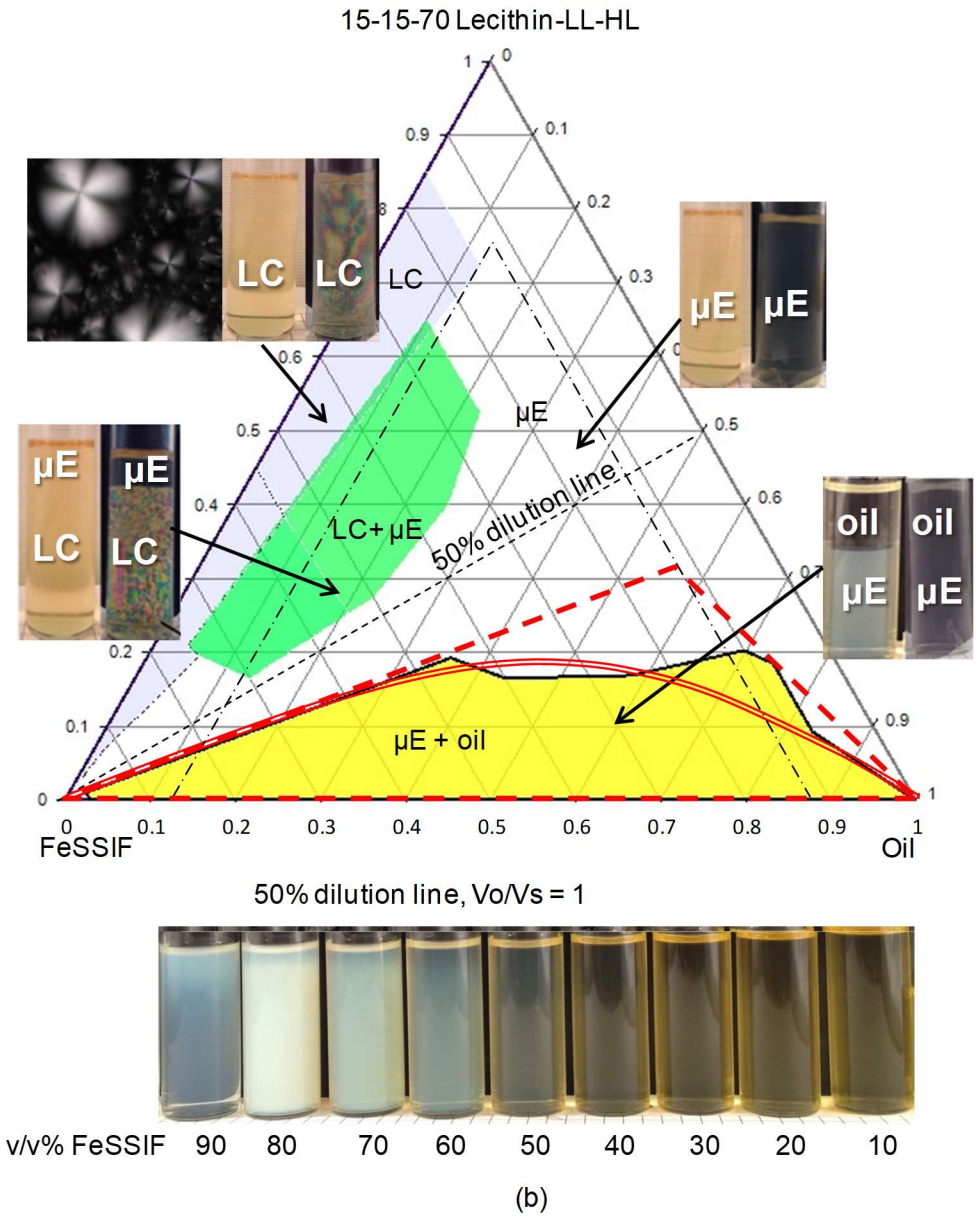

Figure 2-7. (a) Volume-based TPD for the system 15-15-70 lecithin-Peceol-polyglycerol caprylate. The pictures indicate example vials. The vial on the right was taken through crossed polarizers. The dashed line boundary corresponds to the μE+oil phase boundary predicted by the simple HLD-NAC method. The double line boundary was produced with the surfactant continuum HLD-NAC method. The coloured region at the bottom of the diagram corresponds to the experimentally-determined 2-phase region of co-existence of μE + excess oil phase. (b) Vials obtained at different FeSSIF content, along the D50 (50.0% surfactant) dilution line. The uncolored area, labelled as "μE", represent single phase microemulsions.

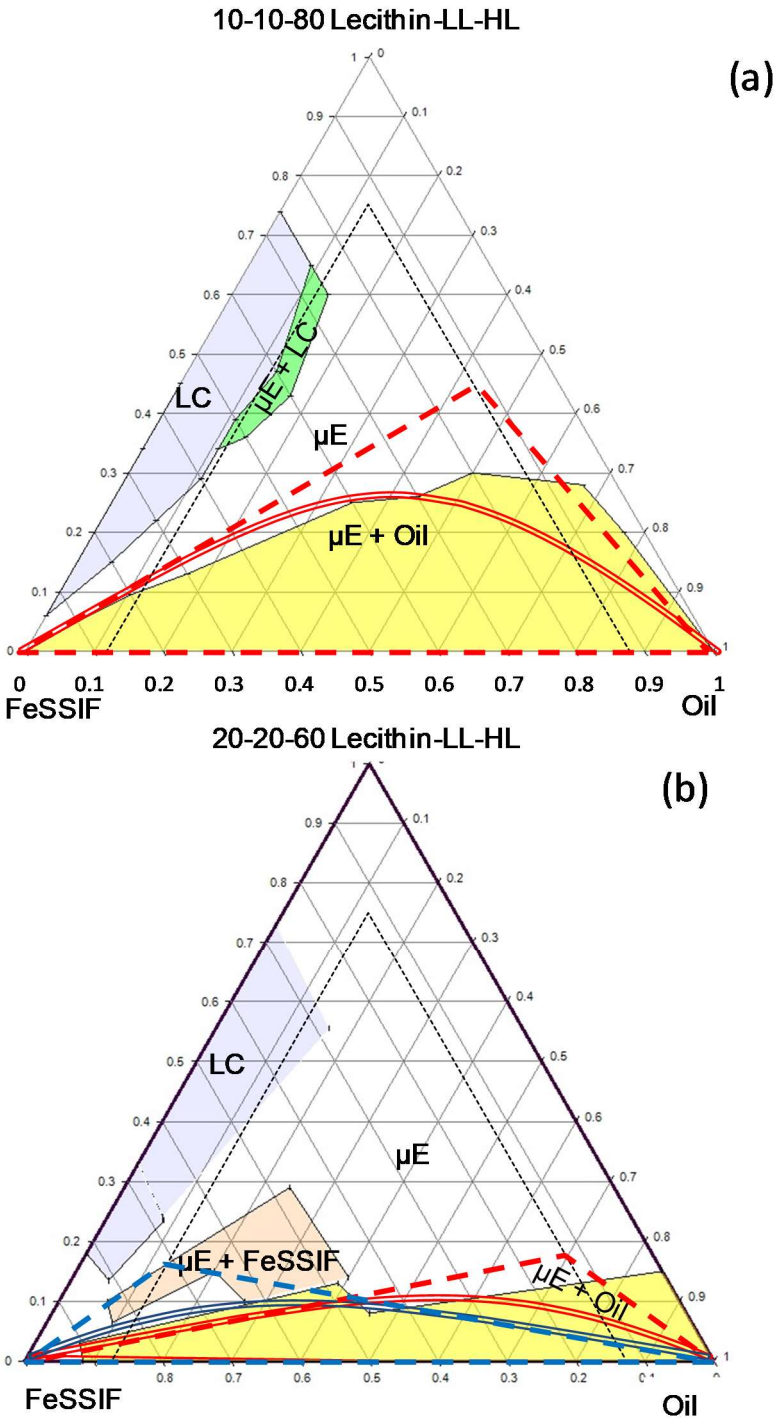

Figure 2-8. Volume-based TPDs for the systems (a) 10-10-80 and (b) 20-20-60 lecithin-Peceol-polyglycerol caprylate. The dashed line boundaries correspond to the μE+oil (red) or μE+FeSSIF (blue) phase boundary predicted by the simple HLD-NAC method. The double line boundaries were produced with the surfactant continuum HLD-NAC method. The uncolored area, labelled as "μE", represent single phase microemulsions.

For the 10-10-80 formulation, the experimental data in Figure 2-8a indicates that a Φ_{Smin} of 46.0% in the preconcentrate is necessary to obtain a fully dilutable μE, whereas the HLD-NAC predicts Φ_{Smin} 50.9%. This discrepancy is to be expected given the less accurate HLD-NAC predictions of the 10-10-80 phase scan. The simple HLD-NAC method produces substantial over-prediction of the size of the 2-phase region while the surfactant continuum method produces a more accurate prediction, but still under-predicts the size of the 2-phase region near the water discontinuity region. For the 20-20-60 system, the HLD-NAC (simple and surfactant continuum version) predicts the existence of two multiphase regions, which is consistent with the experimental observations in Figure 2-8b. The size of the region of μE + excess FeSSIF was under-predicted by the simple and the surfactant continuum method. Furthermore, we could not observe vials with three-phase systems in the bottom of the ternary diagram, as predicted by the HLD-NAC methods. This is perhaps, due to linker partition issues[13].

For the 10-10-80 and the 15-15-70 system, one observes that the HLD-NAC triangle produced with the simple method over-predicts the size of the 2-phase region, while the surfactant continuum method tends to under-predict the size of the 2-phase region towards the discontinuity lines. The over-prediction of the simple method can be traced back to neglecting the contribution of the surfactant towards the continuous phase volume. The underprediction of the simple method may be associated with not considering that a fraction of the surfactant volume could be part of the dispersed phase volume. On top of these issues, there is the entropic cost of forming a concentrated surfactant phase in equilibrium with an almost surfactant-free oil phase. This entropy contribution is best captured by activity coefficient models, however, the use of these models for microemulsions remains challenging [46]. Monte Carlo models can handle mixing entropy and self-assembly behaviour but can only reproduce the behaviour of idealized systems[47]. Phenomenological models based on Helfrich's curvature model can explain, and predict some of

the features of ternary phase diagrams, but they require knowledge of the spontaneous curvature and bending moduli of the surfactant-oil-water system, which is not readily available [44,48]. Although the HLD-NAC predictions are not completely accurate, they are the only predictive method available that uses input information that can be readily obtained via simple phase scan experiments. The predictions are meant to guide the design of delivery systems or other products and processes that make use of ternary phase diagram information from surfactant-oil-water systems.

To further evaluate the predictive capacity of the HLD-NAC, we proceeded to consider the system of lecithin-cyclohexane-water studied by Angelico et al. at 25°C in the absence of electrolytes[44]. For this system, Cc =5.5 (lecithin only), EACN= 3 for cyclohexane[40], and S =0 (no electrolyte), yielding an HLD = 5.02. For lecithin alone, Vs/As = 14.2Å (calculated using Table 2-2 data for lecithin, and a density of 1 g/ml). With this information and the simple and surfactant continuum method introduced earlier, the 2-phase μE + excess water region can be predicted. Figure 2-9 presents a comparison of the HLD-NAC predictions and the experimental observations of Angelico et al. The simple and surfactant continuum methods do reproduce μE + water phase boundary, and the surfactant continuum method is capable of approximating the LC+ water boundary up to the oil discontinuous region, even though the LC existence cannot be predicted by the HLD-NAC.

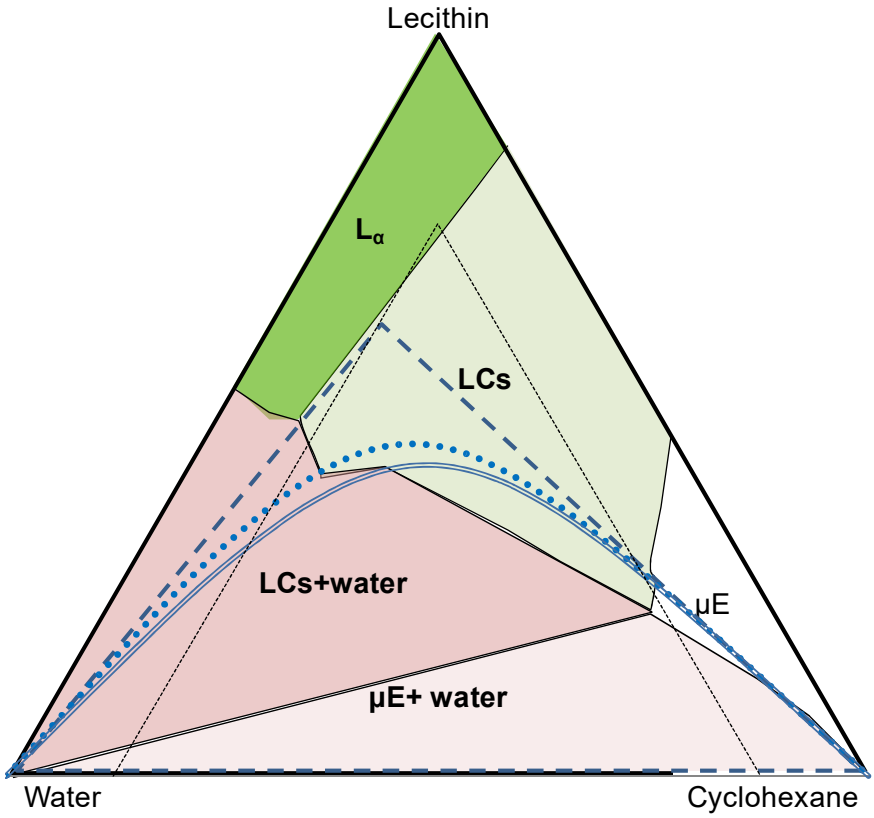

Figure 2-9. TPD for lecithin-cyclohexane-water. The dashed line boundary corresponds to the μE + water phase boundary (volume-based) predicted by the simple HLD-NAC method. The double line boundary (volume-based) and dotted line (mass-based) were produced with the surfactant continuum HLD-NAC method. The shaded areas were determined experimentally (mass-based) by Angelico et al.[44]. The LC region contains various liquid crystalline phases, except for L_α.

2.4.4. HLD-NAC predicted changes in μE properties along a dilution line.

The NAC predictions in Figure 2-5 and Figure 2-6, regarding oil and water discontinuity along a dilution line, suggest that not all Type I μEs are oil-swollen micelles, and by similar reasoning, not all Type II μEs are water-swollen reverse micelles. A confirmation of this prediction would mean that it is necessary to revise the definitions of Type I and Type II μEs in large portions of the

existing literature, including our previous work, that link Type I μEs to oil-swollen micelles and Type II μEs to water-swollen reverse micelles. According to the NAC predictions, those links would only be correct at low volume fractions (less than 12.5%) of the disperse phase.

To explore the question of phase continuity in fully dilutable systems, as well as the properties of μEs along a dilution line, systems with 50.0 v/v% surfactant (as preconcentrate mixed with oil, also known as D50 systems) for the 10-10-80 and 15-15-70 formulations were characterized as a function of FeSSIF content. This characterization included electrical conductivity, hydrodynamic radius via dynamic light scattering, and low shear viscosity.

Figure 2-10a shows the conductivity of the samples as a function of the FeSSIF content. The data is presented in logarithmic scale to show the large changes in conductivities that take place between 10.0 and 20.0% FeSSIF. Changes of similar magnitude were observed by Cabino et al, who suggested that the transition from oil-continuous to bicontinuous occurs at a volume fraction of approximately 14.0% [49]. This fraction is comparable to the fraction predicted by the NAC model of 12.5% (from Figure 2-5). Similar conductivity measurements by Wang et al. showed two marked transition points, one close to 15.0-20.0% water (oil continuous-bicontinuous), and another at 65.0-70.0% water (bicontinuous-water continuous) when diluting μEs containing approximately 70.0% surfactant 30.0% oil (D70 systems) [50]. Similar transitions points have been reported by Lidich et al. for the dilutions of a D80 system1. Fisher et al. reported similar limits for the dilution of a D90 system [51]. Kalaitzaki et al. suggested transition points of 20.0% and 80.0% water for the dilution of a D64 system[3].

Figure 2-10b presents the change in hydrodynamic radius (obtained via DLS) as a function of FeSSIF content. Closer to 10.0% and 80.0% FeSSIF we see large increases in drop size, and the lowest values are obtained closer to the 20.0-40.0% FeSSIF content for both, the 10-10-80 and 15-

15-70 formulations. Since these systems are all single-phase systems with a known volume of oil (V_o), water (V_w) and surfactant (V_S, thus $A_S = V_S/(V_S/A_S)$), it is possible to calculate R_o and R_w using Eq. 2-3. When ϕ_w<0.125 (the discontinuity line), the volume of oil plus surfactant becomes the continuous phase and one calculates R_{o_os} and R_{w_os}. Similarly, when When ϕ_O<0.125, surfactant + water is the continuous phase, and one calculates R_{w_ws} and R_{o_ws}. With these radii, one can calculate H_n, H_{avg}. Using these curvatures and Eq. 2-13 and 2-14, one calculates the real drop radius (R_d) and length (L_d). The hydrodynamic radius can be estimated as $R_h = R_d + L_d/2$+ surfactant tail length (~ 25Å). The values of V_s/A_s are 16.7Å for 10-10-80 and 17.6 Å for 15-15-70. The solid line of NAC-predicted size in Figure 2-10b was calculated using an intermediate value of V_s/A_s = 17 Å. The NAC calculations produce negative L_d values between 12.5% and 75.0% FeSSIF, suggesting that in that range the system becomes bicontinuous. The NAC values (solid line in Figure 2-10b) in between 12.5% and 75.0% FeSSIF do not correspond to R_h, but instead to the inverse of the average curvature, which is the characteristic length for those systems. The DLS-obtained size for bicontinuous systems is not a hydrodynamic radius, but it has been proposed to represent the characteristic length of the microemulsion[49]. That view is supported by the data and NAC predictions in Figure 2-10b.

The experimental values of relative viscosities in Figure 2-10c were calculated as the ratio between the measured viscosity and the ideal mixture viscosity obtained from the Arrhenius equation. The Arrhenius mixing rule indicates that $\ln(\eta_{mixture}) = \phi_1\ln(\eta_1) + \phi_2\ln(\eta_2)$ [52]. For both formulations, the viscosity of pure FeSSIF, η_2= 1 mPa·s. For the 10-10-80 system η_1 = 122 mPa·s , and for 15-15-70, η_1 = 150 mPa·s. The solid line represents the predicted relative viscosity (η_r) using the dilute rigid rods model used by Kiran et al.[32]:

$$\eta_r = 1 + \frac{{L_d}^2}{\pi {R_d}^2}\phi_{disp} \qquad \textbf{2-16}$$

The dilute rigid rods model above tends to overpredict the viscosities for η_r values greater than 2, which is consistent with the data in Figure 2-10c. However, the NAC-predicted trend explains that as L_d grows towards the oil discontinuity limit, the viscosity tends to increase. Once the system breaks into a bicontinuous system, this trend breaks down. Thus far, there is no model to predict the viscosity of the bicontinuous system.

While the visual inspection of the vials in Figure 2-7b, and the experimental data in Figure 2-10b and 10c clearly show substantial transitions near 70.0-80.0% FeSSIF, there is very little evidence of change in the 10-20% FeSSIF region, with the exception of the conductivity changes. The relatively high surfactant content in the 10.0-20.0% FeSSIF region reduced the drop size of the μE and its potential effect on μE viscosity.

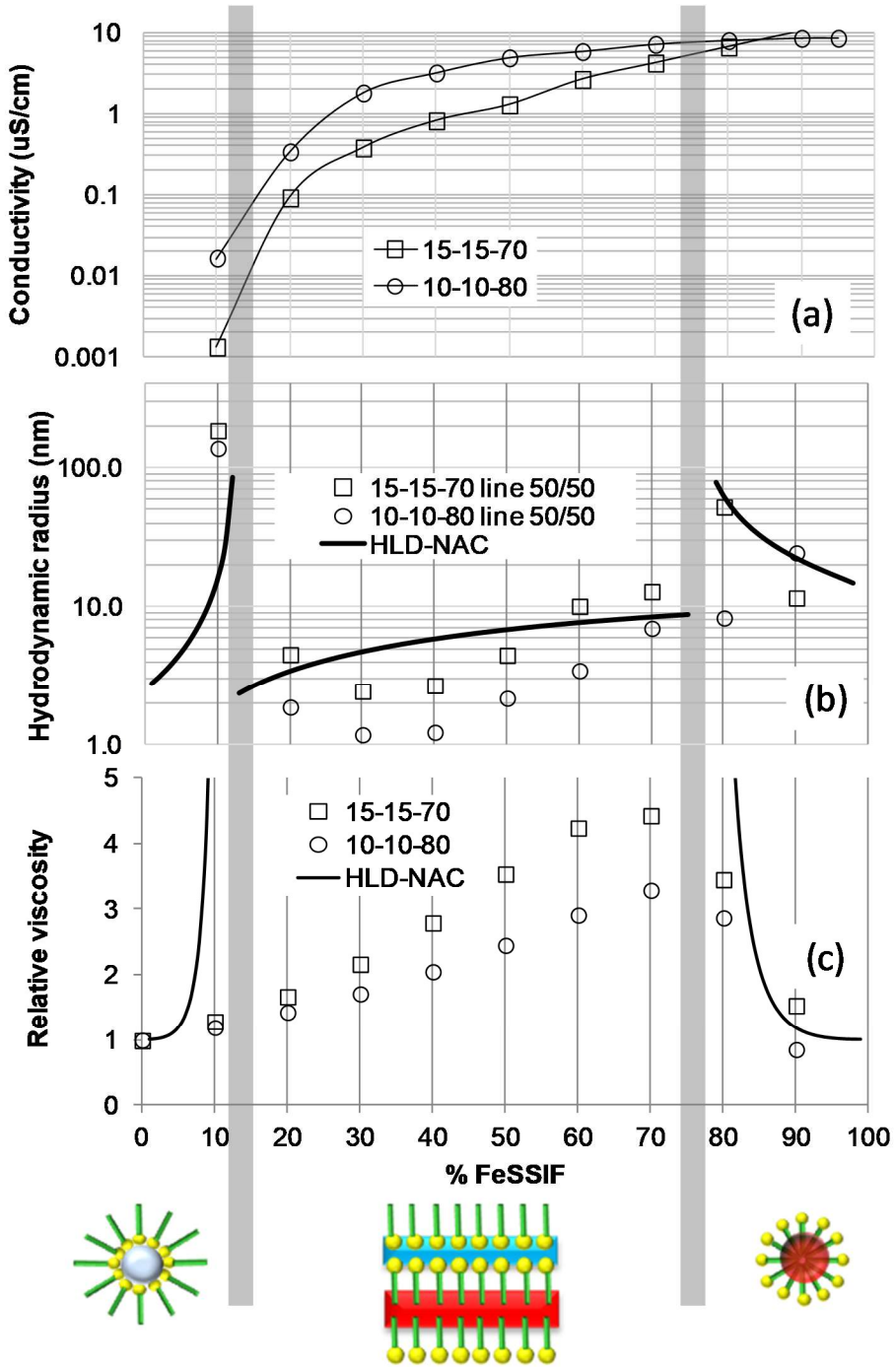

Figure 2-10. Conductivity, hydrodynamic radius (from dynamic light scattering), and the relative viscosity measured at low shear (<100s^{-1}) for the D50 (50.0% surfactant 50.0% oil) line of systems 10-10-80 and 15-15-70 (lecithin-Peceol-polyglycerol caprylate) as a function of FeSSIF content. The dark solid lines represent the values predicted using the HLD-NAC model.

2.5. Conclusions

Constructing an accurate ternary phase diagram (TPD) is a resource-intensive process. To produce fully dilutable μEs we need to know the region occupied by the multiphase phase region, and the minimum surfactant volume fraction in the oil + surfactant mixture (ϕ_{Smin}) required to avoid that region upon dilution with the aqueous phase. Using the HLD-NAC framework, as illustrated in the four cases discussed in this work, one can obtain a conservative estimation of ϕ_{Smin}, suitable for the design of SMEDS, particularly, lecithin-linker SMEDS.

This work introduces a stepwise approach to obtain the necessary HLD (Cc, EACN) and NAC parameters (L, ξ) from phase scans for multi-component lecithin linker μEs, and the use of these parameters in models used to predict TPD solubilization boundaries.

The HLD-NAC is currently the benchmark model for equations of state for surfactant-oil-water systems [18,46,53]. This work explains the assumptions used in a simplified HLD-NAC construction of TPDs used to illustrate the connection between HLD and TPD, and in reservoir simulators of enhanced oil recovery (EOR) [33,34,35]. This work also introduces a new surfactant continuum approach to predict solubilization phase boundaries of TPDs.

The potential applications of predicting solubilization feature of TPDs go well beyond the design of SMEDS. Khorsandi and Johns introduced, and highlighted the importance of, fitted continuous TPD boundaries for reservoir simulations of enhanced oil recovery [36,37,54]. The HLD-NAC surfactant continuum method fully predicts this boundary(ies) with reasonable accuracy.

The surfactant continuum NAC in this work predicts discontinuity limits (~12.5 vol% of the internal phase), which improves over the previous empirical catastrophic phase inversion, and

explains the experimental observations in dilutable μEs 1[,49,50,51]. These predicted limits were consistent with literature observations, and with measurements of conductivity, hydrodynamic radius, and viscosity of diluted μEs. The NAC method introduced in this work also clarifies the effect of surfactant/water/oil ratio on the type of μEs produced.

Future work should consider in more detail the fraction of the surfactant volume that contributes to the continuous phase and to the dispersed phase of the μE, in addition to considerations of entropy and surfactant solubility and partition in the aqueous and oil phases. The use of the surfactant-continuum HLD-NAC for other SOW systems should also be explored.

2.6. References

[1] N. Lidich, E. Wachtel, A. Aserin, N. Garti. Water-dilutable microemulsions for transepithelial ocular delivery of riboflavin phosphate. *J. Colloid Interface Sci.* 2016, 463, 342-8.

[2] J. Marcus, S. Wolfrum, D. Touraud, W. Kunz. Influence of high intensity sweeteners and sugar alcohols on a beverage microemulsion. *J. Colloid Interface Sci.* 2015, 460, 105-12.

[3] A. Kalaitzaki, A. Xenakis, V. Papadimitriou. Highly water dilutable microemulsions: a structural study. *Colloid Polym Sci.* 2015, 193, 1111-9.

[4] M. Klossek, J. Marcus, D. Touraud, W. Kunz. Highly water dilutable green microemulsions. *Colloids Surf. A.* 2014, 442, 105-10.

[5] H. Zhang, Y. Shen, P. Weng, G. Zhao, F. Feng, X. Zheng. Antimicrobial activity of a food-grade fully dilutable microemulsion against Escherichia coli and Staphylococcus aureus. *Int J Food Microbiol.* 2009, 135, 211-5.

[6] P. Balakrishnan, B. Lee, D. Oh, J. Kim, M. Hong. Enhanced oral bioavailability of dexibuprofen by novel solid self-emulsifying drug delivery system. *Eur J. Pharm. Biopharm.* 2009, 72, 539-45.

[7] D. McClements. Nanoemulsions versus microemulsions: terminology, differences, and similarities. *Soft Matter.* 2012, 8, 1719-29.

[8] D. Shah, R. Bagwe, J. Kanicky, B. Palla, P. Patanjali. Improved drug delivery using microemulsions: Rationale, recent progress, and new horizons. *Crit Rev Ther Drug Carrier Syst.* 2001,18, 77-140.

[9] N. Garti , I. Yuli-Amar. Micro- and nano-emulsions for delivery of functional food ingredients. In: Garti N, editor. Delivery and controlled release of bioactives in foods and nutraceuticals. *Woodhead Publishing Limited*; 2008. p. 149–84.

[10] B. Paul, S. Moulik. Uses and applications of microemulsions. *Curr Sci.* 2001, 80, 990-1001.

[11] J. Lawrence. Nanoparticulates As Drug Carriers. In: V. P. Torchilin, editor. Nanoparticulates As Drug Carriers. London: Imperial College Press; 2006.

[12] J. Flanagan, H. Singh. Recent advances in delivery of food-derived bioactives and drugs using microemulsios. In: Mozafari MR, editor. Nanocarrier Technologies: frontiers of nanotherapy. Springer Netherlands; 2006.

[13] D. Sabatini, E. Acosta, J. Harwell. Linker molecules in surfactant mixtures. *Curr Opin Colloid Interface Sci.* 2003,8, 316-26.

[14] E. Acosta, T. Nguyen, A. Witthayapanyanon, J. Harwell, D. Sabatini. Linker-based bio-compatible microemulsions. *Environ Sci Technol.* 2005, 39, 1275-82.

[15] J. Chu, Y-L Cheng, A. Rao, M. Nouraei, S. Zarate-Muñoz, E. Acosta. Lecithin-linker formulations for self-emulsifying delivery of nutraceuticals. *Int J. Pharm.* 2014, 471, 92–102.

[16] E. Acosta, O. Chung, X. Xuan. Lecithin-linker microemulsions in transdermal delivery. *J Drug Deliv Sci Technol.* 2011, 21, 77-87.

[17] P. Gao. Design and Development of Self-Emulsifying Lipid Formulations for Improving Oral Bioavailability of Poorly Water-Soluble and Lipophilic Drugs. In: Williams III RO, Watts AB, Miller D., editors. Formulating Poorly Water Soluble Drugs. Springer N. Y.; 2012. p. 243–66.

[18] A. Boza Troncoso, E. Acosta. Integrated Free Energy Model (IFEM) for microemulsions. *J. Colloid Interface Sci.* 2016, 466, 400-412.

[19] H. Paroor. *Microemulsion: Prediction of the Phase diagram with a modified Helfrich free energy*. Ph.D. Dissertation. Johannes Gutenberg University, Mainz, Germany, 2012.

[20] F. García-Sánchez, G. Eliosa-Jiménez, A. Salas-Padrón, O. Hernández-Garduza, D. Ápam-Martínez. Modeling of microemulsion phase diagrams from excess Gibbs energy models. *Chem Eng J.* 2001, 84, 257-74.

[21] S.V. Patel, S. Patel. Prediction of the solubility in lipidic solvent mixture. *Eur. J. Pharm. Sci.* 2015, 77, 161-9.

[22] R. Nagarajan, E. Ruckenstein. Molecular Theory of Microemulsions. *Langmuir*. 2000, 16, 6400-15.

[23] L. Djekic, S. Ibric, M. Primorac. The application of artificial neural networks in the prediction of microemulsion phase boundaries in PEG-8 caprylic/capric glycerides based systems. *Int J Pharm.* 2008, 361, 41-6.

[24] N. Marasini, T. Tran, B. Poudel, H-G Choi, C.Yong, J. Kim. Statistical modeling, optimization and characterization of spray-dried solid self-microemulsifying drug delivery system using design of experiments. *Chem. Pharm. Bull.* 2013, 61, 184-93.

[25] J-L Salager, R. Anton, D. Sabatini, J. Harwell, E. Acosta, L. Tolosa. Enhancing solubilization in microemulsions—State of the art and current trends. *J Surfactants Deterg.* 2005, 8, 3-21.

[26] V. Nardello, N. Chailloux, J. Poprawski, J-L Salager, J-M. Aubry. HLD concept as a tool for the characterization of cosmetic hydrocarbon oils,. Polym Int. 2003, 52, 602-9.

[27] E. Acosta, J. Yuan, A. Bhakta. The Characteristic Curvature of Ionic Surfactants. *J Surfactants Deterg.* 2008, 11, 145-58.

[28] E. Acosta, E. Szekeres, D. Sabatini, J. Harwell. Supersolubilization in Surfactant Microemulsions. *Langmuir*. 2003, 38, 186-95.

[29] E. Acosta. *Modelling and Formulation of Microemulsions: The Net-Average Curvature Model and the Combined Linker Effect.* Ph.D. dissertation. University of Oklahoma, Oklahoma, 2004.

[30] E. Acosta. The HLD–NAC equation of state for microemulsions formulated with nonionic alcohol ethoxylate and alkylphenol ethoxylate surfactants. *Colloids Surf. A.* 2008, 320,193-204.

[31] E. Acosta, E. Szekeres, J. Harwell, B. Grady, D. Sabatini. Morphology of ionic microemulsions: comparison of SANS studies and the net-average curvature (NAC) model. *Soft Matter.* 2009, 5, 551-61.

[32] S. Kiran, E. Acosta. Predicting the Morphology and Viscosity of Microemulsions Using the HLD-NAC Model. *Ind Eng Chem Res.* 2010, 49, 3424-32.

[33] Abbott, S. *Surfactant Science: Principles and Practice.* Ipswhich, UK (v.1.03). [Web 25 Jan. 2017]. Available from: http://www.stevenabbott.co.uk/practical-surfactants/the-book.php.

[34] L. Jin, Z. Li, A. Jamili, H. Luo, M. Delshad, J. Lu, B. Shiau, J. Harwell, Z. Rui. Development of a Chemical Flood Simulator Based on Predictive HLD-NAC Equation of State for Surfactant. *SPE – Annual Technical Conference Proceedings*, Dubai, Sept. 2016.

[35] L. Jin, A. Jamili, Z Li, J. Lu, H. Luo, B. Shiau, M. Delshad, J. Harwell. Physics based HLD-NAC phase behavior model for surfactant/crude oil/brine systems. *J. Petroleum Sci. Eng.* 2015, 136, 68-77.

[36] S. Ghosh, R. Johns. Dimensionless Equation of State to Predict Microemulsion Phase Behavior. *Langmuir*. 2016, 32, 8969-8979.

[37] S. Khorsandi, R. Johns. Robust Flash Calculation Algorithm for Microemulsion Phase Behavior. *J. Surfactants Deterg.* 2016, 19, 1273-1287.

[38] Ghosh, S. and Johns, R. T. An Equation-of-State Model to Predict Surfactant/Oil/Brine-Phase Behavior. SPE J. SPE-170927-PA. http://dx.doi.org/10.2118/170927-PA, 19 January, 2016.

[39] M. Marques. Dissolution Media Simulating Fasted and Fed States. *Dissolution Technol*. 2004, 11, 16.

[40] S. Zarate-Muñoz, F. Texeira de Vasconcelos, K. Myint-Myat, J. Minchom , E. Acosta. Simplified Methodology to Measure the Characteristic Curvature (Cc) of Alkyl Ethoxylate Nonionic Surfactants. *J Surfactants Deterg.* 2016, 19, 249-63.

[41] A. Mouri, O. Diat, A. El Ghzaoui, I. Ly,C. Dorandeu, J. Maurel. Development of pharmaceutical clear gel based on Peceol®, lecithin, ethanol and water: Physicochemical characterization and stability study. *J Colloid Interface Sci.* 2015, 457, 152-61.

[42] M.J. Rosen. *Surfactants and Interfacial Phenomena.* Hoboken, N.J. (3rd ed.), Wiley-Interscience, New York.(2004).

[43] The 30 day Formulation Challenge Project. Speeding up the transition to greener surfactants [Web 25 Jan. 2017]. Available from: http://vlci.biz/wp-content/uploads/2017/01/Speeding-up-the-transition-to-greener-surfactant.pdf

[44] R. Angelico, A. Ceglie, U. Olsson, G. Palazzo. Phase diagram and phase properties of the system lecithin-water-cyclohexane. *Langmuir.* 2000, 16, 2124-32.

[45] P. Petrov, S. Miklavcic, U. Olsson, H. Wennerstroem. A Confined Complex Liquid: Oscillatory Forces and Lamellae Formation from an L3 Phase. *Langmuir.* 1995,11, 3928-36.

[46] C. Browarzik , D. Browarzik, J. Winkelmann. Modeling of the three-phase equilibrium in systems of the type water + nonionic surfactant + alkane. *Fluid Phase Equilib.* 1010,296, 82-7.

[47] A. Mackie, K. Onur, A. Panagiotopoulos. Phase equilibria of a lattice model for an oil-water-amphiphile mixture. *J Chem Phys*. 1996, 104, 3718-25.

[48] S. Safran, L. Turkevich. Phase diagrams for microemulsions. *Phys Rev Lett*.1983, 50, 1930-3.

[49] F. Caboi, G. Capuzzi, P. Baglioni, M. Monduzzi. Microstructure of Ca-AOT/water/decane w/o microemulsions. *J. Phys. Chem. B.* 1997, 101, 10205-12.

[50] W. Wang, H. Wei, Z. Du, X. Tai, G. Wang. Formation and characterization of fully dilutable microemulsion with fatty acid methyl esters. *ACS Sustain. Chem. Eng.* 2015, 3, 443-50.

[51] S. Fisher, E. Wachtel, A. Aserin, N. Garti. Solubilization of simvastatin and phytosterols in a dilutable microemulsion system. *Colloids Surf. B.* 2013, 107, 35-42.

[52] J. Kendall, A. Wright. The viscosity of liquids. IV. Ideal mixtures of the types ether-ether and ester-ester. *J Am Chem Soc.* 1920, 42, 1776-84.

[53] J . Fraaije, K. Tandon, S. Jain, J-W. Handgraaf, M. Buijse. Method of moments for computational microemulsion analysis and prediction in tertiary oil recovery. *Langmuir*. 2013, 29, 2136-2151.

[54] Khorsandi, S., Qiao, C., & Johns, R. T. Simulation of Surfactant/Polymer Floods With a Predictive and Robust Microemulsion Flash Calculation. *SPE J.* 2016, doi:10.2118/179566-PA

Chapter 3. Design and in vivo Evaluation of an Ibuprofen-loaded Lecithin Linker Self Micro-Emulsifying Delivery System (SMEDS)

3.1. Abstract

A lecithin-linker microemulsion has been used as a platform for designing fully dilutable self-microemulsifying delivery system (SMEDS). This SMEDS formulation was composed of ethyl caprate, lecithin, glycerol monooleate (lipophilic linker, LL) and polyglycerol caprylate (hydrophilic linker, HL) and displayed a fully dilutable path suitable for drug delivery. Introducing ibuprofen as a model active pharmaceutical ingredient (API), resulted in phase behaviour changes that induced a phase separation along the dilution line. To address this issue, the Hydrophilic-Lipophilic Difference (HLD) framework was used to quantify the effect of ibuprofen on the phase behaviour of the formulation. It was determined that introducing ibuprofen produces a positive (lipophilic) HLD shift. The HLD framework was then used to identify an alternative hydrophilic linker and the proportions of LL:Lecithin:HL to restore the fully dilutable path with simulated intestinal fluid (SIF). To evaluate the uptake of ibuprofen in the formulation, the ibuprofen-loaded SMEDS, and suspended ibuprofen in water were administered to male rats at a dose of 25 mg/kg body weight. Plasma concentration profiles showed a higher absorption in SMEDS when compared to the control. The SMEDS formula also increased the circulation time above the therapeutic limit (10 μg/mL plasma). The results of this study suggest that the HLD is a useful tool to quantify the impact of drug-formulation interaction and identify the necessary changes to restore the formulation. A properly designed fully dilutable lecithin linker SMEDS not only improve drug absorption but also increases its circulation time.

3.2. Introduction

Low aqueous solubility is the most common factor limiting the absorption of a wide range of drugs and nutraceuticals [1] Lipid-based delivery systems (LBDS), such as microemulsions (μE) and self-microemulsifying delivery systems (SMEDS) have effectively been used to enhance the solubility and increase the bioavailability of these substances. SMEDS are a water-free mixture of oils and surfactants- including cosurfactant/cosolvents/linkers- that upon exposure to the aqueous phase and with mild agitation spontaneously form microemulsion droplets with a size range of 10-100 nm [2,3]. The distinctive features of SMEDS are high drug solubilization capacity and the ability to transition from water-free pre-concentrate to water-in-oil (w/o) μEs to bicontinuous (BC) μEs to oil-in-water (o/w) μEs upon exposure to gastrointestinal (GI) fluids without phase separation. SMEDS differ from self-emulsifying delivery systems (SEDS) in terms of composition, droplet size, thermodynamic stability and performance [4]. Compared to μEs, the lack of water in SMEDS formulation promotes the stability of both the drug and the formulation against chemical and biological degradation of APIs [5]. This compact pre-concentrate system makes packaging, storage and transportation more affordable.

A review of the formulated SMEDS reveals that the oil phase of SMEDS is generally composed of medium/long chain tri/diglycerides and their derivatives, essential oils or ethyl ester of fatty acids [6]. The surfactants used in SMEDS formulations are typically non-ionic amphiphilic compounds with large head groups and medium-chain fatty acid tail. They include polyoxyl glycerides, ethoxylated glycerides, and esters of polyglycerols, propylene glycol and polyethylene glycol. Cremophor (polyethoxylated hydrogenated castor oil) is the most common surfactant. The data shows that using a single surfactant does not lead to a dilutable formulation and a mixture of surfactants and cosolvents (short chain alcohols) are required to balance the

hydrophilicity/lipophilicity of the system and enhance the solubilization [7,8]. However, some surfactants cause adverse effects such as irritating the GI mucosa, undesirable interactions with other excipients and instability of the oils and the drug [9].

Multiple mechanisms have been proposed on how SMEDS improve the bioavailability of poorly soluble drugs. SMEDS not only improve the solubilization of the drug but also enhances membrane fluidity, opening of tight junctions between the epithelial cells and increasing lymphatic transport system [10,11,12,13,14]. Lymphatic absorption through chylomicrons has gained attention since it avoids first-pass metabolism by the liver [15]. SMEDS formulations have been examined for various hydrophobic drugs in parenteral, dermal and transdermal applications, but the majority of the work has examined the oral administration of poorly soluble drugs [16].

A new era started in drug delivery when Novartis marketed Neoral®, a SMEDS formulation loaded with cyclosporine A (CyA). Numerous comparative clinical studies showed superiority of Neoral® in reducing the time to reach peak blood concentration (T_{max}) and increasing peak blood concentration (C_{max}) and area under the curve (AUC), indicating a faster and greater uptake of the drug [17,18]. Following the success of SMEDS for pharmaceuticals, the application of SMEDS was extended to the delivery of nutraceuticals. There are many reports in the literature showing the effectiveness of μE-based systems for improving the absorption of poorly soluble nutraceuticals such as curcumin [19,20,21], CoQ10 [22,23] or vitamins A and D [24]. However, most of the formulations have used ethoxylated surfactants and alcohols.

The increased in bioavailability of lipophilic drugs by SMEDS is attributed to different mechanisms such as a) prolongation of gastrointestinal residence time, solubilizing the drug, increased intestinal wall permeability and enhance trans-cellular absorption, Overcoming the unstirred water layer barrier, inhibiting efflux pump activity and reducing enterocyte-based

metabolism[25],[26],[27],[28],[29],[30],[31]. Stimulation of lymphatic transport is also plays an important role. This pathway increases the bioavailability by eliminating first-pass metabolism in liver. A recent in vivo study, when the chylomicron flow of lymphatic system was blocked, the bioavailability of the drug (in terms of AUC) dropped by 27% [32]. O'Driscoll has reported that the contribution of lymphatic transport for LBDS could reach up to 50% [33]. In an in vivo experiment, Iwanaga et al.[34] showed that in loaded microemulsions, partitioning of drug in the intestinal cells to the lymphatic system is independent of the chain length of the oil component of microemulsions and concluded that the mechanism of bioavailability enhancement with microemulsions is different from that of emulsions. One of the most intriguing questions regarding the process of vehicle transport is whether the microemulsion systems are interacting with the naturally occurring bile salt mixed micelles (BSMM). The in-vitro experiments show that the interaction between microemulsion (μE) micelles and BSMM results in formation of a new complex micellar system (μE-BSMM) with different properties [35] .

Despite their effectiveness in increasing the solubility of poorly soluble ingredients, there are numerous challenges in formulating SMEDS that limit their widespread use [36]. Formulating fully dilutable μEs – so-called U-type microemulsion [37,38] - is challenging particularly for food systems since the choices of surfactants and carrier oils are limited. Nonionic and zwitterionic surfactants (such as polyglycerol esters of fatty acids and phospholipids) are preferred since they are more biocompatible [39]. However, formulating dilutable SMEDS using these surfactants is not a simple task. Phase behaviour upon dilution, droplet size and drug solubilization/loading capacity are among the questions the formulator needs to consider. Constructing ternary phase diagrams (TPDs) can answer these questions. However, mapping detailed TPDs is a time-consuming process.

In ternary surfactant-oil-water (SOW) systems, various multi-phase systems may be formed. Phase continuity over dilution (full dilutability) is a key factor in designing SMEDS. This could be achieved by balancing the oil: surfactant ratio in a way that the pre-concentrate undergoes the transition (W/O→BC → O/W) without phase separation. Graphically, this is the case in a ternary phase diagram where the dilution line does not cross the multiphase region. Any point on oil-surfactant axe contains no water and represent a potential SMEDS formulation. The dilution line in a ternary phase diagram connects the oil-surfactant axe to the water vertex (red lines in Figure 3-1). Each point on the dilution line –regardless of water content – has a constant ratio of surfactant to oil. In Figure 3-1, any dilution line below D50 crosses the two-phase (μE + oil) region in which phase separation occurs and is not fully dilutable and therefore not a SMEDS. In a ternary phase diagram, the surfactant-water axis often contains liquid crystals (LC) as illustrated in Figure 3-1. The area in between the LC and multiphase region (oil+μE) is of particular interest. Therefore, there is a fixed area with optimum oil: surfactant ratio where infinite dilution is possible. In Figure 3-1, only the formulations with a surfactant: oil ratio of 70:30 to 50:50 (denoted as D70 and D50) form fully dilutable μE, and hence they can correctly be named as SMEDS. The challenge in designing a SMEDS is finding the appropriate formulations that produces a phase behaviour with a fully dilutable path.

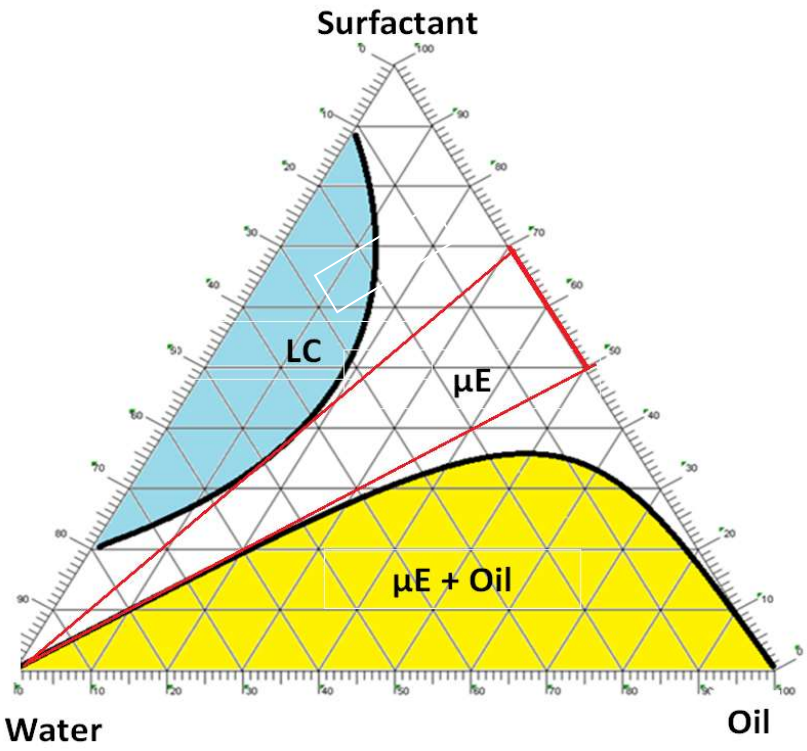

Figure 3-1: A schematic ternary phase diagram showing 2-phase system of microemulsion and oil, single-phase fully dilutable microemulsion, and liquid crystal regions. The red lines represent the extreme dilution lines (D70 and D50).

Lecithin-based formulations are desirable in formulating food-grade delivery vehicles since lecithin has a GRAS status and is approved for food and drug use. However, the lecithin molecule is too lipophilic and its critical packing parameter (CPP) is relatively high (0.8), which promotes the formation of structures like lamella and other liquid-crystal phases. [40,41]. Therefore, additives are needed to adjust the system. Cosurfactants, such as medium molecular weight alcohols make the interface more flexible, however, most medium chain alcohols such as butanol and pentanol can dissolve cell membranes or may cause allergic reactions [42]. Hydrophilic and lipophilic linkers are suitable alternatives to resolve these issues. Linkers are amphiphilic surfactant-like additives that modify the interfacial properties of microemulsion systems to facilitate the co-solubilization of oil and water[43]. Hydrophilic linkers (HL), having a large hydrophilic polar head group and a short carbon tail, enhance the interaction between the surfactant layer and the aqueous phase, and

increase the interfacial area. Lipophilic linkers (LL), on the other hand, typically with twelve or more carbons in their alkyl chain and relatively small polar head group segregate near the tails of the surfactants; improving the interaction between the surfactant and the oil [44]. Mixtures of HL and LL can replace cosurfactants/cosolvents in microemulsion formulations [45] and serve as potential safe excipient for designing delivery system for drugs and nutraceuticals. Accordingly, we have developed a number of lecithin linker microemulsions as delivery systems for oral[46]and transdermal [47,48,49]administration of drugs and nutraceuticals.

This project builds on the concept of linker-based μEs to design a platform for self-micro emulsifying delivery system (SMEDS) that can be engineered according to the active pharmaceutical ingredient (API) of interest.

The conventional approach to find a fully dilutable system is based on constructing ternary phase diagrams for each formulation. Using the Hydrophilic-Lipophilic Difference–Net Average Curvature (HLD-NAC) model, Nouraei and Acosta proposed a methodology to optimize the formulations and predict the minimum oil-surfactant ratio beyond which a fully dilutable path is obtained [50]. The original objective of this work was to evaluate the *in vivo* performance of lecithin linker SMEDS loaded with ibuprofen. However, as it will be explained later, the introduction of ibuprofen changed the SMEDS phase behaviour upon dilution. While the unloaded SMEDS of Nouraei & Acosta [50] was fully dilutable, loading even 1%wt of ibuprofen resulted in phase separation during dilution. Ibuprofen is a nonsteroidal anti-inflammatory drug (NSAID) with a LogP of 3.97 and pKa of 4.5and contains a benzene and carboxylic acid group, as illustrated in Figure 3-2.

It is well-known that the drug-formulation interactions can cause changes in the physicochemical properties of diluted formulations including electrical conductivity, pH and viscosity[51,52,53,54,55].

However, the effect of drug loading on phase behaviour upon dilution and the shape of TPDs is not amply discussed in the literature and requires further investigation. Pestana compared the ternary phase diagrams for loaded and unloaded lecithin/tween 80 μEs showing that the addition of amphotericin significantly expands the emulsion region at the expense of the μE region[56]. We have already reported that loading a lecithin linker SMEDS formulation with β-sitosterol at 3% level diminishes the microemulsion region in the ternary phase diagram [46]. It is reported that loading curcumin in SMEDS reduces the single-phase self-emulsifying region in ternary phase diagrams[21]. Balakrishnan also reported that increasing drug loading reduces self-emulsification region and efficiency of the self-emulsification process[57].

There is also a gap in the literature in identifying strategies to restore the fully dilutable μE region after drug loading. The first step in any reformulation is quantifying the change due to drug loading. Currently there is not a comprehensive methodology to quantify the impact of drug loading. Consequently, the current practice for restoring the formulation to a fully dilutable state is trial and error. In this work, we introduce a mathematical approach to reformulate the system and correct for the effect of drug loading.

Incorporating an API to the formulation influences the hydrophilicity-lipophilicity of the system and therefore the critical questions to be answered are a) how to quantify the shift in hydrophilicity-lipophilicity and b) how to adjust the ratios of the components within surfactant mixture as well as oil: surfactant ratio to compensate for the change. This work is an attempt to answer these critical questions. Since the phase behaviour of the original platform formulation was explained and predicted by HLD-NAC framework, it was hypothesized that the model can also be used to quantify the drug-SMEDS interaction and to predict the required changes to restore the phase behaviour. HLD is an equation that correlates the formulation variables (oil polarity, surfactant

hydrophilicity) and field variables (temperature and salinity) with phase behaviour. For a non-ionic surfactant system, the equation is [50]:

$$\boldsymbol{HLD = b * (S) - k * EACN + Cc + c_T(T - 25) + f(A)} \quad \textbf{(3-1)}$$

Where "S" is the electrolyte concentration (g NaCl/100 ml), "EACN" is the equivalent alkane carbon number; "Cc" is the characteristic curvature of the surfactant, "T" is the temperature of the system (˚C), "f (A)" is a function of alcohol or cosolvents concentration. Finally, K, c_T, and b are empirical constants for a given system[58].A hydrophilic (or lipophilic) system has a negative (or positive) HLD values and generates O/W (or W/O) microemulsions with excess oil (or water). When HLD approaches zero, a bicontinuous microemulsion is formed. In this work, we applied the HLD concept to quantify the shift in hydrophilicity of the system and to predict the required changes in the formulation to compensate for the effect of loading ibuprofen and restore the fully dilutable path. Then, *in vivo* oral bioavailability studies were performed to investigate the role of SMEDS in ibuprofen uptake.

3.3. Materials and Methods

3.3.1. Materials

SMEDS components included ethyl decanoate, (≥98%, FCC, FG) purchased from Sigma - Aldrich (Oakville, ON,Canada), L-alpha-lecithin, granular (technical grade, from soybean oil) obtained from Acros Organics (NJ– USA), polyglyceryl-6-caprylate (Dermofeel® G6CY, 100%) and hexaglycerol Caprylate (Caprol® 6GC8, 100%) were donated by Kinetik Technologies (Morris, NJ, USA) and ABITEC Corporation (OH, USA), respectively. Glycerol monooleate (Peceol™) was a gift from Gattefossé (Etobicoke, ON, Canada). Glacial acetic acid (ACS, ≥99.7%) dipotassium monohydrogen phosphate anhydrous (>95%), phosphoric acid, glacial acetic acid

(ACS, ≥99.7%) were purchased from Fisher Scientific Canada (Markham, ON, Canada). Sodium chloride (>99.0%), and sodium hydroxide (ACS reagent grade) were purchased from Bioshop® Canada. Sodium taurocholate hydrate ≥97.0% (TLC), (S)-(+)-Ibuprofen (ReagentPlus®, 99%), flufenamic acid (analytical standard), sodium taurocholate hydrate (≥97.0%), and cyclohexane (ACS reagent, ≥99.5%) were purchased from Sigma Aldrich Canada. Acetonitrile (HPLC grade) and phosphoric acid (85%) were purchased from Caledon (Georgetown, ON, Canada). Octyl-decyl pentaethylene glycol (C8–10E5, DehydolR OD5®, 100% active) was a gift from BASF(Wyandotte, MI, USA) and was used as a reference surfactant in salinity scans.

3.3.2. Methods

HPLC system: High-performance liquid chromatographic system (PerkinElmer, USA), equipped with an autosampler and Shimadzu UV–visible detector (Model—SPD 10A), was used for the analysis. Twenty µL of samples were fractionated on C18, 4µ column (L 150mm, ID 4.6mm) and their absorbance was registered at λ=222 nm.

Preparation of mobile phase: The method introduced by Jahan et al was adopted and modified[59]. Briefly, 1.75 g of potassium phosphate dibasic (K_2HPO_4) was dissolved in 900mL of deionized water. The pH was adjusted to 6.85 with phosphoric acid, followed by the addition of water to a final volume of 1L. This pH was selected to be at least two units above the pKa of the drug. For ibuprofen, pKa is reported to range from 4.42 to 4.85[60]. The pump was adjusted to mix the buffer and acetonitrile at a ratio of 55:45, v/v, with a flow rate of 0.7 mL/ min.

HPLC standards and plasma samples: A stock solution of ibuprofen in acetonitrile were made with a concentration of 10,000 ppm. Fifty µL of this stock solution was added to 950 µL blank plasma to make 1 ml of stock plasma (500 ppm ibuprofen). The stock plasma was used to

make standard plasma concentrations. For the HPLC analysis, 50 µL of plasma and standard samples were diluted with 150 µL acetonitrile and then spiked with 50 µL Flufenamic acid solution in acetonitrile as internal standard. The samples were vortexed, centrifuged (10000 rpm, 5 min) and the supernatant was filtered using 0.2 µm syringe microfilter. Twenty µL of the filtrate was injected to HPLC.The ratio of ibuprofen AUC to the flufenamic acid AUC was calculated for each standard to construct standard curve and calculate drug concentrations in samples. A linear calibration curve was obtained in the range of 1-100 µg/ml with a correlation (R^2) of 0.986.

Oral bioavailability: Male Sprague-Dawley rats (350 ± 20 g), supplied by Charles River Laboratories Canada, and were acclimatized for a week at the Division of Comparative Medicine (DCM) lab in a temperature-controlled environment with free access to water and food. Rats were randomly assigned to two groups (5 animals in each) depending on whether they received ibuprofen in suspension (control) or in SMEDS. These preparations were administered to animals by oral gavage at a dose of 25 mg/kg. Blood samples (100 µL) were withdrawn through the saphenous vein at 5, 10, 20, 30, 45, 60, 90, 120, 240 and 480 minutes after administration and collected in Heparin-coated tubes. The plasma was separated by centrifugation and stored at −20 °C for later analysis. For the control group, Ibuprofen was suspended in 0.1% (w/v) of sodium carboxy methylcellulose (Na-CMC) solution using a high shear homogenizer. The suspension was shaken immediately before use. The SMEDS was loaded with 5% (w/w) ibuprofen. All the *in vivo* experiments were conducted at the Division of Comparative Medicine (DCM) laboratories at University of Toronto and procedures were conducted according to the guiding principles in the use of animals, as adopted by the University Animal Care Committee (UACC).

Phase scan: The detailed procedure for phase scans is explained elsewhere[50]. Briefly, a series of surfactant solutions of increasing salinity (0, 5, 10, 15, 20, 25, 30 g NaCl/100 mL) with equal

volumes of aqueous and oil phases were prepared. The total surfactant concentration was 10 wt. % unless otherwise stated. To prepare the phase scans, 3 ml of the saline solution containing the required salt, 3 ml of ethyl decanoate (oil) and 0.67 g of lecithin+ linkers (density 1.0 g/ml) were vortex-mixed in 2 dram vials at room temperature. The phases were left to equilibrate at room temperature for two weeks before recording the phase volumes. The optimum salinity was chosen when a middle phase μE with equal excess oil/water were observed.

Preparing Fed-state simulated intestinal fluid (FeSSIF): The composition of the fed-state simulated intestinal fluid (FeSSIF) used in this work is a slightly modified version of the USP formulation reported by Marques [61]. In a 1L graduated flask, sodium hydroxide, sodium chloride and glacial acetic acid were dissolved in water (101, 203, 144 mM, respectively). Then lecithin and sodium taurocholate were added to final concentration of 3.75 and 15 mM. The pH was adjusted to 6.8.

Table 3-1: Composition of fed state simulated intestinal fluid (FeSSIF)

Components	**mM**
NaOH	101
NaCl	203
Acetic Acid	144
Sodium taurocholate	15
Lecithin	3.75
pH	Adjusted to 6.8

Constructing ternary phase diagrams: Stock solutions of varying weight ratios of oil (ethyl caprate) to surfactant/linker mixtures (from 10:90 to 90:10) were prepared (represented by each dilution line in ternary phase diagram). The surfactant-mixture consisted of lecithin (main surfactant), glycerol monooleate (lipophilic linker) and hexaglycerol caprylate (hydrophilic linker) at fixed ratios (10:10:80 for GC6Y, 15:15:70 for 6GC8). Dilution lines, from 5% to 99% aqueous phase, were made by adding appropriate amounts of FeSSIF to each of oil-surfactant mixtures in

glass vials and shaken gently until thorough mixing was achieved. Dilution behaviours were monitored immediately after formation (within two hours) and after being given time to equilibrate (two weeks). Transparent single-phase samples that did not exhibit birefringence (i.e. no lamellar or hexagonal liquid crystal) or highly viscous nature (no cubic liquid crystal) were identified as μEs. The observed phases were plotted on a pseudo-ternary phase diagram, with the three axes representing FeSSIF, oil and the surfactant-mixture. The stable microemulsion domain and other existing fields were identified by delineating the phase boundary. Prosim software was used to illustrate the data and produce the phase diagrams. Wherever two evaluated points were different, the average coordinates between the two was assigned as the point for the borderline.

SMEDS Preparation: The oil (ethyl caprate) was mixed with the surfactant mixture which consists of lecithin, Peceol^{TM}, Dermofeel® G6CYand/or Caprol® 6GC8. The optimum ratio of components of surfactant mixture and the ratio of oil: surfactant mixture was selected so that the mixture forms a fully dilutable path in a ternary phase diagram. The loaded SDMEDS was prepared by dissolving the drug in SMEDS on a weight basis.

Preparation of ibuprofen suspension: Ibuprofen powder was passed through a 100-mesh sieve (150 μm), suspended in 1% (w/w) of sodium-CMC solution for a concentration of 0.5% w/v. The suspension was shaken immediately before use.

Determination of the characteristic curvature (Cc) of Caprol 6GC8®: this surfactant was mixed with a reference surfactant, Dehydol OD5® with known Cc of - 0.96, in different ratios (10:90. 20:80, 30:70, 40:60 and 50:50), and optimum middle phase μEs were obtained using cyclohexane as oil. The optimum salinity (S*) for every ratio was determined as a function of the molar fraction of test surfactant in the mixture, obtaining the linear correlation $S^*=48.2^*X_{6GC8}+12.0$ ($R^2=0.996$). The slope of this regression line in was used to calculate the Cc of Caprol 6GC8

as Cc6GC8 = Cc_{OD5} –b*slope of the linear regression, where b=0.13 for Dehydol OD5. Details of the development of this method and equations can be found elsewhere [62]. The calculation yielded a Cc= -7.2 for Caprol 6GC8®.

3.4. Results and discussion

3.4.1. SMEDS-drug interaction

The original SMEDS platform was formulated using ethyl caprate as oil, lecithin (Lec) as the main surfactant, glyceryl mono-oleate as lipophilic inker (LL) and polyglyceryl caprylate as hydrophilic linker (HL). A schematic representation of the interface of the linker formulation is illustrated in Figure 3-2. The hydrophilic linker in this formulation was a 6-glycerol ester of caprylic acid.

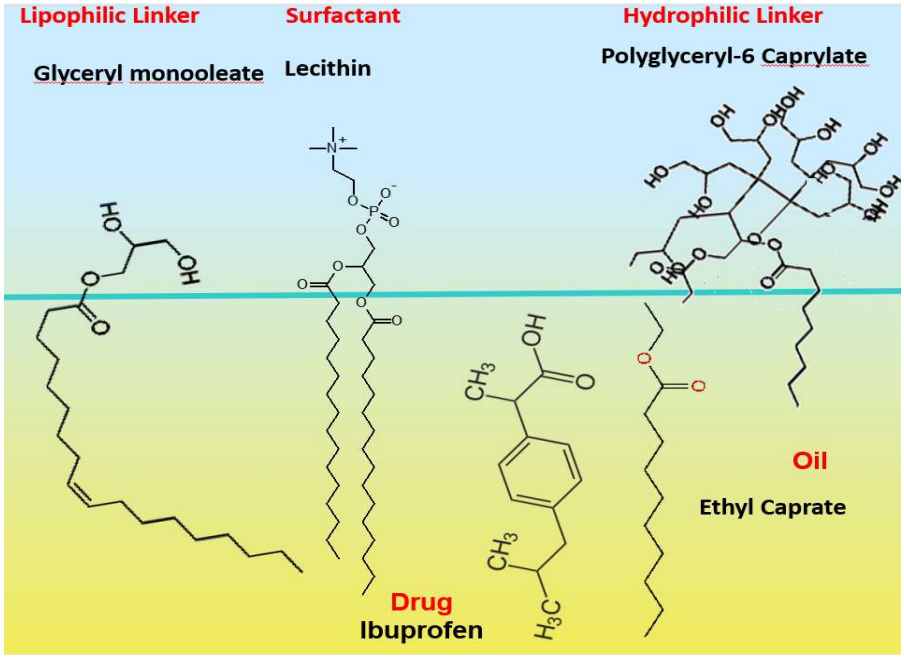

Figure 3-2: Schematic of the interface of lecithin linker microemulsion, loaded with ibuprofen.

The ternary phase diagram for the original platform SMEDS formulation of 10:10:80 ratio of LL:Lec:HL, described in previous chapter [50], displayed a wide single-phase microemulsion region, ranging from 80:20 to 50:50 surfactant: oil ratios.

Figure 3-3 (top) illustrates the dilutions behaviour of SMED at 75:25 ratio with fed-state simulated intestinal fluid (FeSSIF), indicating a fully dilutable 1-phase µE without a phase separation. However, upon loading the original platform SMEDS with ibuprofen the dilution phase behaviour changed dramatically. In dilutions with more than 35% aqueous phase, a phase separation (water +µE) occurred.

Figure 3-3 (bottom) shows the dilutions of the SMEDS loaded with 5% ibuprofen. Adding ibuprofen to the system changes its properties in a way that the surfactants can no longer solubilize the entire aqueous phase in oil and hence expels an excess aqueous phase.

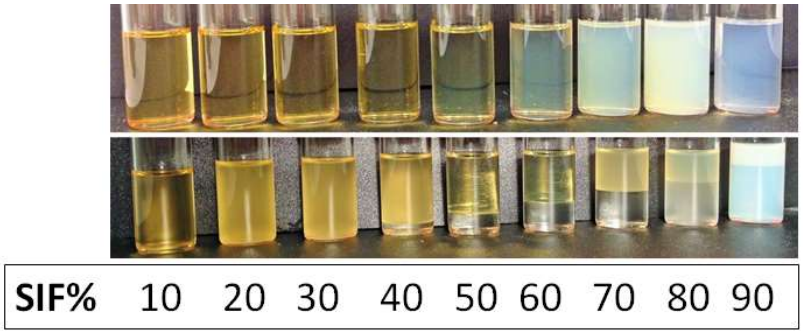

Figure 3-3: Top: the phase behaviour of the original platform10-10-80 formulation at 75:25 Surfactant: Oil. Top: the unloaded SMEDS, Bottom: the same formulation when loaded 5% ibuprofen. The aqueous phase is FeSSIF.

The TPD for loaded SMEDS showed no region of fully dilutable µE. Instead, it was mainly occupied with 2-phase systems of µE+oil or µE+water, as shown in Figure 3-4.

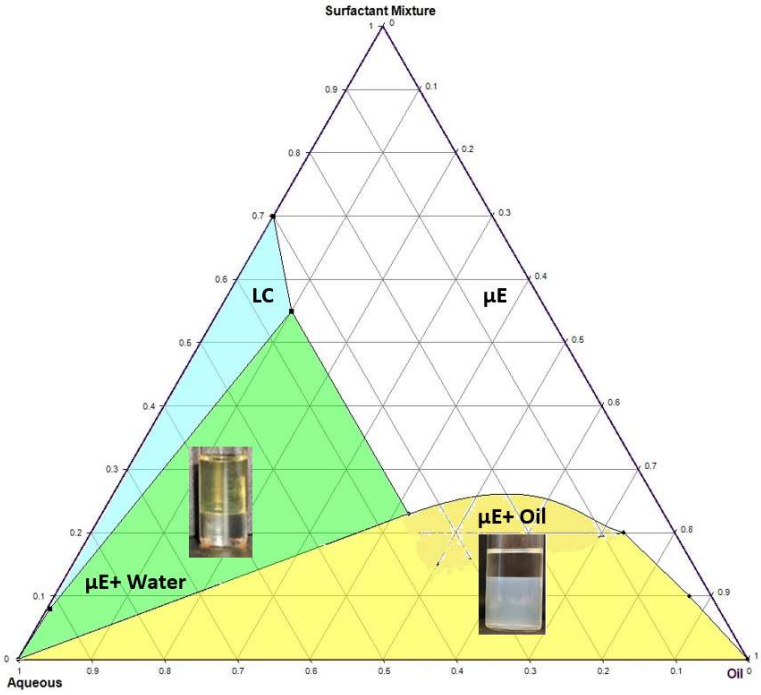

Figure 3-4: Ternary phase diagram for the original SMEDS platform loaded with 5% ibuprofen. The surfactant mixture contains LL:Lec:HL ratio of 10:10:80.

The formation of μE + excess water system with ibuprofen suggests that the addition of drug increases the surfactant-oil affinity in comparison to the surfactant-water interactions. Ibuprofen, when considered as part of oil phase, is a polar oil and decreases the oil hydrophobicity. The impact of polar oils in oil mixtures has been investigated in applications such as oil recovery [63,64,65], and in the flavour and fragrance industry [66]. However, for lipid-based drug delivery systems, the effect of polar oils has not been addressed in surfactant-oil-water (SOW) systems. The most common indicator used in predicting oil polarity in pharmaceutical industry is the octanol/water partition coefficient, but it does not take into account the role of surfactant. The equivalent alkane carbon number (EACN) used in the HLD framework has been used as an alternative to quantitatively define the role of polar oil in the mixture. Most non-polar oils have positive EACN values and polar oils tend to have negative values[67]. For a mixture of oils, the EACN of the mixture can be calculated as [68]:

$$\mathbf{EACN}_{mix} = \sum \boldsymbol{X_i}\, \boldsymbol{EACN_i} \qquad \textbf{(3-2)}$$

where X_i and $EACN_i$represent the volume fraction and EACN of oil i, respectively. Kiran and Acosta showed that due to its polar nature, asphaltenes (a component in bitumen) greatly affects the hydrophilic–lipophilic nature of bitumen and causes a reduction in $EACN_{mix}$and concluded that low EACN for asphaltenic oils provides them with some amphiphilic properties [65]. In food and cosmetic industries, a major challenge in product development is that introducing a flavour or fragrance alters the physicochemical and organoleptic properties of the product. Tchakalova & Fieber showed that polar fragrances greatly impact the whole $EACN_{mix}$[66]. Rearranging Eq.3-2, the EACN of the oil "1" when mixed with oil "2" can be calculated as:

$$\boldsymbol{EACN_1 = \frac{EACN_{mix} - (X_2 * EACN_2)}{X_1}} \qquad \textbf{(3-3)}$$

To quantify the changes in phase behaviour produced by ibuprofen, the HLD shift (and $EACN_{mix}$) of the SMEDS was assessed via salinity scans. By definition, the optimum salinity (S*) is the salinity in which a bicontinuous phase is formed containing equal volumes of oil and water solubilized, corresponding to a HLD value of zero. A salinity phase scan revealed that for unloaded SMEDS, S*~25 g NaCl/100 mL, but for SMEDS loaded with 5% ibuprofen, S*~3 g NaCl/100 mL (Figure 3-5).

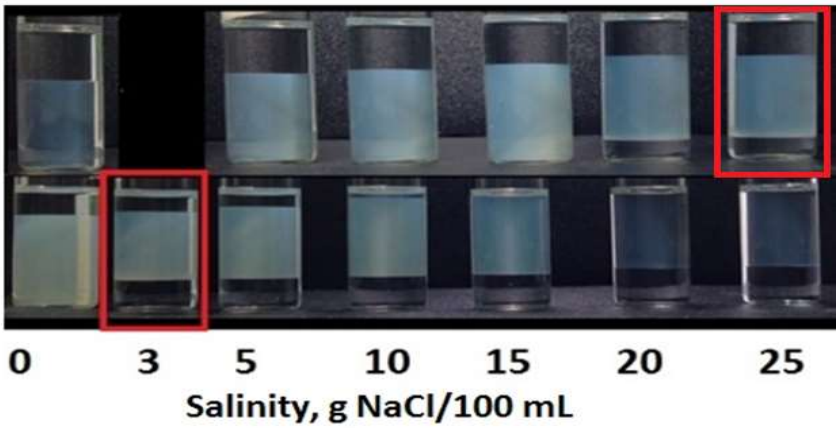

Figure 3-5: top: the phase san for unloaded SMEDS, bottom: The corresponding phase scan for loaded SMEDS with 5% ibuprofen

It is known (from experiments and the HLD equation) that when the system is formulated with an oil of low EACN, the phase transition (I-->III) occurs at lower salinity S* [69]. The data in Figure 3-5 suggests that ibuprofen as a low or even negative EACN to explain the substantial reduction in the optimum salinity. To assess the EACN of ibuprofen, the HLD equation (Eq. 3-1) can be simplified at optimum (HLD*=0) considering that the experiments were conducted at 25 °C ($\alpha_T \cdot (T-25)=0$), without alcohol (f(A)=0), thus, $HLD^* = 0 = b(S^*) - k(EACN) + Cc = 0$ Designating the optimal salinity for the unloaded system as S^*_1 with $EACN_1$ and for the loaded system as S^*_2 with $EACN_{mix}$, since the Cc in both cases is constant (the same surfactant formulation), then, $HLD^*_2 - HLD^*_1 = 0 = b(S^*_2 - S^*_1) - k(EACN_{mix} - EACN_1)$, then the $EACN_{mix}$ can be calculated as:

$$\mathbf{EACN_{mix} = (b/k)\,(S^*_2 - S^*_1) + EACN_1} \qquad \mathbf{(3\text{-}4)}$$

As per Figure 3-5, $(S^*_2 - S^*_1) = 3 - 25 = -22$. The EACN of ethyl caprate has been determined to be 5.5, and the surfactant constants to be b=0.12, and k=0.17 [50]. Replacing these values in Eq.3-4, one obtains $EACN_{mix} = -10.0$. To assess the EACN of ibuprofen we can now use Eq. 3-3 with the known value of $EACN_{mix}$, using the EACN of ethyl caprate as $EACN_2$, and the volume fraction of ibuprofen ($x_1 = 0.11$) and ethyl caprate ($x_2 = 0.89$) in the oil phase. From Eq. 3-3, one would estimate the EACN of ibuprofen ($EACN_1$) as -135. This extremely negative EACN is not unprecedented. Baran et al calculated the EACN of polar chlorocarbons in negative range (-5 to -22) [68].Szekeres et al. assessed the EACN of dodecanol in μEs of mixtures of limonene and dodecanol as ranging from -20 to -100, depending on the concentration of dodecanol in the oil[64]. As indicated by Szekeres et al. and Kiran et al., there is a fraction of the polar oil that segregate near the surfactant tails, behaving as surfactant-like molecules. In principle, polar oils should be treated as both, oil and surfactant (thus having an EACN and a Cc) but the HLD does not have an additional equation to account for the fraction of the polar oil that behaves as a surfactant and the fraction that behaves as oil. Work to find/predict that fraction is still ongoing. At the moment, we

can only refer to the EACN of -135 for ibuprofen as an apparent EACN, applicable to the conditions of the experiment. For organic compounds with ionizable groups (i.e. carboxylic acid for ibuprofen), certain pH ranges could produce additional surfactant species resulting from the dissociation of the ionizable group. This also applies to ibuprofen as the pH of the FeSSIF was 6.8, larger than the pKa of ibuprofen of 4.5. Given the mass transfer and dissociation reactions at the interface, it is also difficult to say what fraction of ibuprofen is in dissociated state. Once again, the apparent EACN accounts for all those combined phenomena of interfacial segregation and dissociation at the interface.

3.4.2. Restoring the dilutable path using the HLD framework

To restore the formulation using the HLD framework, is convenient to rewrite Eq. 3-1 in terms of formulation changes from a condition "i" to condition "ii", considering that in both conditions the formulations remains at 25°C, and without alcohol:

$$\Delta HLD = HLD_{ii} - HLD_i = b(S_{i\,i} - S_i) - k(EACN_{ii} - EACN_i) + (Cc_{ii} - Cc_i) \quad (3\text{-}5)$$

Labeling the unloaded (original) formulation as condition "i", and the restored formulation loaded with ibuprofen as condition "ii", the reformulation exercise should produce an HLD_{ii} that is equivalent to that of the original formulation HLD_i. Another consideration is that both formulations should be dilutable with FeSSIF, which has a given electrolyte composition, thus $S_{ii} = S_i$. According to Eq. 3-5 there are two ways to address the problem, by changing ethyl caprate for other oil that can maintain the same EACN as the original formulation or to change the surfactant composition (change Cc) to compensate for the changes in EACN. The EACN solution would require using Eq. 3-3 with $EACN_{mix} = EACN_i = 5.5$; $x_2 = 0.11$; $EACN_2 = -135$; $x_1 = 0.89$. Under those conditions, the required oil should have $EACN_1 = 23$. To achieve this large EACN would require

the use a highly hydrophobic oil, similar to squalane. These highly hydrophobic oils are difficult to solubilize in μEs, thus an unpractical solution.

The second strategy to restore the formulation is to find a Cc_{ii} that can compensate for the change in EACN. From Eq. 3-5, considering $HLD_{ii}=HLD_i$, $S_{ii}=S_i$ (FeSSIF), $EACN_i=5.5$, $EACN_{ii} = -10.0$, then $Cc_{ii} = Cc_i +0.17(-10.0-5.5) = Cci -2.63$. In other words, we need a surfactant mixture more hydrophilic (negative Cc) than the original formulation to compensate for the introduction of ibuprofen. It is reasonable to increase the surfactant-water (hydrophilic) interactions given the earlier observation that the introduction of ibuprofen strengthened the surfactant-oil interaction.

The value of Cc_i can be assessed using the linear mixing rule, $Cc_{mix}= \sum x_j Cc_j$ where x_j is the molar fraction of surfactant "j" in mixture with the rest of the surfactants in the system, and Cc_j is the characteristic curvature of each surfactant[70]. In case of the original platform lecithin linker formulation, using the values in Table 3-2, $Cc_i = -1.16$.

Table 3-2: Characteristic curvatures of lecithin and linkers in the original platform SMEDS formulation.

	Lecithin	**Lipophilic Linker** (Peceol)	**Hydrophilic Linker** (*Dermofeel® G6CY*)
MW	750	488	593
Weight ratio	10	10	80
# of mole	0.013	0.020	0.135
x_j	0.079	0.121	0.800
Cc_j	5.5	6.6	-3
$\Sigma x_j Cc_j$	- 1.16		

The target Cc_{mix} value in the restored formulation should be close to Cc_{ii}=-1.16-2.63 = -3.79. A quick look at Table 3-2 illustrates that no matter what ratio we use, we cannot restore the formulation changing the ratio of the existing linkers. The most hydrophilic component in Table 3-2, the hydrophilic linker is still not hydrophilic enough (Cc=-3).

The choices for food grade hydrophilic linkers with extremely negative Cc are limited. The Caprol 6GC8® was found to meet these requirements. As explained in the methods section, Caprol 6GC8® has a Cc of -7.2, sufficient to shift the Cc of the mixture from -1.16 to -3.79. Dermofeel® G6CY and Caprol® 6GC8 are both described as being polyglycerol caprylates by their respective manufacturers. However, their Cc is significantly different. Polyglycerol esters of fatty acids can be synthesized in linear, hyper-branched, dendritic polyglycerol, or as a mixture of them[71]. This variation in chemical structure could explain their different Cc values.

To obtain the appropriate ratio of lecithin : peceol (lipophilic linker) : Caprol® 6GC8 (hydrophilic linker) to obtain a $Cc_{mix} \sim$ -3.8, similar calculations as those presented in Table 3-2 were conducted using various combinations of lecithin and linkers. Table 3-3 presents the ratio that was finally selected (the ratio could be further optimized to obtain an exact Cc match, but the rounded ratio of 15:15:70 was found to be enough to restore the formulation) .

Table 3-3: Characteristic curvatures of lecithin and linkers in the loaded and restored SMEDS formulation.

	Lecithin	**Lipophilic Linker** (Peceol)	**Hydrophilic Linker**
MW	750	488	593
Weight ratio	15	15	70
# of mole	0.020	0.031	0.118
Xi	0.118	0.183	0.699
Cc	5.5	6.6	-7.2
ΣXi Cci	- 3.2		

To test if the restored formulation recovered the original HLD (S*~30 g NaCl/100 mL), a salinity scan was conducted with the formulation of Table 3-3. As shown in Figure 3-6, the formulation of Table 3-3 has S* ~ 22.5 g NaCl/100 mL.

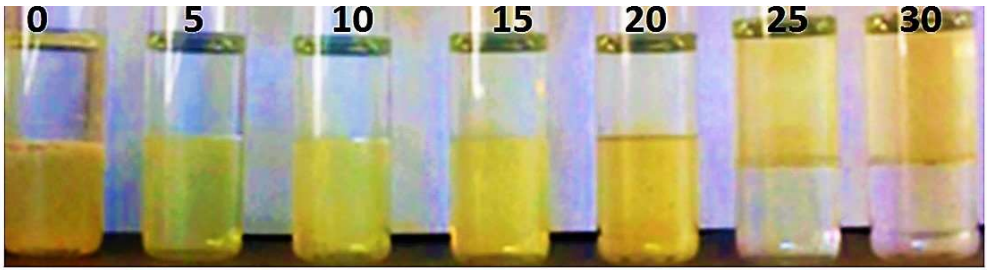

Figure 3-6: The phase scan for loaded SMEDS from 0 to 30 g NaCl/100 mL of the SMEDS formulation of Table 3-3

To examine the single-phase dilutability, the ternary phase diagram of the loaded and restored SMEDS was constructed, as shown in Figure 3-7. The dilution line of the D60/40 line is also depicted in Figure 3-8.

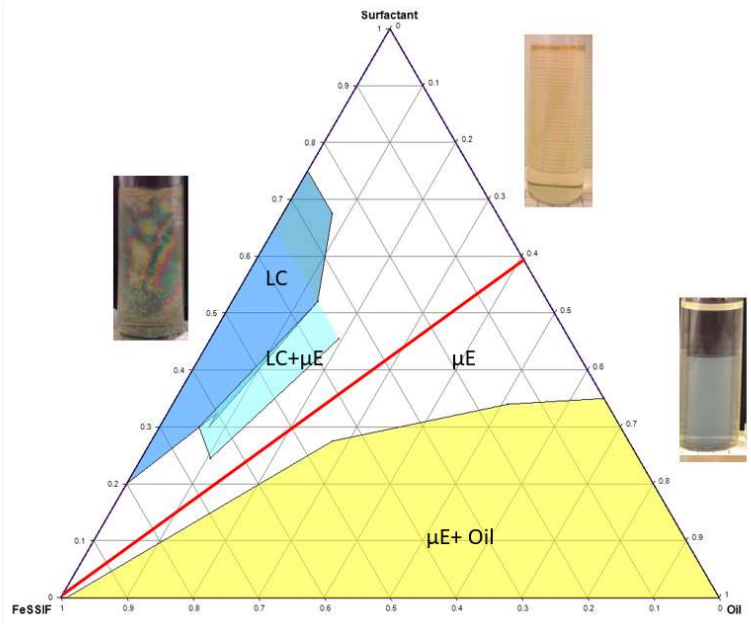

Figure 3-7: Ternary phase diagrams for restored formulation loaded with 5% ibuprofen.

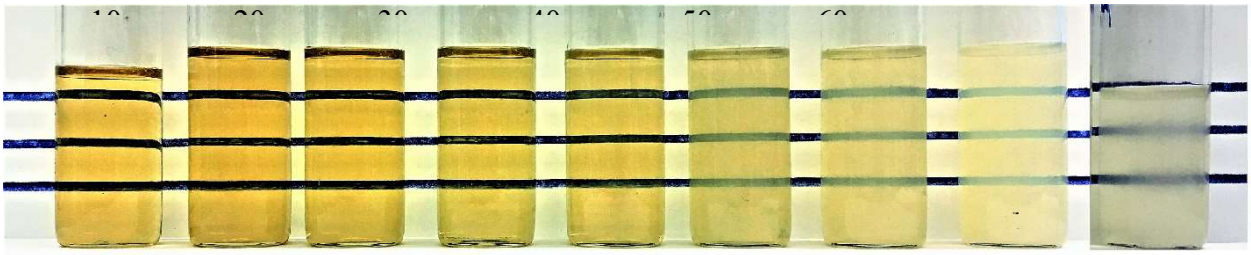

Figure 3-8: Dilution profile of SMEDS restored and loaded with 5% w/w ibuprofen. The numbers indicate the wt% of FeSSIF along the D60/40 line. The blue lines in the background show transparency of the microemulsions.

The ample single phase μE region in Figure 3-7 and the transparency of the systems in the D60/40 (no phase separation, emulsions, precipitate formation or liquid crystal formation detected) line further confirms that using the HLD as guideline to restore the formulation after loading ibuprofen was a suitable and timely strategy (the reformulation took less than a month).

The 60:40 system depicted in Figure 3-8 was selected to test the *in vivo* uptake of ibuprofen-loaded in SMEDS. One way to conduct a preliminary assessment of the potential usefulness of the formulation to improve *in vivo* absorption is to determine the average drop size and viscosity of

the formulation upon dilution [46]. Figure 3-9 presents the drop size (determined via dynamic light scattering) and the viscosity (at shear rate of 100±50 s^{-1}) along the D60/40 line as a function of the wt% of FeSSIF. The drop size remains below 10 nm for most of the dilution process, and in all cases below 100 nm. These drop sizes are quite useful in increasing the uptake of nano-scale droplet or particle delivery systems[72]. Although the viscosity is relatively high at low dilution, this might be beneficial to slow down the emulsification process in the stomach to secure that most of the emulsification takes place in the intestine, where the formulation was designed to act (via the use of FeSSIF). The changes in drop size and viscosity relates to transitions in the shape of the μEs drops as discussed elsewhere [50]. Considering the data presented in Figure 3-8, it's worth noting that the dilutions between 20% and 80% FeSSIF, are indeed bicontinuous systems and not in W/O or O/W microemulsions. Therefore, that droplet size measured by DLS for these dilutions do not correspond to actual droplets size. As shown in previous work [50], for lecithin linker microemulsions, the DLS data for bicontinuous systems represent the characteristic length ξ which is the inverse of the average curvature (*Ha*).

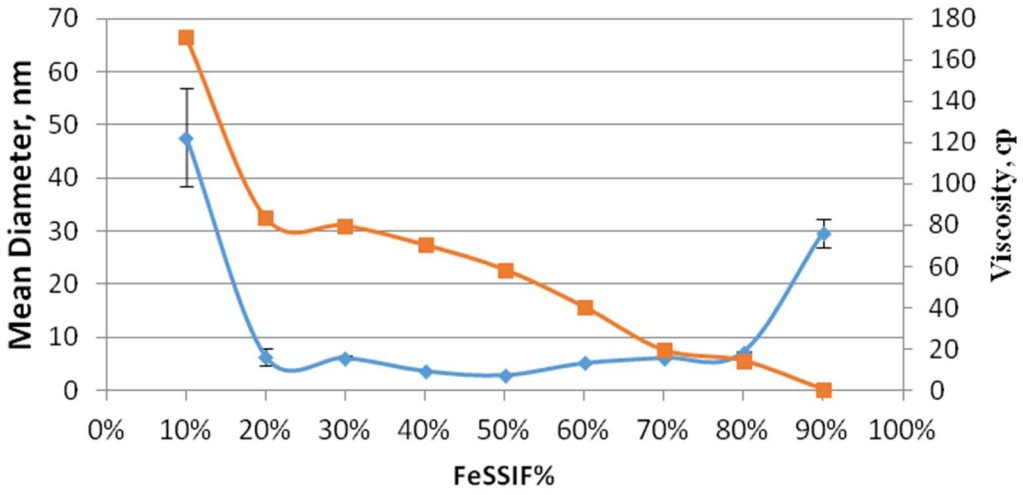

Figure 3-9: Drop size (right axis) and viscosity (left axis) of the diluted SMEDS along the 60/40 dilution line at 25 °C. The viscosity data are based on the average viscosity measured at shear rates ranging from 80-120 s^{-1} (n=40). The error bars represent the standard deviation. For most cases, the bars are too small to be visualized.

The phase behavior of the lecithin linker SMEDS, was confirmed to be thermo-reversible and pH –reversible. To simulate SMEDS phase behavior in the absorption site (intestine), FeSSIF was used as diluting media. To investigate the interaction of SMEDS with acidic conditions of stomach, the SMEDs were diluted with simulated gastric fluid (HCl 1 N). It was noticed that SMEDS does not self-disperse in pH 1 to 2 and the bulk of the SMEDS remains intact. However, when the acidic dilution is neutralized, self-micro emulsification occurs. In terms of thermostability, the experiments showed that after frequent heating-cooling cycles the phase behavior was recovered after returning to room temperature.

Pharmacokinetic (in vivo uptake) of the fully dilutable ibuprofen-loaded SMEDS.

The D60 SMEDS was selected as the candidate delivery system for Ibuprofen. The detailed formulation of this system is listed in Table 3-4: Composition of ibuprofen-loaded (and restored) SMEDS used in the *in vivo* study..

Table 3-4: Composition of ibuprofen-loaded (and restored) SMEDS used in the *in vivo* study.

Components		**Wt%**
Oil	Ethyl Caprate	38
Surfactant	Lecithin	8.5
Lipophilic Linker	Glycerol monooleate	8.5
Hydrophilic Linker	Caprol 6GC8	40
Drug	(S)-(+)-Ibuprofen	5

The formulation was dosed at 25 mg Ibuprofen/kg b.w. to male Sprague-Dawley rats (350 ± 20 g). The control formulation was a powder suspension of ibuprofen in a carboxymethyl cellulose (CMC) solution also dosed at 25 mg/kg b.w. The reason for selecting ibuprofen as a model drug was partly because of there are several studies comparing μE-based formulas and suspension versions of the drug, as will be discussed later. A second reason to select ibuprofen as a model

drug is because it was one of the drugs (in preliminary screening studies) that caused the most changes in phase behaviour as noted earlier. Finally, ibuprofen is a drug that although effective and common, is not completely absorbed, thus the importance of improving its uptake to avoid waste and its potential endocrine disrupting effects associated with that waste[73].

The rats were allowed access to water and food before and during the duration of the experiment. One of the reasons for the use of a fed-state condition is that the formulation was designed for fed-state condition. The other reason for using fed-state condition is that the clinical recommendation is to take ibuprofen and other NSAIDs after meals to minimize the effects of the drug on the lining of the stomach [74]. A few preliminary experiments were conducted in fasted animals but the plasma concentration curves were highly variable, which could be associated with differences in the composition of the gastric juices. However, these variable results are more likely associated with the differences in the concentration of lipids in the intestinal fluid of the fasted animals, which would suggest that the lipids in the intestinal fluid facilitate the formation of SMEDS.

The plasma concentration curves obtained with the D60 SMEDS (composition of Table 3-4) and with the control suspension are shown in Figure 3-10. The solid lines in Figure 3-10 were obtained after fitting the data to a single compartment model programmed in the PKsolver software [75.] Table 3-5 includes a summary of the pharmacokinetic parameters obtained from the fitted curves, along with their standard deviation, and the 2-tailed t-student probability (p_{value}) for the null hypothesis of not difference between the control and SMEDS pharmacokinetic data.

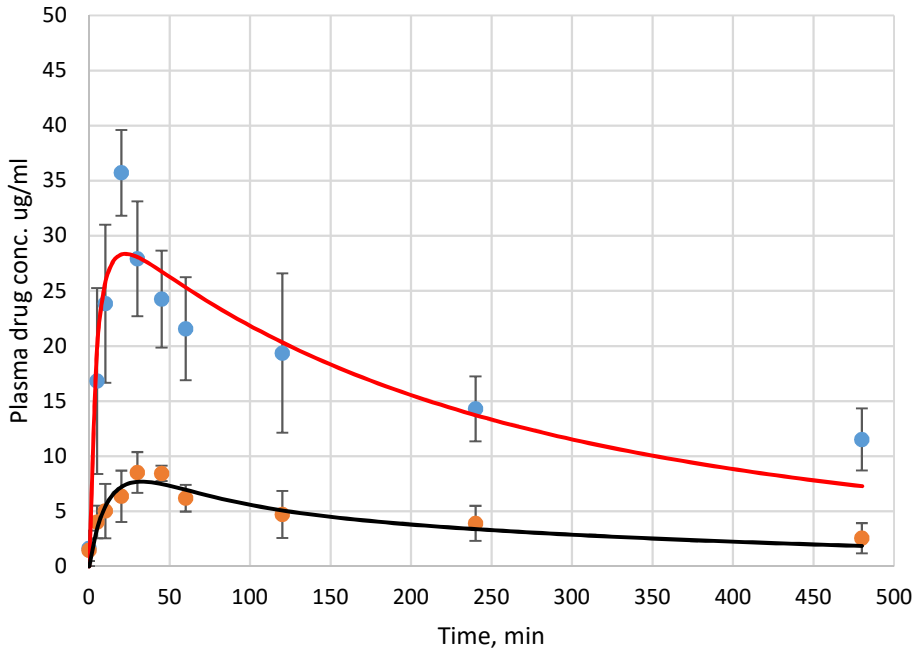

Figure 3-10: Plasma concentration-time profile of ibuprofen in rats after oral administration of 25 mg/kg b.w. Ibuprofen in SMEDS (blue circles) and water suspension (orange circles). The error bars represent the standard deviation (SD) of 6 repeats. The solid lines represent the single compartmental fit; $C_t=A(e^{-k10t} - e^{-kat})$.

Table 3-5: Pharmacokinetic parameters for orally administered ibuprofen in SMEDS and in aqueous suspension

Parameter	Unit	Value SMEDS	Value Control	p_{value}
T_{max}	min	22.1 ± 8.0	42 ± 22	6.4E-02
C_{max}	µg/ml	28.9 ± 3.4	8.2 ± 1.0	5.5E-08
AUC $_{0-t}$	µg/ml*min	(7.3 ±2.2)*10^3	(1.85±0.79)*10^3	2.0E-04
A	µg/ml	32.1±3.3	9.7±1.7	4.0E-08
k_a	1/min	0.23 ±0.11	0.08±0.04	1.1E-02
k_{10}	1/min	0.004±0.002	0.012 ± 0.012	1.4E-01

k_a: Absorption rate constant and k_{10}: elimination rate constant.

The data in Figure 3-10 revealed that the SMEDS formulation produced plasma concentrations higher than the ibuprofen suspension. The pharmacokinetic parameters in Table 3-5 show that the relative bioavailability (AUC $_{test}$/AUC $_{control}$) was improved by 3.4 folds. The C_{max} was increased

3. 8 times. The average T_{max} was shortened to 50% of that of the control group, however the relatively high null probability of p_{value} =0.06 (not difference between control and SMEDS) is the result of the high standard deviation obtained with the control sample. The increase in absorption of the drug when it was loaded in SMEDS can be attributed to the role of surfactant micelles in enhancing the apparent solubility of the drug and likely increasing the permeation through the intestinal wall. Amidon et al. have shown that surfactant micelles produce a significant increase in apparent solubility of a hydrophobic drug [76] and the micelle complexation of the drug increases the exposure of the drug to intestinal epithelial cells [77]. The size of the micelles, being less than 100 nm (Figure 3-9), should also facilitate the absorption of the drug via passive absorption mechanisms as it has been shown in various nanoparticle bioavailability studies [72]. If the micelles, as indicated in Figure 3-9, maintain a size lower than 10 nm during part of the absorption process then the paracellular mechanism of transport is also possible where micelles can penetrate through the junctions in between epithelial cells [72,78]. The substantial increase in drug uptake with the SMEDS formulation of this work justifies further studies exploring the details of the transport mechanism obtained with these systems.

Another important feature of the data in Figure 3-10 is that the ibuprofen plasma concentration of the SMEDS formulation remains high in the blood after an extended period of time. This can be explained on the higher absorption rate constant (k_a) for the SMEDS formulation (p_{value} = 0.01) while the elimination rate constant (k_{10}) for SMEDS is approximately the same (p_{value} = 0.14) or slightly lower than that of the control. The high absorption rate constant for SMEDS means that the drug will be easy to absorb while its elimination rate remains approximately the same, leading to a high plasma concentration for an extended period of time. Efficacy studies have shown that in humans, the onset of pain relief occurs 15- 20 minutes post dosing when the mean plasma concentration of ibuprofen reaches 7 μg/ml, but for maximum pain relief, the concentration should

remain above 10 μg/ml[79]. The data shown in Figure 3-10 suggests that the lecithin-linker SMEDS formulation reaches 7 μg/ml sooner than the control and can maintain a concentration higher than 10 μg/ml for about 5 hours.

The AUC in time-plasma drug concentration graphs obtained from in-vivo experiments, such as the data presented in Figure 3-10, can be used to calculate the (relative)bioavailability which is different from the concept of bioaccessibility. Bioavailability represents the fraction of drug that reaches the systemic circulation after oral administration, GI digestion, absorption, metabolism, and tissue distribution. In contrast, bioaccessibility represent the fraction of ingested active ingredient that is released from the food matrix in the GI tract and potentially becomes available for uptake by intestinal epithelium cells in the intestinal lumen [80]. Bioaccessibility is evaluated by in vitro tests in which the fraction of active compound released into mixed micelles after digestion is quantified [81]. In fully dilutable SMEDS dilutions, the drug is already present in a micellar system and therefore could be considered as fully bioaccessible. This clearly shows the importance of full dilutability in microemulsions in order to ensure enhanced bioavailability. In such systems, the formation of micellar systems – a prerequisite for enhanced absorption- is guaranteed where as in other system such as SEDS or partially dilutable systems; the risk of creaming or drug precipitation exists.

The work of Alexis et al.[82] might be relevant to explain the apparent trend of slower clearance with the lecithin-linker SMEDS. Alexis et al. reviewed the factors affecting the drug clearance of nanoparticle delivery systems, finding that surface composition, size and charge are the factors associated with long-circulating effects. The authors argued that highly hydrophilic compounds on the surface of the nanoparticle disrupt the protein-drug interactions that would induce drug clearance. Furthermore, they indicate that smaller particles (10-100 nm) have a lower rate of

hepatic uptake and filtration and therefore remain longer in plasma. For ibuprofen, hepatic metabolism is the predominant route of elimination through enzymatic reactions, particularly for the unbound drug in plasma[83]. Finally, Alexis et al.[82] indicated that nano-particles with neutral or negatively charged surface have a longer retention time, while positively charges particles are cleared sooner. The formulated linker-SMEDS is rich (40%) in polyglycerol esters that impart a hydrophilic and neutrally charged structure to the oil-swollen micelles, and upon dilution it creates ultrafine microemulsion droplets (<35 nm) with a highly hydrophilic interface, all of which may explain the long-lasting effect of ibuprofen in lecithin-linker SMEDS. However, this interpretation presumes that the micelle SMEDS survive or reorganize after the intestinal adsorption. The SMEDS component might also just changed the composition of the chylomicrons in a way that reduced the elimination rate of the drug. These are all outstanding questions that require further studies.

To put the findings of Table 3-5 in the context of other SEMDS or μE-based ibuprofen delivery systems, Table 3-6 compares the relative pharmacokinetic parameters of four delivery systems, including the lecithin-linker SMEDS of this work. In terms of composition, systems 1 through 3 used polyethylene glycol esters (PEG) -based surfactants whereas the lecithin-linker SMEDS is PEG-free. Although most PEG-based surfactants are relatively mild, they tend to have a role in increasing the permeability of epithelial tissue that may lead to irritation. The PEG-free lecithin-linker formulation has been shown to act in a different manner as it does not increase the permeability of epithelial tissue, but instead uses lecithin micelles as carriers that accumulate in the epithelial tissue, imparting an extended release profile [43,48]. To perform the comparison among the studies in Table 3-6 (that have different experimental conditions), the ratios of pharmacokinetic parameters of formulation to control have been calculated. Table 3-6 shows that μE -based systems

significantly increase the ibuprofen uptake causing an increase in C_{max} and AUC (almost to the same ratio) and decrease in T_{max}. (except for case 2). The data suggests that our lecithin linker SMEDS platform increased the C_{max} and reduced T_{max} to a greater extent than the other formulations. In the case of ibuprofen this is of critical importance because in fed-state condition it has been shown that C_{max} tend to be low and T_{max} high compared to fasted conditions, but yet again the guidelines suggest to dose after meals to minimize side effects [74].

Out of the systems summarized in Table 3-6, the closest experimental conditions to the current work were those of the work of You et al.[84] (system 3) as that team also used a dose of 25 mg/kg b.w. The T_{max} obtained by You et al. was close to 30 minutes with their most efficient formulation, and close to for 45 minutes for their control, both values are similar to those in Table 3-5. The control of You et al. (also ibuprofen suspension), however, was able to reach C_{max} ~ 30 μg/ml, versus the lower value of ~ 8 μg/ml achieved in our control group. The reason for this discrepancy might be explained by the fact that our specimens were slightly older (larger) than those used by You et al, or because in their experiments the rats were in a fasted state (known to increase ibuprofen C_{max}[74]). The optimal SMEDS of You et al. achieved a C_{max} ~ 70 μg/ml but that concentration rapidly decreased to 8 μg/ml after 4 hours and was completely cleared by 8 hours. If one looks at the data (not the model fit) for SMEDS in Figure 3-10 one realizes that although C_{max} ~ 35 μg/ml (about half that of You et al.), the average plasma concentration remains close to 10 μg/ml even after 8 hours. This observation is in line with those obtained in transdermal delivery with lecithin-linker system where it was found that these formulations do not increase the permeability of the tissue (fast transport), but instead uses the epithelial tissue as an in-situ depo for the drug, effectively producing an extended release behaviour[43]. Such extended release behaviour might not be fully represented by the single compartment model used to fit the data in

Figure 3-10 as that model fails to properly fit the peak C_{max} and the ibuprofen concentration at 8 hours. Once again, further studies are needed to gain a better understanding of the mechanism of transport with these lecithin-linker SMEDS in oral delivery.

Table 3-6. Pharmacokinetic parameters of µE-based ibuprofen delivery systems.

Dosage Form	Components	Dose (mg/kg BW)	Droplet Size (nm)	T_{max} test/ T_{max} control	C_{max} test/ C_{max} Control	$T_{1/2}$ (hr)	AUC test/ AUC control	Time above 10 ppm	Ref.
Solid SEDDS	PEG-5 Oleate, PEG-8 Caprylic/Capric Glycerides, Propylene glycol monocaprylate	10	220	0.93	2.1	3.9	2.1	4	57
µE	**PEG**-40 Hydrogenated Castor Oil , Diethylene glycol monoethyl ether	10	57	1.3	1.9	2.16	1.9	4.5	85
µE	Tween 80, PEG-35 Castor oil, PEG400, caprylic/capric triglyceride, Glyceryl monolinoleate	25	40	0.66	2.3	1.2	1.5	4	84
SMEDS	Ethyl caprate, **Lecithin**, Glyceryl monooleate, Hexaglycerol caprylate	25	10-30	0.52	3.52	4	3.6	>8	This work

When comparing the pharmacokinetics data for ibuprofen one should be cautious. Since R-(-) ibuprofen converts to the S-(+) enantiomer [86]. Therefore, type of administered ibuprofen needs to be considered and data from non-stereospecific drug could be different when the disposition of the

individual enantiomers. Also, many studies indicate that the pharmacokinetics of ibuprofen and ibuprofen-plasma protein binding capacity are dose-dependent and administrating higher doses result in an increased drug clearance and a reduced AUC of the total drug [87,88]. Considering the dose effect, perhaps the fairest comparison is that among the study of You et al. [84], which uses similar dose and study conditions.

3.5. Conclusions

The drug-lipid interaction in lipid-based delivery systems can produce substantial changes in the phase behaviour of the original drug-free delivery system. The conventional approach to deal with these situations is to embark in empirical reformulation efforts that can take significant amount of time and resources and may not result in a successful formulation. This work introduced a more rational approach to the problem using the HLD framework as the guide for such reformulation work. The reformulation work was conducted in two stages, the first was to quantify the impact of the drug via the use of salinity scans and determining the optimal salinity (S*) and the shift in HLD value with regards to the original formulation. This shift was then used to identify strategies (change of surfactant or change of carrier oil), and the most likely approach that would lead to a successful formulation. The method was used to reformulate a lecithin-linker SMEDS platform that could incorporate 5% ibuprofen. The *in vivo* experiments showed that this formulation could increase the relative bioavailability of ibuprofen by 3-4-fold compared to an aqueous suspension of ibuprofen, and impart extended release-like features that are not commonly observed in other SMEDS formulations.

3.6. References

[1] Yu LX, Amidon GL, Polli JE, Zhao H, Mehta MU, Conner DP, et al. Biopharmaceutics Classification System: The Scientific Basis for Biowaiver Extensions. Pharm Res. 2002;19(7):921–5.

[2]Pouton CW. Lipid formulations for oral administration of drugs: non-emulsifying, self-emulsifying and "self-microemulsifying" drug delivery systems. Eur J Pharm Sci. 2000;11:S93–8.

[3]Pouton CW. Formulation of self-emulsifying drug delivery systems. Adv Drug Deliv Rev. 1997 Apr;25(1):47–58.

[4]Hauss DJ, editor. Oral Lipid-Based Formulations: Enhancing the Bioavailability of Poorly Water-Soluble Drugs. CRC Press; 2007.

[5]Hauss DJ. Oral lipid-based formulations. Adv Drug Deliv Rev. 2007 Jul 30;59(7):667–76.

[6]Gibson L. Lipid-Based Excipients for Oral Drug Delivery. In: Hauss DJ, editor. Oral lipid-based formulations : enhancing the bioavailability of poorly water-soluable drugs. New York: CRC Press; 2007. p. 33–62.

[7]Wang W, Wei H, Du Z, Tai X, Wang G. Formation and characterization of fully dilutable microemulsion with fatty acid methyl esters as oil phase. ACS Sustain Chem Eng. 2015;3(3):443–50.

[8]Yaghmur A, Aserin A, Garti N. Phase behavior of microemulsions based on food-grade nonionic surfactants: effect of polyols and short-chain alcohols. Colloids Surfaces A Physicochem Eng Asp. 2002 Sep;209(1):71–81

[9]Djekic L, Primorac M. Microemulsion Systems Application in Delivery of Poorly Soluble Drugs. In: Fanum M, editor. COLLOIDS IN DRUG DELIVERY. CRC Press; 2010. p. 245–70.

[10] Porter CJH, Trevaskis NL, Charman WN. Lipids and lipid-based formulations: optimizing the oral delivery of lipophilic drugs. Nat Rev Drug Discov. 2007 Mar;6(3):231–48.

[11] Talegaonkar S, Azeem A, Ahmad FJ, Khar RK, Pathan S a, Khan ZI. Microemulsions: a novel approach to enhanced drug delivery. Recent Pat Drug Deliv Formul. 2008 Jan;2(3):238–57.

[12] O'Driscoll CM. Lipid-based formulations for intestinal lymphatic delivery. Eur J Pharm Sci. 2002 Jun;15(5):405–15.

[13] Fatouros DG, Karpf DM, Nielsen FS, Mullertz A. Clinical studies with oral lipid based formulations of poorly soluble compounds. Ther Clin Risk Manag. 2007 Aug;3(4):591–604.

[14]Porter CJ, Charman WN. In vitro assessment of oral lipid based formulations. Adv Drug Deliv Rev. 2001 Oct 1;50 Suppl 1:S127-47.

[15]Yáñez J a, Wang SWJ, Knemeyer IW, Wirth M a, Alton KB. Intestinal lymphatic transport for drug delivery. Adv Drug Deliv Rev. Elsevier B.V.; 2011 Sep 10;63(10–11):923–42.

[16]Djekic L, Primorac M. Microemulsion Systems Application in Delivery of Poorly Soluble Drugs. In: Fanum M, editor. Colloids in Drug Delivery. CRC Press; 2010. p. 245–70.

[17]Choc MG. Bioavailability and pharmacokinetics of cyclosporine formulations: Neoral vs Sandimmune. Int J Dermatol [Internet]. 1997 Dec;36 Suppl 1:1–6. Available from: http://www.ncbi.nlm.nih.gov/pubmed/9466213

[18] Van Mourik IDM, Thomson M, Kelly DA. Comparison of pharmacokinetics of neoral and sandimmune in stable pediatric liver transplant recipients. Liver Transplant Surg. 1999;5(2):107–11

[19] Cui J, Yu B, Zhao Y, Zhu W, Li H, Lou H, et al. Enhancement of oral absorption of curcumin by self-microemulsifying drug delivery systems. Int J Pharm. 2009;371(1–2):148–55.

[20]Setthacheewakul S, Mahattanadul S, Phadoongsombut N, Pichayakorn W, Wiwattanapatapee R. Development and evaluation of self-microemulsifying liquid and pellet formulations of curcumin, and absorption studies in rats. Eur J Pharm Biopharm. Elsevier B.V.; 2010;76(3):475–85.

[21]Wu X, Xu J, Huang X, Wen C. Self-microemulsifying drug delivery system improves curcumin dissolution and bioavailability. Drug Dev Ind Pharm. 2011;37(1):15–23.

[22]Onoue S, Uchida A, Nakamura T, Kuriyama K, Hatanaka J, Tanaka T, et al. Self-nanoemulsifying particles of coenzyme Q10 with improved nutraceutical potential. PharmaNutrition. Elsevier B.V.; 2015;3(4):153–9.

[23]Kommuru TR, Gurley B, Khan M a, Reddy IK. Self-emulsifying drug delivery systems (SEDDS) of coenzyme Q10: formulation development and bioavailability assessment. Int J Pharm. 2001 Jan 16;212(2):233–46

[24]Liu Y, Jiang X, Wang X. Prescription design and bioavailability assessment of self-microemulsifying system of vitamin AD. Lat Am J Pharm. 2015;34(1):3853.

[25] Porter CJH, Trevaskis NL, Charman WN. Lipids and lipid-based formulations: optimizing the oral delivery of lipophilic drugs. Nat Rev Drug Discov. 2007 Mar;6(3):231–48.

[26] Talegaonkar S, Azeem A, Ahmad FJ. Microemulsions: a novel approach to enhanced drug delivery. Recent Pat Drug Deliv Formul. 2008 Jan;2(3):238–57.

[27] Fatouros DG, Karpf DM, Nielsen FS, Mullertz A. Clinical studies with oral lipid-based formulations of poorly soluble compounds. Ther Clin Risk Manag. 2007 Aug;3(4):591–604.

[28] Hauss DJ. Oral lipid-based formulations. Adv Drug Deliv Rev. 2007 Jul 30;59(7):667–76.

[29]Porter CJ, Charman WN. In vitro assessment of oral lipid-based formulations. Adv Drug Deliv Rev. 2001 Oct 1;50 Suppl 1:S127-47.

[30] Dahan A, Hoffman A. Rationalizing the selection of oral lipid based drug delivery systems by an in vitro dynamic lipolysis model for improved oral bioavailability of poorly water soluble drugs. J Control Release. 2008 Jul 2;129(1):1–10.

[31]Rao J, McClements DJ. Food-grade microemulsions, nanoemulsions and emulsions: Fabrication from sucrose monopalmitate & lemon oil. Food Hydrocoll. 2011 Aug;25(6):1413–23.

[32] Wu L, Bi Y, Wu H. Formulation optimization and the absorption mechanisms of nanoemulsion in improving baicalin oral exposure. Drug Dev Ind Pharm. 2018;44(2):266–75.

[33] O'Driscoll CM. Lipid-based formulations for intestinal lymphatic delivery. Eur J Pharm Sci. 2002 Jun;15(5):405–15.

[34]wanaga K, Higashiyama Y, Miyazaki M, Kakemi M. Enhancing mechanism of intestinal absorption of highly lipophilic compounds using microemulsion - Quantitative analysis of the partitioning to the mesenteric lymph in intestinal cells. Asian J Pharm Sci. 2014;10(3):186–93.

[35]Rozner S, Shalev DE, Shames AI, Ottaviani MF, Aserin A, Garti N. Do food microemulsions and dietary mixed micelles interact? Colloids Surf, B. 2010 May 1;77(1):22–30.

[36] Dokania S, Joshi AK. Self-microemulsifying drug delivery system (SMEDS) - challenges and road ahead. Drug Deliv Inf Healthc. 2015;22(6):1521–0464.

[37] Shevachman M, Garti N, Shani A, Sintov AC. Enhanced percutaneous permeability of diclofenac using a new U-type dilutable microemulsion. Drug Dev Ind Pharm. 2008 Apr;34(4):403–12.

[38] Spernath A, Aserin A, Garti N. Phase transition induced bywater dilution in phospholipid U-type food-grade microemulsions studied by DSC. J Therm Anal Calorim. 2006;83(2):297–308.

[39]Feedap AF, Ramos F, Rychen G, Saarela M, Villa RE, Wallace RJ, et al. Safety and efficacy of lecithins for all animal species. EFSA J. 2016;14(8):e04561.

[40]Aboofazeli, R, C.B. Lawrence, S.R. Wicks MJL. Investigations into the formation and characterization of phospholipid microemulsions. Int J Pharm. 1994;111(1):63–72.

[41] Tenjarla S. Microemulsions: an overview and pharmaceutical applications. Crit Rev Ther Drug Carr Syst. 1999;16(5):461–521.

[42]De Weck AL, Bundgaard H, editors. Allergic Reactions to Drugs Volume 63 of Handbook of Experimental Pharmacology. Springer; 2012. 342 p.

[43] Yuan J. Linker-based lecithin microemulsions as transdermal drug delivery systems, Doctoral dissertations. University of Toronto; 2009.

[44] Sabatini DA, Acosta E, Harwell JH. Linker molecules in surfactant mixtures. Curr Opin Colloid Interface Sci [Internet]. 2003 Nov;8(4–5):316–26.

[45] He C-X, He Z-G, Gao J-Q. Microemulsions as drug delivery systems to improve the solubility and the bioavailability of poorly water-soluble drugs. Expert opin drug Deliv. 2010 Apr;7(4):445–60.

[46]Chu J, Cheng Y-L, Rao AV, Nouraei M, Zarate-Muñoz S, Acosta EJ. Lecithin-linker formulations for self-emulsifying delivery of nutraceuticals. Int J Pharm. 2014;471(1–2):92–102.

[47]Acosta, E., Chung, O., Xuan X. Lecithin-linker microemulsions in transdermal delivery. J Drug Deliv Sci Technol. 2011;21(1):77–87.

[48]Yuan JS, Acosta EJ. Extended release of lidocaine from linker-based lecithin microemulsions. Int J Pharm. 2009 Feb 23;368(1–2):63–71.

[49]Xuan X-Y, Cheng Y-L, Acosta E. Lecithin-Linker Microemulsion Gelatin Gels for Extended Drug Delivery. Pharmaceutics [Internet]. 2012 Jan 31 [cited 2012 Aug 26];4(1):104–2.

[50]Nouraei M, Acosta EJ. Predicting solubilisation features of ternary phase diagrams of fully dilutable lecithin linker microemulsions. J Colloid Interface Sci. 2017.

[51] Djordjevic L, Primorac M, Stupar M. In vitro release of diclofenac diethylamine from caprylocaproyl macrogolglycerides based microemulsions. Int J Pharm. 2005; 296:73–9.

[52] Djordjevic L, Primorac M, Stupar M, Krajisnik D. Characterization of caprylocaproyl macrogolglycerides based microemulsion drug delivery vehicles for an amphiphilic drug. Int J Pharm. 2004;271(1–2):11–9.

[53] Djekic L, Primorac M, Jockovic J. Phase Behaviour, Microstructure and Ibuprofen Solubilization Capacity of Pseudo-Ternary Nonionic Microemulsions. J Mol Liq. Elsevier B.V.; 2011;160(2):81–7.

[54] Hathout RM, Woodman TJ, Mansour S, Mortada ND, Geneidi AS, Guy RH. Microemulsion formulations for the transdermal delivery of testosterone. Eur J Pharm Sci. Elsevier B.V.; 2010;40(3):188–96.

[55] Milović M, Djuriš J, Djekić L, Vasiljević D, Ibrić S. Characterization and evaluation of solid self-microemulsifying drug delivery systems with porous carriers as systems for improved carbamazepine release. Int J Pharm. 2012 ;436(1–2):58–65.

[56]Pestana KC, Formariz TP, Franzini CM, Sarmento VH V, Chiavacci LA, Scarpa M V, et al. Oil-in-water lecithin-based microemulsions as a potential delivery system for amphotericin B. Colloids Surfaces B Biointerfaces. 2008;66(2):253–9.

[57]Balakrishnan P, Lee B-J, Oh DH, Kim JO, Hong MJ. Enhanced oral bioavailability of dexibuprofen by a novel solid self-emulsifying drug delivery system. Eur J Pharm Biopharm. Elsevier B.V.; 2009 Aug;72(3):539–45.

[58] Kiran SK, Acosta EJ. HLD–NAC and the Formation and Stability of Emulsions Near the Phase Inversion Point. Ind Eng Chem Res. 2015;54(25):6467–79.

[59] Jahan S, Islam J, Begum R, Kayesh R, Rahman A. A Study of Method Development, Validation, and Forced Degradation for Simultaneous Quantification of Paracetamol and Ibuprofen in Pharmaceutical Dosage Form by RP-HPLC Method. Anal Chem Insights. 2014;2014(9):17–25.

[60] Domañska U, Pobudkowska A, Pelczarska A, Gierycz P. pKa and solubility of drugs in water, ethanol, and 1-octanol. J Phys Chem B. 2009;113(26):8941–7.

[61] Marques M. Dissolution Media Simulating Fasted and Fed States. Dissolution Technol. 2004;11(2):16.

[62] S. Zarate-Muñoz, F. Texeira de Vasconcelos, K. Myint-Myat, J. Minchom , E. Acosta. Simplified Methodology to Measure the Characteristic Curvature (Cc) of Alkyl Ethoxylate Nonionic Surfactants. J Surfactants Deterg. 2016, 19, 249-63.

[63] Szekeres E, Acosta E, Sabatini DA, Harwell JH. Modeling solubilization of oil mixtures in anionic microemulsions: II. Mixtures of polar and non-polar oils. J Colloid Interface Sci. 2006;294(1):222–33.

[64] Szekeres E, Acosta E, Sabatini DA, Harwell JH. Preferential solubilization of dodecanol from dodecanol-limonene binary oil mixture in sodium dihexyl sulfosuccinate microemulsions: Effect on optimum salinity and oil solubilization capacity. J Colloid Interface Sci. 2005;287(1):273–87.

[65]Kiran SK, Acosta EJ, Moran K. Evaluating the hydrophilic-lipophilic nature of asphaltenic oils and naphthenic amphiphiles using microemulsion models. J Colloid Interface Sci. Elsevier Inc.; 2009 Aug 1;336(1):304–13.

[66]Tchakalova V, Fieber W. Classification of fragrances and fragrance mixtures based on interfacial solubilization. J Surfactants Deterg. 2012;15(2):167–77.

[67]EACN | Practical Surfactants Science | Prof Steven Abbott [Internet]. [cited 2017 Mar 6]. Available from: https://www.stevenabbott.co.uk/practical-surfactants/eacn.php

[68]Baran Jr. JR, Pope GA, Wade W., Weerasooriya V, Yapa A. Microemulsion Formation with Mixed Chlorinated Hydrocarbon Liquids. J Colloid Interface Sci. 1994;168:67.

[69]Phan TT, Harwell JH, Sabatini DA. Effects of Triglyceride Molecular Structure on Optimum Formulation of Surfactant-Oil-Water Systems. 2010;189–94.

[70] Acosta, E. J.; Yuan, J. S.; Bhakta, A. S. The Characteristic Curvature of Ionic Surfactants. J. Surfactants Deterg. 2008, 11, 145-158.

[71]Zhang H, Grinstaff MW. Recent advances in glycerol polymers: Chemistry and biomedical applications. Macromol Rapid Commun. 2014;35(22):1906–24.

[72] Acosta, E. Bioavailability of nanoparticles in nutrient and nutraceutical delivery (2009) Current Opinion in Colloid and Interface Science, 14 (1), pp. 3-15.

[73] Gonzalez-Rey, M., Bebianno, M.J. Does non-steroidal anti-inflammatory (NSAID) ibuprofen induce antioxidant stress and endocrine disruption in mussel Mytilus galloprovincialis? (2012) Environmental Toxicology and Pharmacology, 33 (2), pp. 361-371.

[74] Moore, R.A., Derry, S., Wiffen, P.J., Straube, S. Effects of food on pharmacokinetics of immediate release oral formulations of aspirin, dipyrone, paracetamol and NSAIDs - A systematic review (2015) British Journal of Clinical Pharmacology, 80 (3), pp. 381-388.

[75]Zhang Y, Huo M, Zhou J, Xie S. PKSolver: An add-in program for pharmacokinetic and pharmacodynamic data analysis in Microsoft Excel. Comput Methods Programs Biomed. 2010;99:306–14.

[76]Amidon GL, LoÈbenberg R. Modern bioavailability, bioequivalence and biopharmaceutics classi ® cation system. New scienti ® c approaches to international regulatory standards. Eur J Pharm Biopharm. 2000; 50:3–12.

[77]Miller JM, Beig A, Krieg BJ, Carr RA, Borchardt TB, Amidon GE, et al. The solubility-permeability interplay: Mechanistic modeling and predictive application of the impact of micellar solubilization on intestinal permeation. Mol Pharm. 2011;8(5):1848–56.

[78] Sha, X., Yan, G., Wu, Y., Li, J., Fang, X. Effect of self-microemulsifying drug delivery systems containing Labrasol on tight junctions in Caco-2 cells (2005) European Journal of Pharmaceutical Sciences, 24 (5), pp. 477-486.

[79]Mehlisch DR, Sykes J. Ibuprofen blood plasma levels and onset of analgesia. J Clin Pract. 2013; 67:3–8.

[80] Carbonell-capella, J. M., Buniowska, M., Barba, F. J., Esteve, J. & Fr, A. Analytical Methods for Determining Bioavailability and Bioaccessibility of Bioactive Compounds from Fruits and Vegetables : A Review. *Compr. Rev. food Sci. food Saf.* **13,** 155–171 (2014).

[81] Ahmed, K., Li, Y., Mcclements, D. J. & Xiao, H. Nanoemulsion- and emulsion-based delivery systems for curcumin : Encapsulation and release properties. *Food Chem.* **132,** 799–807 (2012).

[82]Link C, Alexis F, Pridgen E, Molnar LK. Factors Affecting the Clearance and Biodistribution of Polymeric Nanoparticles. Mol Pharm. 2008;5(4):505–15.

[83]Satterwhite J., Douglas F. Effects of age and dose on the pharmacokinetics of Ibuprfen in rats. Drug Mataboism Dispos. 1991;19(1):61–7.

[84]You X, Xing Q, Tuo J, Song W, Zeng Y, Hu H. Optimizing surfactant content to improve oral bioavailability of ibuprofen in microemulsions : Just enough or more than enough ? Int J Pharm. Elsevier B.V.; 2014;471(1–2):276–84.

[85]Hu L, Yang J, Liu W, Li L. Preparation and evaluation of ibuprofen-loaded microemulsion for improvement of oral bioavailability. Drug Deliv. 2011;18(1):90–5.

[86] Davies NM. Clinical pharmacokinetics of ibuprofen. The first 30 years. Clin Pharmacokinet. 1998;34(2):101–54.

[87] Jung DT, Shah A, Jung D. Dose -dependent Pharmacokinetics of Ibuprofen in the Rats. Drug Metab Dispos. 1987;15(2):151–154;

[88] Rainsford K, editor. Ibuprofen: A Critical Bibliographic Review. Taylor & Francis Ltd.; 2005. 595 p.

Chapter 4. Gelled Self - Microemulsifying Delivery System (G-SMEDS)

4.1. Abstract

A lecithin-linker self-microemulsifying delivery system (SMEDS) was used as the oil phase to develop a self-dispersing organogel platform in which the release rate could be modified by the gelator concentration. The fully dilutable SMEDS formulation is composed of ethyl caprate (oil), lecithin (main surfactant), and glycerol esters of fatty acids as lipophilic and hydrophilic linkers. Two phytosterols (β-sitosterol and γ-oryzanol) at 1:1 mass ratio were used as low molecular weight gelators (LMWG). The changes in thermal and mechanical properties of the gel during heating/cooling cycles were evaluated as a function of gelator concentration. The results showed that gel strength (elastic modulus G'), melting point (expressed in terms of shear rate transition temperature) and gel firmness (rupture point) increases along with increasing gelator concentration. The micrographs showed the gradual formation of Maltese cross spherulite crystalline structures during cooling and gel formation. The microscopic observation showed gradual formation of spherulite structure during gel formation. Different from other organogels, the SMEDS organogels display a large viscous modulus (G") that maybe responsible for the controlled release properties. While liquid SMEDS, instantly self (micro)emulsified upon exposure to the aqueous phase, the gelled SMEDS showed an extended release profile (1-4 days) at experimental conditions. Video-microscopy studies, and batch release studies suggest that the limiting factor for the self-microemulsification process in gelled SMEDS is the water diffusion into the gel. Fitting the experimental to a combined diffusion + erosion model suggests that both diffusion and erosion influence the release mechanism.

4.2. Introduction

The poor solubility of hydrophobic bioactive ingredients (drugs and/or nutraceuticals) tends to limit their uptake via oral administration as only a small fraction of the suspended or emulsified active can dissolve and pass through the intestinal walls. Lipid-Based Drug Delivery System (LBDDS), in particular, microemulsions (μE) and Self-Microemulsifying Drug Delivery System (SMEDS), are promising strategies to enhance solubilization, absorption and bioavailability of poorly soluble bioactive ingredients. μEs and SMEDS improve the bioavailability by two mechanisms: a) increasing the concentration of the drug by solubilization in nano-sized (micellar) carriers, and b) increasing the permeability of the intestinal wall and/or using passive transport mechanisms, especially for carriers with less than 100 nm in diameter [1]. SMEDS can be considered as concentrated μE (a latent microemulsion), containing isotropic mixtures of oil, surfactant/cosurfactant (or lipophilic/hydrophilic linkers) that spontaneously form O/W nano-sized droplets (10-200 nm) upon dilution and mild agitation in intestinal fluids.

SMEDS typically show a burst release profile due to the relatively fast nature of the self-emulsification process [2]. When frequent administration is unpleasant or impractical, extended (prolonged) release profile is preferred. The United States Pharmacopeia (USP) classifies the release profiles into two main groups: immediate and modified. The latter includes the delayed release (enteric coating) and extended (controlled) release [3]. Some of the issues with immediate release dosages include the need for frequent administration, high fluctuation in drug concentration over time, and more importantly the risk of exceeding therapeutic range and exposure to toxic levels. For example, the therapeutic range of ibuprofen, a common non-steroidal anti-inflammatory drug (NSAID) is 8 to 30 μg/ml [4,5] but the typical plasma concentration curves show a peak concentration (which could be greater than the 30 μg/mL), followed by a relatively fast

decay to concentrations below 8 μg/mL, where the drug is ineffective. Ideally, the release profile would be controlled in a way that the release is slow enough to avoid the peak concentration but fast enough to make up for the losses due to elimination processes, thus providing a nearly constant concentration, within the therapeutic range, for an extended period.

For hydrophobic actives, μE-based delivery systems improve the solubility of the drug via solubilization in the lipid core of micellar carriers, but the fast dissolution (burst release) works against the idea of maintaining the concentration nearly constant in the plasma. To achieve the goal of nearly constant concentration, we need to slow down the release and find a way to increase the residence time of the delivery system in the intestinal tract [6]. To increase the residence time in the epithelia tissue, such as intestine, the use of bioadhesives has been proposed as well as the formation of in-situ patches of lecithin-linker formulations [7],[8],[9]. This article specifically aims at the issue of burst release and finding a method to extend the process of self-emulsification (release) over the course of hours, and potentially days.

There are three main mechanisms to achieve extended release that require controlling (a) diffusion of the active from a solid matrix, (b) dissolution of the solid matrix, or (c) mechanical erosion of the solid matrix [10]. A common practice in the pharmaceutical industry is to modify the release profile by coating tablets and capsules with delayed/extended release polymers, or embedding the active ingredient within a controlled release solid matrix. Other techniques include microencapsulation or physical adsorption onto solid carriers to produce a free-flowing powder with micron-sized particles [11],[12]. There are several reports in the literature using encapsulation techniques to achieve an extended release profile for vitamin D_3 [13],[14], beta-carotene and curcumin [15]. Another method to produce controlled release products is via melt granulation/extrusion (spheronisation) which produces granules, pellets and beads containing slow-releasing polymers.

Depending on the chemical properties of the coating polymers, the release profile or dissolution rate could be delayed or extended for several hours [16].

Another approach to transforming liquid systems into solid-like systems is gelation. Gels are viscoelastic soft materials that return to their original state following an applied stress up to a certain limit. Macroscopically, they present the bulk properties of a solid but microscopically they contain liquid phase embedded in an elastic network of polymers (conventional gelators) or supramolecules (low-molecular-weight gelators, LMWG) or even assembled solids. In hydrogels, the predominant liquid phase is aqueous whereas in organogels it is an oil. LMWGs have gained attention in the food industry since they can be used to solidify edible oils to produce margarine with without trans fats. LMWG form self-assembled 3D-structures held together by noncovalent bonds including π-stacking, van der Waals forces, and hydrogen bonds [17].

Since the mid-1990s, the use of organogels in drug delivery systems has been investigated. One of the earlier articles on the topic were authored by Murdan and Florence in the late 90s [18],[19]. In that article, the authors introduced the use of mixtures of sorbitan monostearate (SMS) and polysorbate 20 in an oil phase. The authors indicated that the surfactant mixtures formed a 3D structure of fibrils that provided the solid-like properties of the gel. The authors later investigated the release mechanism from this SMS gel [20] via videomicroscopy of the gels in contact with water and found that water penetrated the gel and produced the emulsification of the oil, destroying the organogel depo within minutes. The authors indicated that more stable organogels would be required if organogels for drug delivery were to be used in intramuscular or subcutaneous injections. Although not always referenced in terms of drug delivery, an even earlier version of surfactant-based organogels (starting in 1991) are lecithin-based organogels (LO) or pluronic-lecithin organogels (PLO), which have been actively explored as a transdermal delivery system [21]. Another

surfactant-based gelator, dibutyllauroylglutamide (or GP1) has been used to produce organogels for transdermal delivery [22]. Lim et al. [22] found that increasing the concentration of GP1 not only increased the elastic modulus of the gel (G'), but it also was able to reduce the rate of mass transfer from the gel up to half that of the system without gelator. The reduction in release rate was not extremely substantial, but at least provided some potential for the gelator concentration to be a potential variable that could be used to control the release rate. In 2008, Vintiloiu and Leroux [17] introduced what is still to date, the most cited review on organogel delivery systems. At that time, the authors commented on the evolution of organogels towards more stable gelators that, different from sorbitan monostearate (SMS) gels, would allow the matrix to remain stable for a longer period of time. The authors commented that using N-stearoyl l-alanine methyl or ethyl ester (SAM or SAE, respectively), sub-cutaneous release systems could be designed to release for up to two weeks. Another very interesting surfactant-like gelator is 12-Hydroxy stearic acid (HSA) because of its food grade status and its ability to form gels at low gelator concentrations [23],[24]. In addition to low molecular weight (surfactant-like) gelators (LMWG), various polymers have also been used. Recent studies comparing the release of drugs from Carbopol (cross-linked polyacrylic acid polymers) organogels and from GP1 organogels finding similar transdermal flux, and that in both cases the flux decreased with increasing gelator concentration [25].

Thus far, organogels and microemulsion-based drug delivery systems have been mutually exclusive. The only publication thus far on microemulsions and organogels compares two different regions of the surfactant-oil-water (SOW) ternary phase diagram, one at low surfactant concentration where stable emulsions are formed (considered organogels by the authors), and a region at high surfactant concentrations where microemulsions are formed [26].

The approach explored in this work differs from previous work, first in that we believe is important to separate the role of gelator from that of the surfactant used to emulsify or solubilize the drug, thus allowing us to tune the formulation for desired drug solubilization/release and for the mechanical properties of the gel. This work also differs in that we use self-microemulsifying drug delivery systems (SMEDS) as the continuous oil media for the organogel. Use of SMEDS as continuous oil phase represents a challenge for many surfactant-like gelators, which are soluble or dispersible in SMEDS. For this reason, we concentrated on mixtures of phytosterols (β-sitosterol, γ-oryzanol) as our food-grade LMWGs. These gelators have been used as an alternative method for solidifying edible oils [27]. These phytosterols are dissolved in hot oil and upon cooling form hydrogen bonds and self-assemble into a helical ribbon structure (hollow tubes) with a diameter of 6.7 - 8.0 nm that ultimately makes a solid network of the gel [20], [28], [29]. These phytosterols gelators are considered nutraceuticals because of their ability to lower cholesterol levels in the bloodstream [30].

Previous work in our group [31] used β-sitosterol + γ-oryzanol as LMWG to develop phytosterol-based organogels for controlled-release systems. These organogels were designed for applications as intravitreal implants. Neither β-sitosterol nor γ-oryzanol alone form gel with oils and only their mixtures (40:60 to 60:40) form a network of phytosterol fibrils. A 50:50 weight ratio was used in that previous work. A wide range of polar surfactant-like oils was evaluated, having HLB values ranging from 0 to 19. The resulting gels were characterized in terms of rheology, firmness, thermal properties, etc. The oils with HLB values of 4-6 (such as propylene glycol monocaprylate) showed maximum sterol solubility, but also high minimum gelator concentration, as shown in Figure 4-1. It seems at these HLB values, the hydrophilic-lipophilic character of the sterols matches the polar nature of the oil. This match (high sterol solubility) was also confirmed by Hansen solubility parameters (dispersion, polar, and hydrogen bonding

interactions) [32]. Some of these organogels were selected to conduct release studies of dexamethasone – dissolved in the polar oil and gelled with the phytosterols – in a saline solution to simulate the aqueous environment of the vitreous. All the formulations evaluated showed a 14-day lag time where no dexamethasone was release. For organogels produced with polyglyceryl-3 polyricinoleate (Dermofeel PR®, HLB ~9) the organogel plugs released 75% of the loaded dexamethasone, following a zero order (linear) release for 6 months (when the studies were terminated). On the other hand, medium chain triglycerides (Labrafac CC®, HLB~0) organogels released 95% of dexamethasone, following a nearly zero order, in 2 months, as shown in Figure 4-2.

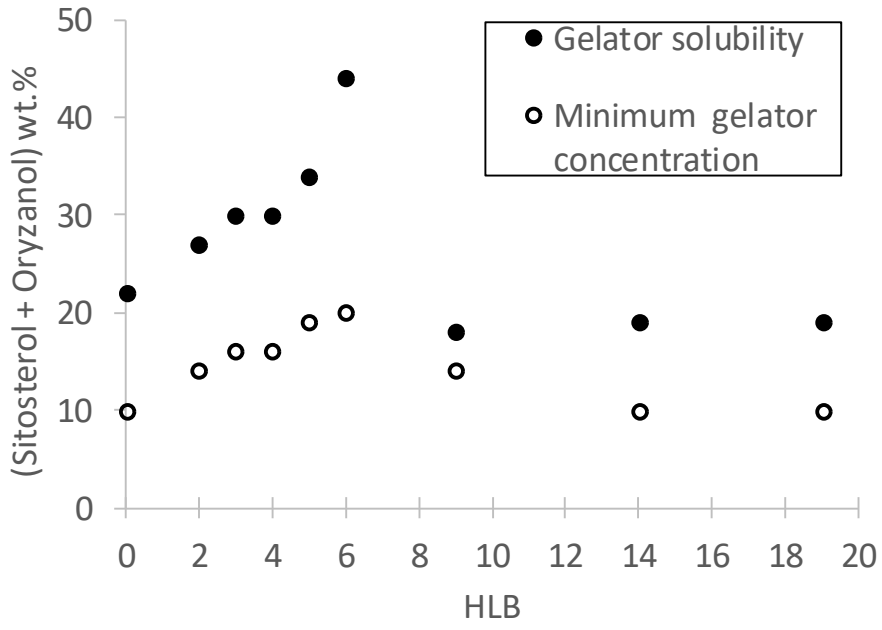

Figure 4-1: Effect of oil phase HLB on the minimum total gelator concentration (β-sitosterol + γ-oryzanol at 1:1 mass ratio) and on the total gelator solubility at 90°C. Data obtained from Chung [31]

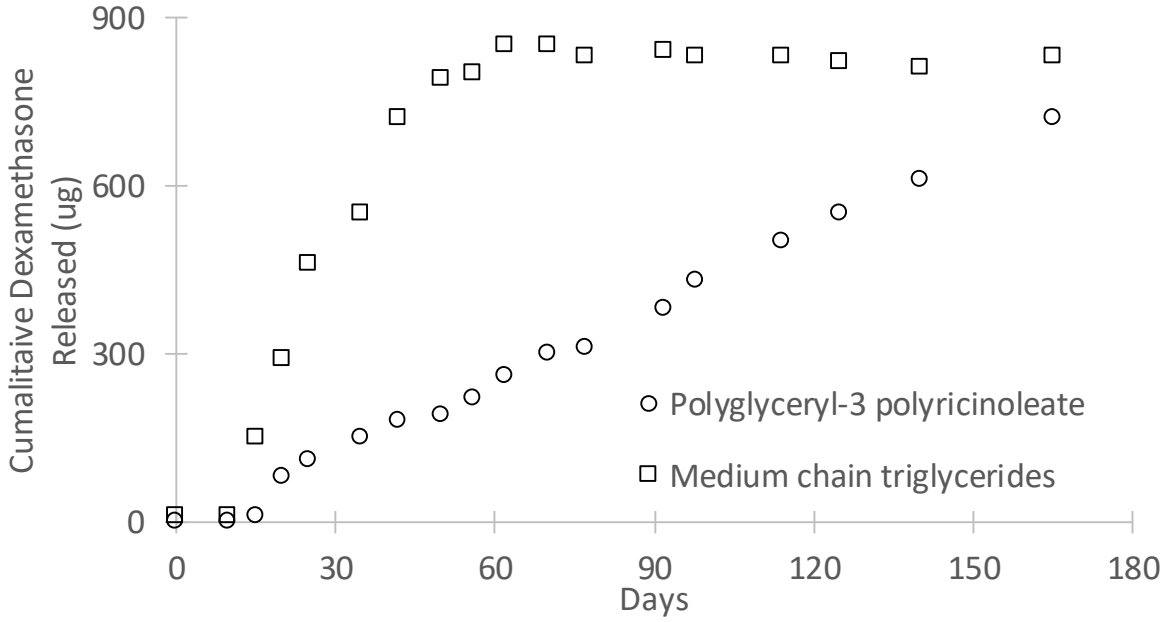

Figure 4-2. Cumulative dexamethasone base release from phytosterols (16 wt % total phytosterols) organogels loaded with 1000µg of dexamethasone. Data obtained from Chung [31].

The features of the release profiles of Figure 4-2 show longer extended release than those previously reported with organogels (~two to three weeks, as indicated by Vintiloiu and Leroux [17] . However, the time scale of phytosterol-polar oil organogels is similar to those reported by the group of Siepmann for lipid implants [33] [34]. Most of these lipids implants are hot water-in-oil emulsions that upon cooling produce a solid matrix where water-soluble components (e.g. propranolol hydrochloride or water-soluble peptides) are encapsulated and slowly released. The group of Siepmann identified that several lipid implant systems follow a first order release that was modeled using an effective diffusion coefficient. However, their data also included several zero order release systems where the release profile was highly dependent on the type of oil used. Chung also observed, as reflected in Figure 4-2, changes in the slope of the zero-order release with the type of oil used, and he could correlate the slope with the partition coefficient of the drug

between the oil used in the organogel and the aqueous phase [20]. According to that correlation, when the drug had a higher affinity for the oil phase, the rate of release decreased. Chung proposed that the mass transfer was limited by the transport between the aqueous side of the organogel-water interface and the bulk aqueous phase, such that Flux ~ K_L*$K_{w/o}$*C_{oil}; where K_L is the mass transfer coefficient, $K_{w/o}$ is the partition coefficient of the drug between water and oil, and C_{oil}, is the concentration of the drug in the oil phase of the organogel. According to this mechanism, the role of the solid network of the organogel is not to slow down the mass transfer of the oil, but simply provide mechanical stability to the oil phase during the long-term release. In fact, one of the disadvantages of Chung's organogels is that they were not degraded even after 6 months of in-vitro release in a buffer solution. It is possible, however, that for in-vivo release, enzymatic degradation could lead to the disintegration of the gel.

To summarize the state of the art on gel delivery, alkyl amino acid-based organogels (GP1, SAM, SAE) can provide weeks of release time that are said to be controlled for the breakdown of the enzymatic breakdown of the gel [35]. In the absence of a process that breaks down the organogel, phytosterol-based organogels could deliver for months via a release mechanism that seems to be controlled by the affinity of the drug for the oil of the organogel [31]. Organogels that rely on emulsification of the oil tend to release their load within minutes [20]. In all these cases, the organogel is considered more of a depot for the drug, not as a way of enhancing the bioavailability of the drug itself [36,37].

By introducing self-microemulsifying lecithin-based drug delivery systems (SMEDS) as the continuous oil media for the organogel we expect to improve over conventional SMEDS in providing a more controlled release (over the current immediate release for those systems), and to improve over past organogel delivery systems by using the oil (lecithin-linker SMEDS) media as a way to facilitate the ability of the drug to absorb and permeate through epithelial tissues [9]. Because the surfactant species in the delivery system (lecithin and linkers) are not the building blocks of the organogel (as in the case of SMS), the organogel should maintain some of its structure as the SMEDS is released. Because the oil (SMEDS) is eventually solubilized in aqueous media, the organogel-SMEDS has its own method of controlling the release that would not depend on enzymatic processes.

The lecithin-linker SMEDS considered in this work were previously developed for the delivery of lipophilic drugs in transdermal and oral delivery [38]. These formulations have been found to be non-toxic, non-irritant and to produce an "in-situ" patch because they can penetrate epithelial tissue without increasing the permeability of the tissue [9] . The lipophilic linker (glycerol monooleate) in the formulation improves the interaction of lecithin (surfactant) with the oil (ethyl caprate), and help prevent the formulation of lecithin liquid crystals and gels. The hydrophilic linker (polyglycerol caprylate) helps improves the interaction of lecithin with the aqueous phase. The ratio of linkers can be modified to obtain different types of microemulsions. For systems that are solubilized in water, more hydrophilic linker is required. Table 4-1 introduces a summary of the fully dilutable SMEDS composition used in this work [39].

Table 4-1: SMEDS composition

	Surfactant (Lecithin)	**Lipophilic Linker** (Peceol)	**Hydrophilic Linker** (Dermofeel G6CY)	**Oil** (Ethyl caprate)
HLB	~ 6	~ 4	~ 15	~ 0
D50 w/w ratio	7.5	7.5	35	50
D70 w/w ratio	10.5	10.5	49	30

The first part of this work looks at the mechanical properties and phase behaviour of D50 SMEDS with varying levels of β-sitosterol + γ-oryzanol (1:1 ratio), while the second part of the article concentrates on the release studies from these systems. The SMEDS did not affect the mechanical properties imparted by the sterols, but provided the desired self-emulsification behaviour that produced a more controlled release over the course of several days.

4.3. Materials and Methods

4.3.1. Materials

SMEDS components including Ethyl decanoate, ≥ 98% were purchased from Sigma - Aldrich (Oakville, ON, Canada), polyglyceryl-6-caprylate (Dermofeel® G6CY, 100%) was donated by Kinetik Technologies (Morris, NJ, USA). Glycerol monooleate (PeceolTM) was a gift from Gattefossé (Etobicoke, ON, Canada). Glacial acetic acid (ACS, ≥ 99.7%) dipotassium monohydrogen phosphate anhydrous (>95%), phosphoric acid, glacial acetic acid (ACS, ≥ 99.7%) and L-alpha-lecithin, granular (from soybean oil) were purchased from Fisher Scientific Canada (Markham, ON, Canada). Sodium chloride (> 99.0%), and sodium hydroxide (ACS reagent grade) were purchased from Bioshop® Canada (Burlington, ON, Canada). Sodium taurocholate hydrate

≥ 97.0% (TLC), sodium taurocholate hydrate (≥ 97.0%), β-Sitosterol (> 70%) and solvent blue 35 98% (as a marker) were purchased from Sigma Aldrich Canada. Acetonitrile (HPLC grade) and phosphoric acid (85%) from Caledon (Georgetown, ON, Canada). γ-Oryzanol was a gift from Tsuno Rice Fine Chemicals (Wakayama, Japan).

4.3.2. Methods

SMEDS preparation: The oil (ethyl caprate) was mixed with the surfactant mixture which consists of lecithin, Peceol™, and Dermofeel® G6CY, as per Table 4-1. The optimum ratio of components of surfactant mixture and the ratio of oil: surfactant mixture was selected so that the mixture forms a fully dilutable path in a ternary phase diagram and was detailed somewhere else 39. For this work, we used 15% -15%- 70% ratio of the lipophilic linker (LL), lecithin and hydrophilic linker (HL) at different oil to surfactant ratios. The loaded SDMEDS was prepared by dissolving the marker in SMEDS on a weight basis.

Fed-state simulated intestinal fluid (FeSSIF): The composition of the fed state simulated intestinal fluid (FeSSIF) used in this work is a slightly modified version of the USP formulation reported by Marques [40]. In a 1L graduated flask, sodium hydroxide was dissolved to a concentration of 101 mM, sodium chloride to a concentration of 203 mM, and glacial acetic acid to a concentration of 144 mM. Lecithin and sodium taurocholate were also added to a final concentration of 3.75 and 15 mM, respectively. The pH of the solution was 6.8.

Preparation of organogel: The SMEDS was used as the organic solvent for the gelators (β-Sitosterol and γ-Oryzanol in equal weight ratios). The gelators were added at varying amounts (1-30 wt. % of gel). The mixtures were heated in a temperature-controlled water bath to 90˚C and then maintained at that temperature until the gelators were fully dissolved in the oil phase,

producing a transparent/translucent solution. After vortex mixing, the samples were cooled down to room temperature where the system solidified over the course of 48 hours.

Differential Scanning Calorimetry (DSC): Thermal properties of gels were analyzed using a TA Instruments DSC Q100. Approximately 10 mg of organogel or dispersion samples and their references were placed into aluminum hermetically sealed pans. A nitrogen gas purge was used at 50mL/min. The thermographs were recorded over a temperature range of 20-90°C at a heating rate of 5°C/min. The nitrogen purge gas maintained at a flow rate of 50 ml/min. Organogel samples were tested using a heat-cool-heat cycle, where upon reaching 20°C after the cooling cycle, the system was kept isothermal for 5 minutes before commencing the second heating cycle. Dispersion samples were tested using single heating and cooling cycles.

Gel Rheology: A Carri-Med CSL2 Rheometer (TA Instruments, USA) was used to the rheology of the gels. A 4-cm stainless steel parallel-plate geometry was attached, and a newly prepared hot melted gel was poured onto the lower rheometer plate held at 90°C. The temperature of the lower plate was controlled via Peltier Plate. The platform was raised until a gap size of 200μm between the geometry and the lower plate was achieved, obtaining even sample distribution. The shear stress (τ), shear strain (γ) and frequency were kept constant at 75Pa, 0.001 (0.1%) and 10rad/s, respectively. All tests on gels were operated at shear strains within the linear viscoelastic (LVE) region. The dynamic moduli G' and G'' (Pa) were recorded during heating and cooling cycles as a function of temperature. For heating profile experiments, the molten gel at 90°C was poured on the controlled-temperature plate of the rheometer and set to be cooled to 20°C in 90 minutes, then left to rest at 20°C for another 90 minutes. At that point, the oscillatory experiment was commenced, and the sample was heated from 20°C to 90 °C at the rate of 0.78°C/min. For cooling profile experiments, the values of G' and G" were obtained as a function of temperature when

cooling the gel from 90°C to 20°C at two cooling rates: 0.78°C/min (cooling in 90 min) and at 1.56°C/min (cooling in 45 min).

Gel Firmness: A TA-XT2i Texture Analyzer (Stable Microsystems) was used to measure gel firmness (g) in gels. Gel solutions were heated to 90°C until a molten liquid was obtained and then poured in 20mL vials. The liquids were then cooled to room temperature and periodically and slowly stirred by hand until gelation occurred. Gels were allowed to rest for 48 hours before starting the texture analysis. A TA57-R (d=7mm)-1"R steel dye was used to penetrate the gel at 0.1mm/s to a depth of 10mm. Force was recorded as the peak or plateau gel strength. The measurement was limited to a maximum of 6000 g of compressive force.

Release test using solvent blue 35 as marker: 32+/-5 mg of melted gel (loaded with 5% w/w solvent blue 35) was poured into aluminum pans (6 mm diameter, 2mm height) and let to cool down and solidify at room temperature for 24 hrs. The disk-shaped gels were then placed in 1-dram glass vials and 3 mL of FeSSIF was added. The vials then placed into an isothermal shaker with 100 rpm and the temperature was adjusted to 37°C. At specific time intervals, the aqueous phase of the vials was removed for analysis and the vials were re-filled with fresh FESSIF. The absorbance of the collected samples was measured via spectrophotometry. The modeling of the data was processed by DDSolver software [41].

Release test using ibuprofen: A modified formulation of SMEDS formulation (LL:Lec:HL 90:5:5, D80:20) was prepared to prepared drug loaded G-SMEDS. This alteration was required to avoid phase separation during dilution as explained in section 3.4.1. The samples were made and treated as above, however, after removing the aqueous phase of the vials, they were diluted with acetonitrile (3X) to extract ibuprofen from micellar systems. The HPLC methodology to measure drug concentration from gelled SMED is explained in section 3.3.2.

Spectrophotometry and data processing: The concentration of the solvent blue dye was determined via its absorbance at 600 nm obtained with an Ocean Optic UV-VIS spectrophotometer (model HR2000). To minimize scattering, the samples were centrifuged and filtered. The spectra were recorded between 300 and 800 nm. The scattering profile between 300- 550 nm and 650- 800 nm was used to fit a polynomial curve corresponding to the baseline adsorption that account for the intrinsic scattering of the sample. The difference between the absorbance at 600 nm and the fitted baseline at 600 nm was used to determine the concentration of the solvent blue dye.

4.4. Results and Discussion

4.4.1. The effect of gelator concentration on gel strength

Figure 4-3 shows the relation between the gelator concentrations (from 12 to 20% w/w) and the gel firmness (F) and elastic modulus (G') of the SMEDS and polyglyceryl-3-polyricinoleate (PGPR) gels at 37 °C in heating ramps. The data in Figure 4-3 suggests that with increasing gelator concentration, the strength of the organogels of SMEDS and PGPR increases in the same way, as expressed via the elastic modulus (G') increases and the gel firmness (F). This observation can be interpreted as indicating that the strength of the gels is mainly dominated by the assembly of the gelators into fibrils, which seem to have similar mechanical properties in the different oils. This finding is consistent with that of Chung when comparing different polar oils [31] .

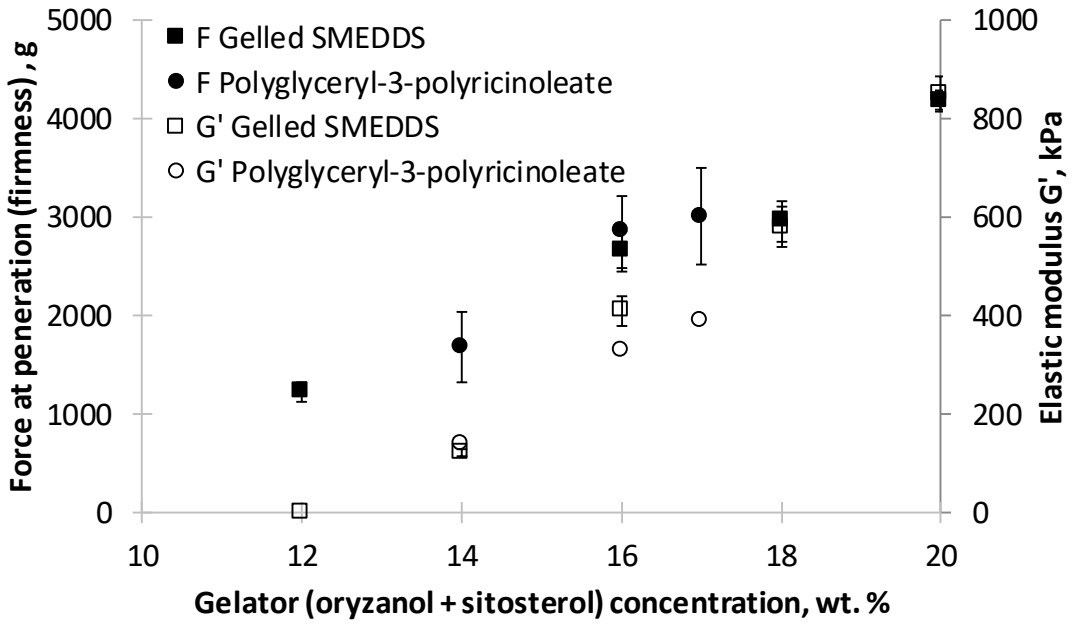

Figure 4-3. Gel firmness (force at the point of probe penetration, solid symbols) at 25°C and elastic modulus G' (open symbols) at 37°C obtained with D50 SMEDS and polyglyceryl-3-polyricinoleate gels as a function total gelator concentration (β-sitosterol + γ-oryzanol at 1:1 mass ratio). Data for polyglyceryl-3-polyricinoleate gels obtained from Chung [31].

One difference between SMEDS and PGPR organogels is that the range of gelator concentration for gel formation is broader for SMEDS. As mentioned in the introduction, the range of gelator concentration for gel formation depends on the polarity of the oil phase, as expressed via the HLB, and illustrated in Figure 4-1. To assess the HLB of the D50 SMEDS, the estimated HLB values for each of the individual components, presented in Table 4-1, can be used. These estimated HLB values were introduced after reviewing product data sheets of various surfactant suppliers. For the case of lecithin, HLB values ranged from 4 to 8, so an average of 6 was used. For ethyl caprate, no value was found in the literature, but its chemical structure is similar to medium chain triglycerides (MCT, HLB=0). Using the weight ratios of Table 4-1, the HLB of D50 SMEDS is expected to be close to 6, similar to that of propylene glycol monocaprylate. According to Figure 4-1, at HLB= 6 one tends to have the largest gelator concentration range for gel formation. This

large range was certainly observed for the D50 SMEDS system, but the minimum gelator concentration for D50 SMEDS gels was 12 wt.%, substantially lower than the 20 wt.% indicated in Figure 4-1. The maximum solubility of the gelator mixture could not be properly determined in D50 SMEDS because when adding 30 wt.% of total gelator concentration, although there is evidence of dissolution of the gelator, the solution becomes too viscous and mild agitation cause the formation of the gel even at high temperature.

4.4.2. Temperature-dependent gel properties

Figure 4-4 presents the shear rate required to maintain a constant shear stress 75 Pa during the rheology experiments. At low temperatures, that shear rate is low because of the large stress caused by the elastic (solid-like behaviour) and the viscous properties of the gel. However, as the gel losses its solid-like behaviour as it undergoes melting, a larger shear rate is required to maintain the stress constant. This sudden increase in the shear rate at a given temperature is here taken as evidence that the gel has reached its melting point. Conventional methods of identifying the melting point such as the temperature at the cross point between G' and G" or the onset of an endothermic peak in scanning calorimetry studies produced ranges of values that, although consistent with those of the transition shear rate method, were not as precise as those of the shear transition method.

Figure 4-5 presents the melting point obtained from Figure 4-4 (expressed as 1000 times the inverse of the absolute melting temperature in Kelvins) correlated to the molar fraction of the gelator (in natural log form) calculated using the sum of the molar fraction of the oryzanol and the molar fraction of sitosterol in the system.

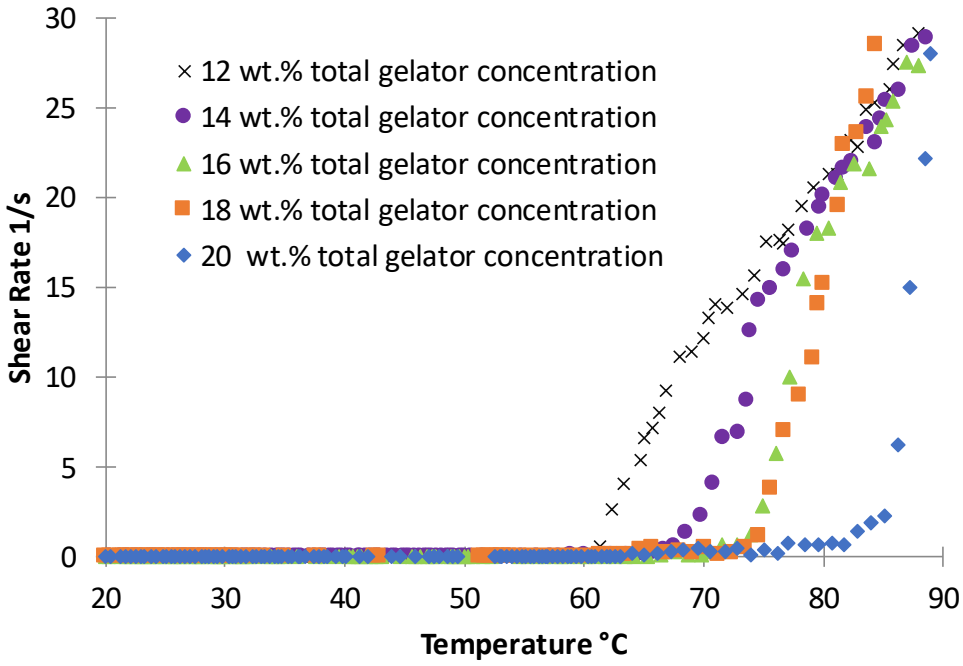

Figure 4-4. Shear rate required to maintain a total oscillatory stress of 75 Pa during the heating cycle experiments for D50 SMEDS organogels. Experiments conducted with a heating rate of 1°C/min, 10 rad/s, and 0.1% strain. The temperature at which the shear rate increases substantially (e.g. 85°C for 20% total gelator) is considered as a signature for the melting point of the gel.

The purpose of the plot of Figure 4-5 is to estimate the enthalpy of "melting" (or disassociation) of the gelator in the media of interest. To compare the results obtained in this work, the data obtained by Chung [31] and by Bot and Agterof [27] are included. The reason to include those two sets of data is that in both cases, the mass ratio of sitosterol and oryzanol was 1:1 and the molecular weight of the oil phase ranged between 500 and 800 g/mol, both of which are conditions similar to those used in this work. As evidenced by the data in Figure 4-5, the dependence of melting point on gelator concentration is very similar for all the three systems, suggesting that despite the differences in the polar nature of the three different oils, the self-assembly of the gelators in the oil occurred in a similar fashion and with a similar enthalpy of association/dissociation. The enthalpy of melting or dissociation, calculated by Bot and Agterof as $\Delta Hm = -R*(\partial \ln(x)/\partial(1/T))$ was

estimated as 26 kJ/mol [28]. Using the slope of Figure 4-5 (corresponding to $\partial \ln(x)/\partial(1000/T)$) for D50 SMEDS, the estimated enthalpy of dissociation is 22 kJ/mol. As suggested by the positive sign of the enthalpy, the dissociation process is endothermic and should be identifiable in a scanning calorimetry experiment.

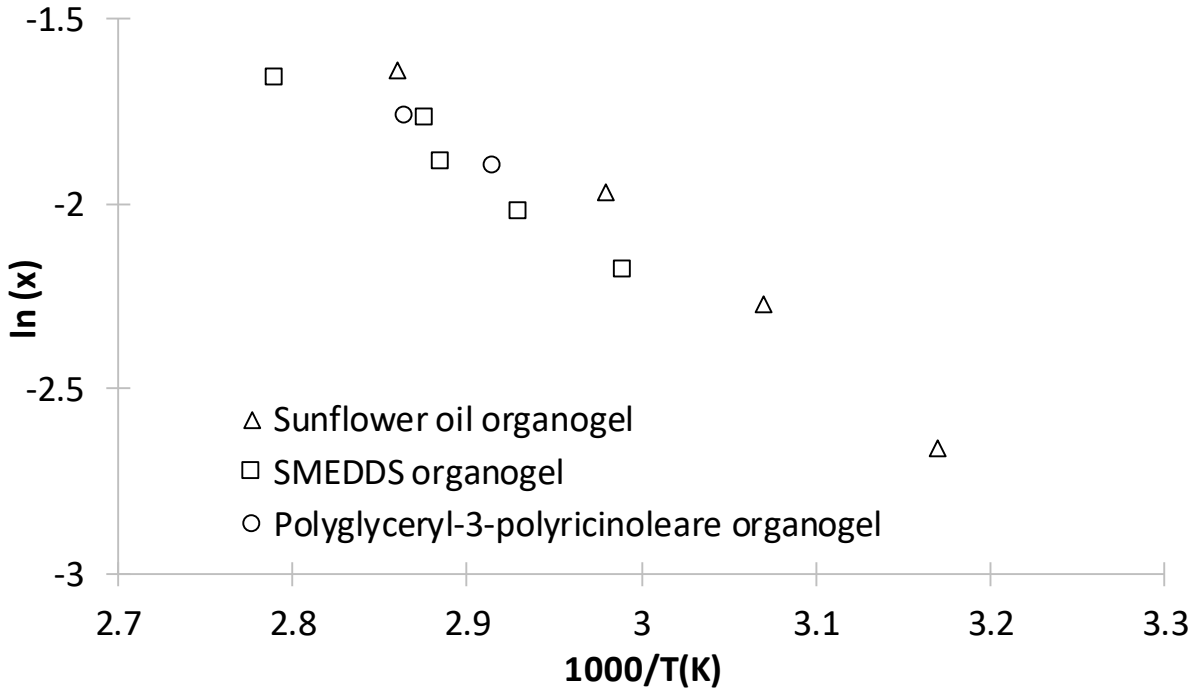

Figure 4-5: Effect of gelator concentration (expressed as ln(x), the natural log of the sum of the molar fraction of β-sitosterol and γ-oryzanol) on the melting temperature of the gel (expressed as 1000 times the absolute melting temperature in Kelvins, or 1000/Tm) for gels prepared with β-sitosterol + γ-oryzanol at 1:1 mass ratio and D50 SMEDS, polyglyceryl-3-polyricinoleate, and sunflower oil gels as oil phases. Data for polyglyceryl-3-polyricinoleate gels obtained from Chung [31]. Data for sunflower oil obtained from Bot and Agterof [27].

To confirm the presence of an endothermic peak when heating the organogel (a signature of the dissociation of gelator fibrils), DSC studies for 18 and 20 wt.% total sterols were conducted on D50 SMEDS gels during heating (dotted line) and cooling (solid line). Figure 4-6 presents those findings. The endothermic peaks for gelator dissociation were observed in the range of 65-75 °C for 18 and 20 wt.% gelator concentration. The melting temperature for 18 wt.% gelator, according

to Figure 4-4, is 75°C which is consistent with the temperature at the maximum heat flow for that peak. However, for the 20 wt.% gelator the melting temperature from Figure 4-4 is 85°C, but the temperature at the peak heat flow for that system is only 72°C, which further illustrates the reason why the shear rate transition point was used to identify the melting point for these systems.

Another important feature of the melting peaks in Figure 4-6 is their broad nature, nearly spanning 20°C at their base and without a sharp peak that could easily identify the onset of dissociation. The peaks obtained by Chung were nearly 10°C at their base, when using propylene glycol monocaprylate (MW ~ 200 g/mol), and did present a relatively sharp peak with a more definite melting point. Bot et al (ref. 24) obtained broad peaks (more than 20°C at their base) when using various triglycerides as oil phases. It is possible that the relatively high viscosity of triglycerides and D50 SMEDS, as compared to propylene glycol monocaprylate, might have influenced the dynamics of the melting process. Furthermore, all the mixtures presented a symmetric signature pick at 39±5˚C during heating/cooling, even at 5% gelator (data not shown) when the mixture is still in liquid state. The fact that the signature peak is present regardless of the physical state of the sample led us to conclude that this peak cannot be associated with the formation of the organogel, and instead, it may correspond to the crystalline structure of the sterols. Sitosterol monohydrate is the most stable in temperatures below 45 °C and converts to hemi-hydrate at 45°C [42,43].

Finally, another important feature of the cooling thermograms in Figure 4-6 is that the exothermic peak for the re-formation of the gel fibrils upon cooling at 5°C/min is largely missing, meaning that the conditions were not appropriate (particularly providing enough time, and some shear to facilitate the formation of the gel) to induce the re-formation of the gel.

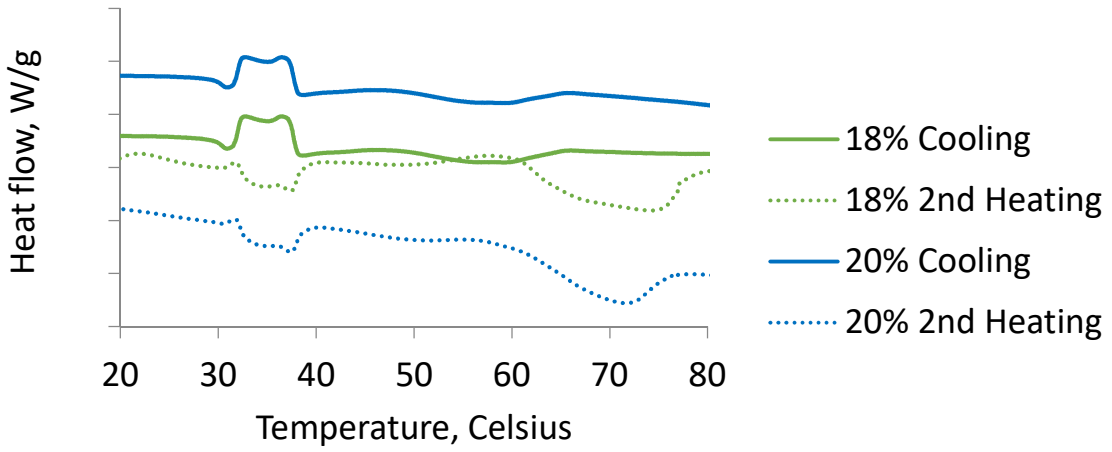

Figure 4-6. Heating and cooling scanning calorimetry thermograms for D50 SMEDS organogels prepared with 18 and 20 wt % total gelator concentration (β-sitosterol + γ-oryzanol at 1:1 mass ratio). Curves were obtained at 5°C/min. each segment in y axe corresponds to 0.02 w/g of heat flow.

To further understand the rheological behaviour of the gelled D50 SMEDS, the changes in G' and G" of the gels during heating from 20 to 90°C were monitored and the results are plotted in Figure 4-7 and Figure 4-8, respectively**.** The data in Figure 4-7 shows that the value of G' tends to increase with increasing gelator concentration but at 18 and 20 wt.% total gelator, the gel strength seems to approach a plateau near 1000 kPa. The work of Chung also shows that with polar oils the oryzanol-sitosterol gels, but in that case the plateau value was near 500 kPa. The largest G' value obtained for oryzanol-sitosterol gels was reported by Sawalla et al. [42] who obtained 2500 kPa when using 16% total sterols at ratios of 4:6 sitosterol: oryzanol in sunflower oil. However, these high G' values reduced to about 10 kPa or less at 40°C and even lower temperatures for systems with lower gelator content. All the gels in Figure 4-7 show a step-wise decrease in their G', one around 40 to 50°C and a more pronounced reduction (on log-scale bases) at temperatures ranging from 60 to 80°C, consistent with the endothermic melting peak in DSC studies (Figure 4-6) and the melting temperatures identified through the shear transition studies (Figure 4-4).

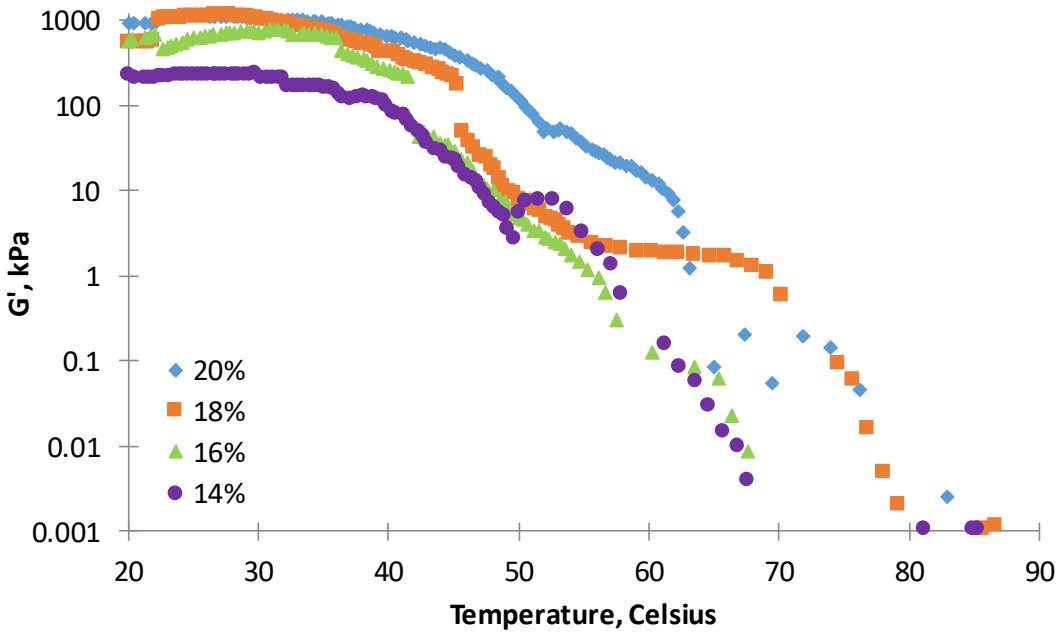

Figure 4-7. Elastic modulus (G') obtained during the heating cycle experiments for D50 SMEDS organogels with total gelator concentration (β-sitosterol + γ-oryzanol at 1:1 mass ratio) ranging from 14 to 20 wt%. Experiments conducted with a heating rate of 0.8 °C/min , 10 rad/s, and 0.1% strain.

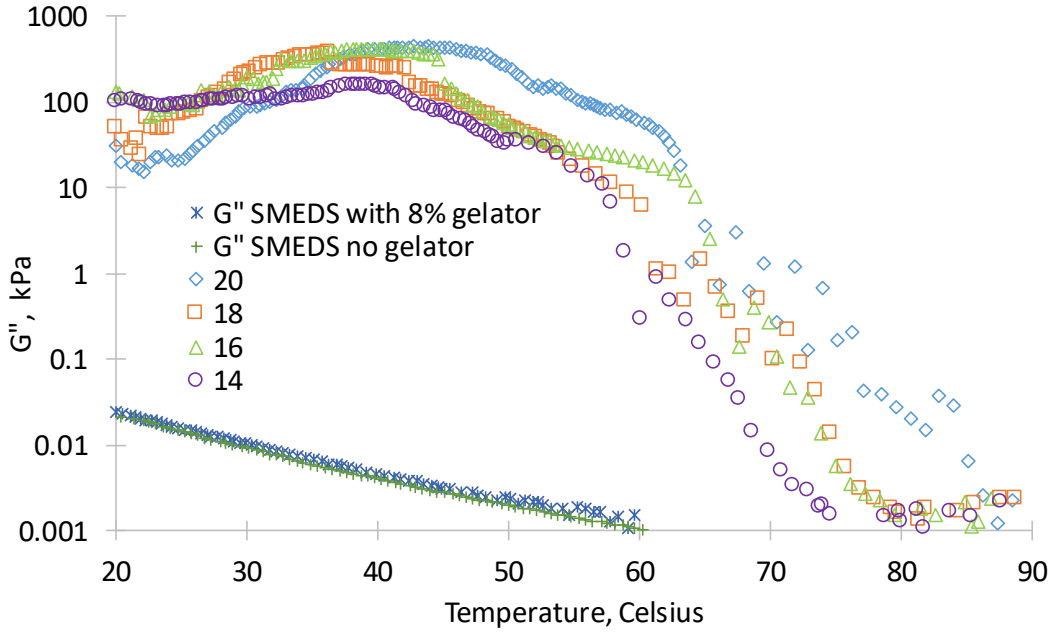

Figure 4-8. Loss (viscous) modulus (G") obtained during the heating cycle experiments for D50 SMEDS organogels with total gelator concentration (β-sitosterol + γ-oryzanol at 1:1 mass ratio) ranging from 14 to 20 wt%. Experiments conducted with a heating rate of 0.8 °C/min, 10 rad/s, and 0.1% strain.

An unexpected result obtained from these studies is the large values of the loss modulus, G", as indicated in Figure 4-8. In all the previous studies in the literature, including the polar oils explored by Chung, the value of G" is substantially lower, by at least one order of magnitude, than the values of G'. In this work, at temperatures ranging from 30 to 50°C the value of G" tends to reach a maximum, and the ratio between G'/G" tend to reduce to values less than 1 at temperatures ranging between 40 to 50°C. Although strictly speaking this cross-over temperature (where G'=G") should be considered the melting of the gel, the DSC studies do not show a structural transition within this temperature range. The onset of melting is closely associated with the temperature range, between 60 and 80°C, where both G' and G" are drastically reduced. These observations are consistent with the findings of Han et al [44] where they observed that introducing lecithin to sitosterol-sunflower oil organogels increased the melting temperature of the organogel to 70 – 80°C, which seemed to correlate with an increase in the length of the crystalline structures formed by the gel.

Figure 4-8 also includes the values of G" for a D50 SMEDS with no gelator and with 8% gelator (below the minimum gelator concentration for gel formation). For those systems, the values of G' were zero and there was no significant difference in G" between 0 and 8% gelator. These intrinsic G" values of the SMEDS system cannot explain the large G" values in the organogel, suggesting that the interactions between the gelator and SMEDS are responsible for the high G".

To assess the dependence between the mechanical properties of the gel during cooling and the cooling rate, Figure 4-9 presents the G' data for D50 SMEDS produced with 14, 16 and 18 wt.% total gelator when the gels were cooled at 0.8°C/min (90 minutes cooling) and 1.6°C (45 minutes cooling). The G' values in Figure 4-9 are lower than those obtained in Figure 4-7 for a gel that was

left to cool down and stay at room temperature for an additional 90 min before being melted. During cooling, the gels form at temperatures ranging from 40 to 60°C, well below the melting point. These discrepancies among cooling and heating cycles and the effect of cooling rate are in agreement with similar studies conducted on hydrogels [37] and organogels [38].

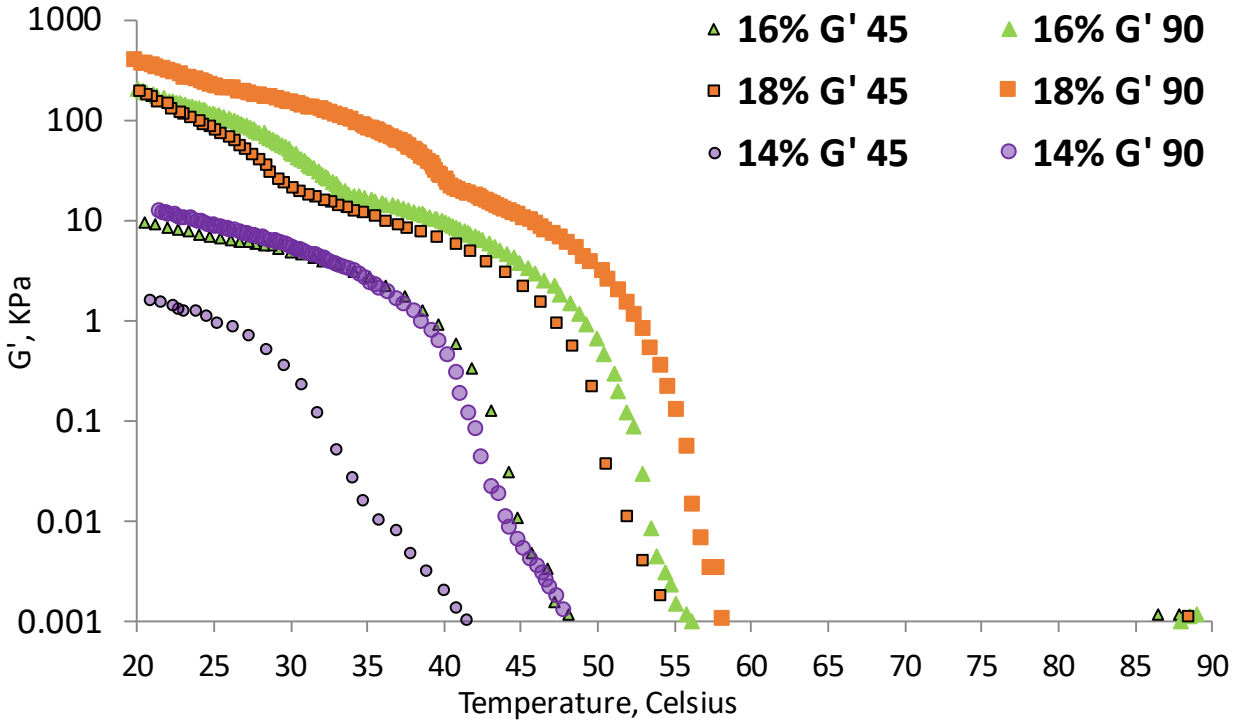

Figure 4-9. Elastic modulus (G') obtained during the cooling cycle experiments for D50 SMEDS organogels with total gelator concentration (β-sitosterol + γ-oryzanol at 1:1 mass ratio) ranging from 14 to 18 wt.%. Experiments conducted with a cooling rate of 0.8°C/min (90 min cooling) and 1.6°C/min (45 min cooling), 10 rad/s, and 0.1% strain.

As it will be evident in the release studies, having gels with large G' and G" is important to impart the desired controlled release properties. The insights offered by the trends in Figure 4-9 prompted us to use slow cooling, simply leaving the gels to rest at room temperature for 48 hours to guarantee the largest G' and G" possible for our systems. Under these slow cooling conditions, we determined that below 10 wt.% total gelator, the phytosterol did not form a gel, and gels produced with 12 wt.% gelator only produced weak gels after 2 days. Increasing gelator concentration reduced the gelling time at room temperature. As indicated earlier, when trying to formulate gels

with more than 22 wt.% gelator, the gel started to form even at the 90°C used to melt sitosterol and oryzanol.

To illustrate the process of gel formation, Figure 4-10 presents polarized light micrographs of a drop D50 SMEDS containing 16 wt.% total gelator that was initially placed at 90°C on a glass slide and was left to cool in ambient air. Initially, the liquid gel shows no specific structure, but over 90 minutes, various growing crystalline structures assemble, forming a three-dimensional gel network. Figure 4-10 also includes a picture of one crystal, which has the typical Maltese cross feature of spherulite structures. These types of spherulite structures have been seen before in various organogels, particularly gels formed with sterols [45,46]

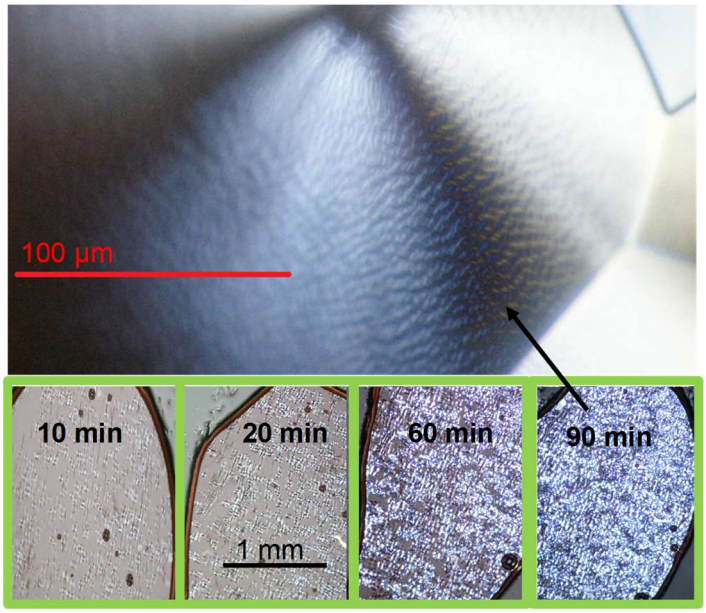

Figure 4-10. Time-lapse polarized light micrographs of a D50 SMEDS gel containing 16 wt.% total gelator. The bright spots are growing crystalline structures formed by the gelator that eventually meet after 90 minutes. The enlarged image corresponds to one crystal displaying the Maltese cross signature of spherulite structures.

4.4.3. Effect of sterols on SMEDS phase behaviour

Figure 4-11 presents a pseudo-ternary phase diagram showing the phase behaviour of D50 SMEDS containing 0 to 30 wt.% total gelator upon dilution with FeSSIF. For systems containing less than 10 wt.% total gelator, the D50 SMEDS – gelator system produces a viscous liquid that can be diluted with FeSSIF (aqueous phase). The series of vials pictured at the bottom of Figure 4-11 shows the progressive dilution of D50 SMEDS in the absence of gelator. The fact that all the systems display a single phase throughout the dilution indicates that in the absence of the gelators the D50 SMEDS is fully dilutable. However, the SMEDS containing 5% gelators rejects excess aqueous phase once the FeSSIF content is greater than 30%

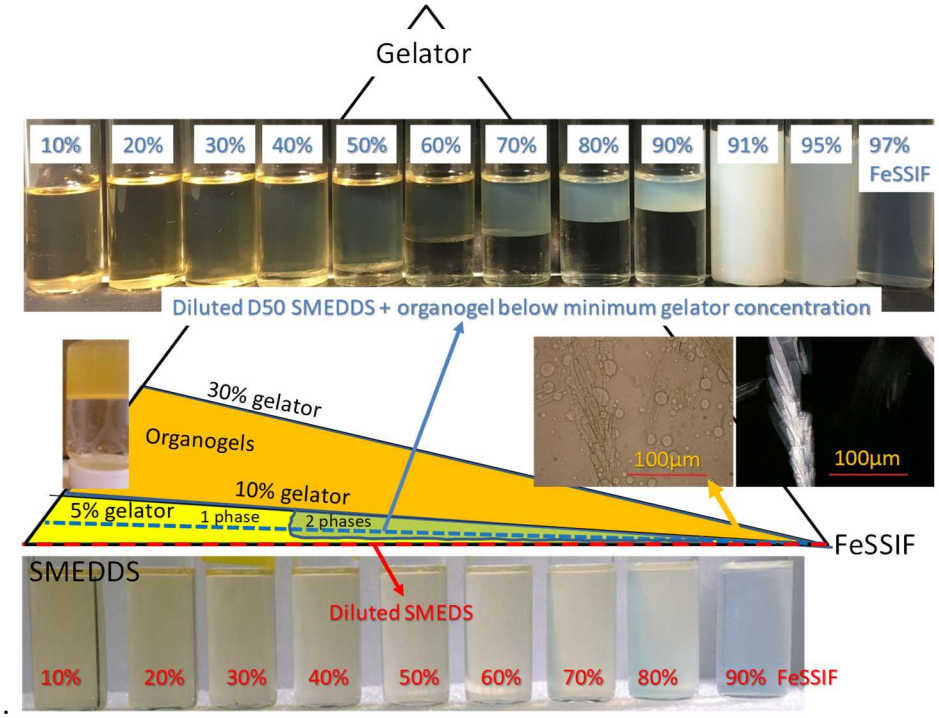

Figure 4-11. Pseudo-ternary phase diagrams of D50 SMEDS (left lower vertex), fed-state simulated intestinal fluid (aqueous phase, lower right vertex) and total gelator concentration (top vertex, β-sitosterol + γ-oryzanol at 1:1 mass ratio). The lower set of vials present the dilution line of SMEDS without organogel. The top set of vials correspond to the dilution line of the SMEDS containing 5% gelator. The micrographs (transmitted and cross-polarized light) correspond to a hot (liquid) D50 SMEDS system containing 16% gelator emulsified in FESSIF.

The rejection of the aqueous phase during the dilution suggests that the addition of the sterols induced a hydrophobic shift in the formulation. In terms of HLD, this would correspond to a positive shift in the HLD, as described in Chapter 3 [47], which is likely the result of the polar nature of the sterols. SMEDS systems with more than 10 wt.% total gelator form organogels. The exposure of already formed (solid) organogels to FeSSIF will be discussed in the next section. However, to generate the diagram of Figure 4-11, hot melt (liquid) mixtures of D50 SMEDS and gelators (from 10 to 32 wt.%) were emulsified in FeSSIF. The resulting systems also have gel-like properties, but different from the original SMEDS organogels where the sterol fibers arrange into spherulite structures, the emulsified hot melt produce a network of sterol hydrates (bright particles in the polarized light - darkfield - micrograph in Figure 4-11) where the aqueous phase is the continuous phase and the SMEDS remains as emulsified drops (drops in transmitted light – bright field – micrograph) within the gel.

4.4.4. Self-emulsification of SMEDS and organogel SMEDS

To observe the self-emulsification behaviour of SMEDS in liquid and gelled states, a small drop of SMEDS or gelled SMEDS containing solvent blue dye was placed on a glass slide, followed by the addition of a few drops of FeSSIF around the SMEDS or gelled SMEDS drop, as illustrated in the schematic of Figure 4-12a. Figure 4-12b shows time-lapse images taken immediately after the addition of water to the D50 SMEDS drop. During the process of self-emulsification, no external shear was introduced and the drops of FeSSIF were carefully placed to avoid disrupting the original drop. The experiment was repeated several times and although Figure 4-12b only shows one of the self-emulsification sequences, they all seem to be initiated by the formation of “fingers” that resemble the finger formation in the “tears of wine” phenomenon. The formation of tears of wine

has been linked to Marangoni effects, which results from inhomogeneities in surface tension. Here the concept would be similar, but referring to the interfacial tension between SMEDS and FeSSIF instead. López-Montilla et al.[48] reviewed the various proposed mechanisms of self-emulsification and identified three potential routes, the first one is interfacial turbulence which is consistent with the description of Marangoni stresses, and is often associated with the formation of streamers, much like those observed in Figure 4-12b. Another mechanism of self-emulsification is the "diffusion and stranding" where a solvent A (soluble in solvent C) carrying solute B (insoluble in solvent C) is placed in contact with solvent C and as the solution of solvent A penetrates solvent C, an insoluble liquid phase containing solute B is formed in the form of an emulsion. Although some articles use this mechanism to explain self-emulsification, this is not relevant for the SMEDS indicated in this work as they are fully solubilized in FeSSIF. Another more controversial mechanism is called the negative interfacial tension driven the process, and might be best characterized as an interfacial tension driven mechanism which differs from the interfacial turbulence in that no streamers are formed, but instead small drops that form a cloud around the interface. Although eventually a cloud is formed around the original location of the SMEDS drop (after 1 minute), these small drops seem to be produced during a second phase of the self-emulsification process.

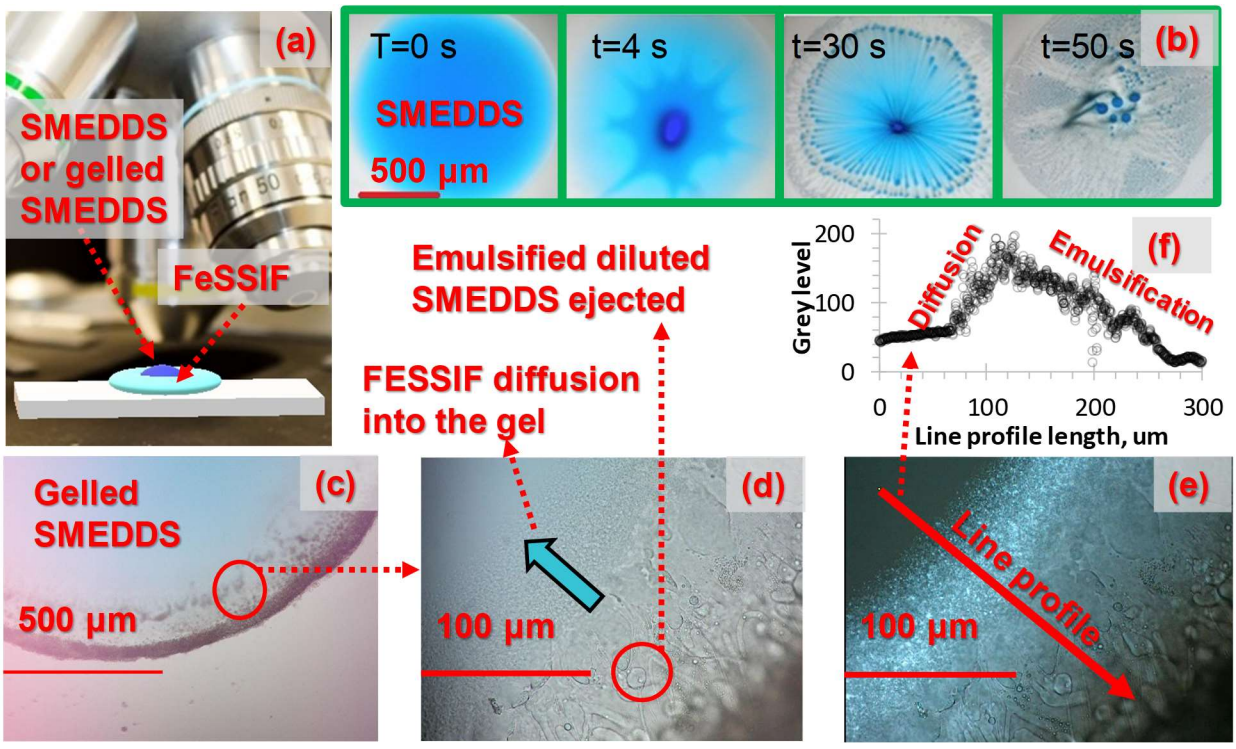

Figure 4-12. Self-emulsification in SMEDS and gelled SMEDS. Experimental setup (a). Time-lapse micrographs of D50 SMEDS self-emulsification (b). Gelled D50 SMEDS with 14 wt.% total gelator after 3 minutes of contact with FeSSIF (c). Transmitted light (bright field) magnified on the self-emulsification front of the gelled SMEDS (d). Polarized light (darkfield) magnification (same as image d) showing the orientation of the line profile (e). Gray level across the line profile of image e (f).

For the gelled SMEDS, a drop of a hot melt of D50 SMEDS (14 wt.% gelator) was allowed to solidify on the glass slide and its interaction with water was monitored. Unlike liquid SMEDS, the dissolution process did not begin immediately. After the addition of water, the edge of the gel starts to expel a stream of droplets (small specs in the aqueous phase in Figure 4-12c). The blue region in the magnified image (50X, Figure 4-12d) and in the drop of Figure 4-12c correspond the solvent blue dye in the gelled D50 SMEDS. The grey areas in Figure 4-12c and 4-12d correspond to the gelator network where SMEDS has been already released and FeSSIF has penetrated. A closer inspection of Figure 4-12c reveals two regions around the edge of the emulsification front, one inner region where FeSSIF is diffusing into SMEDS, and one outer region where the diluted SMEDS, which forms a separated phase as indicated in Figure 4-11, is emulsified and ejected from

the edge of the gel. Figure 4-12e presents an image of the same region presented in Figure 4-12d, but using polarized light. The bright regions in Figure 4-12e correspond to the formation of sterol hydrate crystals that are produced because of the direct contact of sterols and FeSSIF. To quantify the penetration of water from FeSSIF in the gelled SMEDS, Figure 4-12f presents the gray level profile of the line drawn in Figure 4-12d. The larger the gray level value, the brighter the spot in Figure 4-12d. The gray level profile of Figure 4-12f further supports the hypothesis of a two-region front, an aqueous diffusion region and an emulsification region. According to Figure 4-12f, the diffusion thickness is approximately 45μm in length.

4.4.5. In vitro release from SMEDS organogel

Based on the videomicroscopy studies of self-emulsification (Figure 4-12), a hypothesis was formulated that the diffusion of water (in FeSSIF) into the organogel is the limiting step of the process. Diffusion in hydrogels is often limited by using a small gel mesh size, making it small enough to be similar in size to that of the diffusing molecule. In gelled SMEDS the concentration of gelator in organogel is relatively small. Considering the high minimum gelator concentration (~10 wt.%), and that the gelator fiber bundles are relatively large in diameter (~ 1-10 μm strands radiating from the center of the spherulite structure in Figure 4-10), one concludes that the space in between the fibers is in the order of microns, much larger than the size of water molecules trying to diffuse into the gel. The other way to change the diffusivity of the molecules is by changing the viscosity of the gel. The Wilke-Chang equation (an empirical correlation based on the Stokes-Einstein equation) can be used to predict the diffusivity of water in polar oils [49]:

$$D = 7.4 \cdot 10^{-8} \cdot (\psi_B \cdot M_B)^{0.5} \cdot \frac{T}{\mu (V_A)^{0.6}} \qquad \textbf{4-1}$$

where D is the diffusivity in cm^2/s, ψ_B the solvent association factor (assumed to be 1 for most organic solvents), M_B the solvent molecular weight, T the temperature of the system in Kelvins, μ the viscosity of the system in mPa*s, and V_A the molar volume of the solute in cm^3/mol.

According to Eq. 4-1, if one can manage to increase the viscosity of the system (μ), this should result in a reduction in the diffusion coefficient. To increase viscosity in gelled SMEDS there are two avenues, increasing the inherent viscosity of the oil and surfactants in SMEDS, or increasing the viscous loses in the gel structure. For most organogels, the latter would not be possible because the viscous loses, even in other forms of sterol organogels, tends to be substantially small when compared to the elastic component [31]. However, the SMEDS organogels have a significant viscous (loss) modulus, G", as illustrated in Figure 4-8. To investigate the effect of gelator concentration on the release rate from gelled SMEDS, 14 wt.% (G" ~140 kPa) and 18wt% (G" ~320 kPa) total gelator systems were considered. To evaluate the potential effect of the intrinsic viscosity of the SMEDS systems, two different SMEDS systems were considered, the D50 SMEDS investigated throughout this work, and an additional D70 SMEDS (70% surfactant + linkers, 30% oil) that had a larger viscosity. The viscosity of the D50 SMEDS was measured to be 73 mPa*s while the D70 SMEDS had a viscosity of 980 mPa*s.

The gelled SMEDS were loaded with solvent blue 35 dye to quantify the release from the gelled SMEDS. Because the dye is insoluble in water, it could only be released if the SMEDS was released from the gel and diluted with the FeSSIF solution. A hot melt of the gel was poured on a 6-mm aluminum pan. After 24 hours of cooling at room temperature, the pan containing the gelled SMEDS (~ 32 mg) was placed in a vial filled with 3 ml FeSSIF (dilution ratio ~ 100) and orbitally shaken at 100 rpm controlled temperature (37 ºC). Every time a sample was taken, the entire fluid were replaced with a fresh FeSSIF solution. Although this practice was meant to maintain sink

conditions, is important to keep in mind that the SMEDS is fully dilutable at dilution ratios of 10 or larger, thus the release is not expected to be limited by the solubilization of SMEDS in FeSSIF. The endpoint of the release (100% release) process was considered to be when no residual gel SMEDS was observable, and no solvent blue 35 peak was observable in the collected FeSSIF. Figure 4-13 presents the fractional release of gelled SMEDS prepared with 14 and 18 wt.% total gelators and using D50 and D70 SMEDS as gelled organic phase.

According to the data in Figure 4-13, we can confirm that the release from SMEDS organogels produces an extended release profile. Instead of a burst SMEDS release occurring on the span of a few minutes, the gelled SMEDS release over the course of four days. The substantial increase in viscosity obtained when changing the SMEDS composition from D50 to D70 did not produce substantial changes in the release profile, suggesting that the viscosity of the organic phase used as a continuous phase of the gel, at least for SMEDS organogels, does not represent an important factor in the mechanism of release. On the other hand, increasing the total gelator concentration from 14 to 18 wt.% doubled the release time.

To explore the hypothesis of diffusion-controlled mechanism, the early time-release period was considered. According to the hypothesis, the rate-limiting step is the diffusion of water through the gelled SMEDS. Therefore, the rate of mass transfer of water ($\mathring{m}_{water}$) through the surface of the gel in contact with FeSSIF in the early stages of release could be estimated using Fick's first law:

$$\mathring{\boldsymbol{m}}_{\boldsymbol{water}} = \boldsymbol{A}_{\boldsymbol{gel}} * \boldsymbol{D}_{\boldsymbol{app}} * \frac{\boldsymbol{C}_{\boldsymbol{w}_{\boldsymbol{emulsification}}} - \boldsymbol{C}_{\boldsymbol{w}_{\boldsymbol{gel}}}}{\boldsymbol{L}_{\boldsymbol{diff}}} \qquad \textbf{4-2}$$

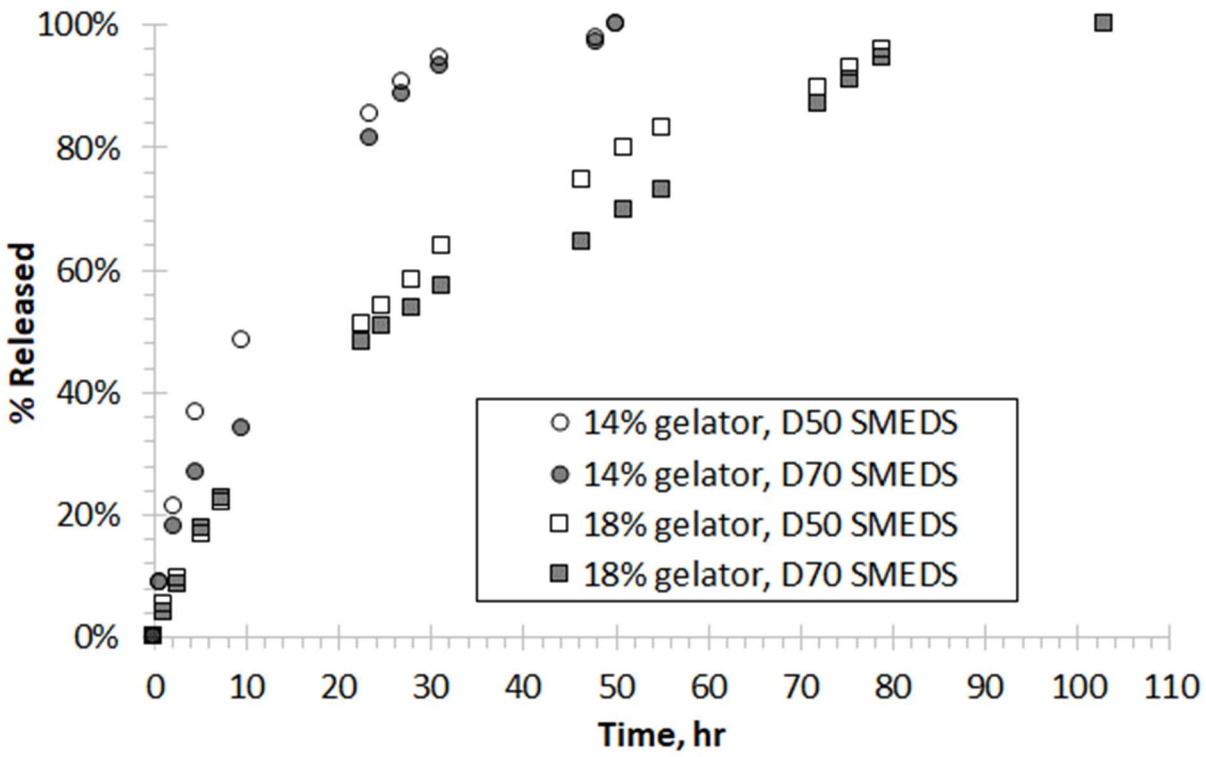

Figure 4-13. The fractional release of solvent blue 35 from D50 SMEDS (open symbols) and D70 SMEDS (filled symbols) in organogels with total gelator concentration (β-sitosterol + γ-oryzanol at 1:1 mass ratio) of 14 wt.% (circles) and 18 wt% (squares). The system remained at 37°C throughout the experiment and the vials.

where A_{gel} (cm^2) is the surface area of the gel in contact with FeSSIF, calculated on the bases of a 6.2 mm diameter disk. D_{app} (cm^2/s) is the apparent diffusivity of water in the gel, which in this case is fitted to the initial release data. $C_{w,emulsification}$ is the concentration of water at the emulsification front of the gel. To estimate $C_{w,emulsification}$ we can consider that according to Figure 4-11, after the water content in SMEDS reaches more than 30%, then the SMEDS would produce a separate phase (emulsify), which would then lead to the emulsification step observed in Figure 4-12. Thus one can estimate $C_{w,emulsification} \sim 0.3$ g/cm^3. In the undiluted edge of the diffusion region in Figure 4-12, then the concentration of water in the gel $C_{w,gel} \sim 0$ g/cm^3. From the line profile in Figure 4-12f, one can estimate a diffusion length (L_{diff}) of approximately 45 μm (4.5E-3 cm), which

may be applicable to the early stages of diffusion as this was determined within the first 5 minutes of release. The value of $\mathring{m}_{water}$ from Eq. 4-2 can be turned into a value of $\mathring{m}_{SMEDS}$ emulsified, once again considering the emulsification boundary of Figure 4-11, whereby 7 parts of SMEDS emulsify for every 3 parts of water that penetrate the SMEDS, in which case $\mathring{m}_{SMEDS} \sim (7/3)*\mathring{m}_{water}$. The early time fractional release can then be considered as $\sim (7/3)*\mathring{m}_{water}*$release time/$m_{SMEDS\ initial}$. Using this approach, the first release point was used to fit the apparent diffusivities (D_{app}) of the 14 and 18 wt.% gels produced with D50 SMEDS, obtaining $D_{app} \sim$ 2.5E-8 cm^2/s and 8.3E-9 cm^2/s, respectively. These fits are illustrated in Figure 4-14a.

To extrapolate the findings to late stages we need to consider that the diffusion length L_{diff} would increase with time, where $L_{diff} \propto \sqrt{(D_{app}*\text{time})}$. There are several models that consider diffusion, but one that is particularly relevant is the shrinking core, diffusion-controlled, ash model for plates, that when considering diffusion from one side, the corresponding release equation would be [50]:

$$X_B = \sqrt{t \cdot \left(C_{SMEDDS,gel} \cdot \frac{L^2}{2b \cdot D_{app} \cdot C_{w,emulsification}} \right)} \qquad \textbf{4-3}$$

where t is the release time, $C_{SMEDS,\ gel}$ is the concentration of SMEDS in the organogel (0.86 and 0.82 g/cm^3 for 14% and 18% organogel, respectively), L is the thickness of the gel in the aluminum pan (0.12 cm), b is the ratio of SMEDS mass released to water that diffuses in (70/30), and D_{app} and $C_{w,\ emulsification}$ is the same terms introduced earlier.

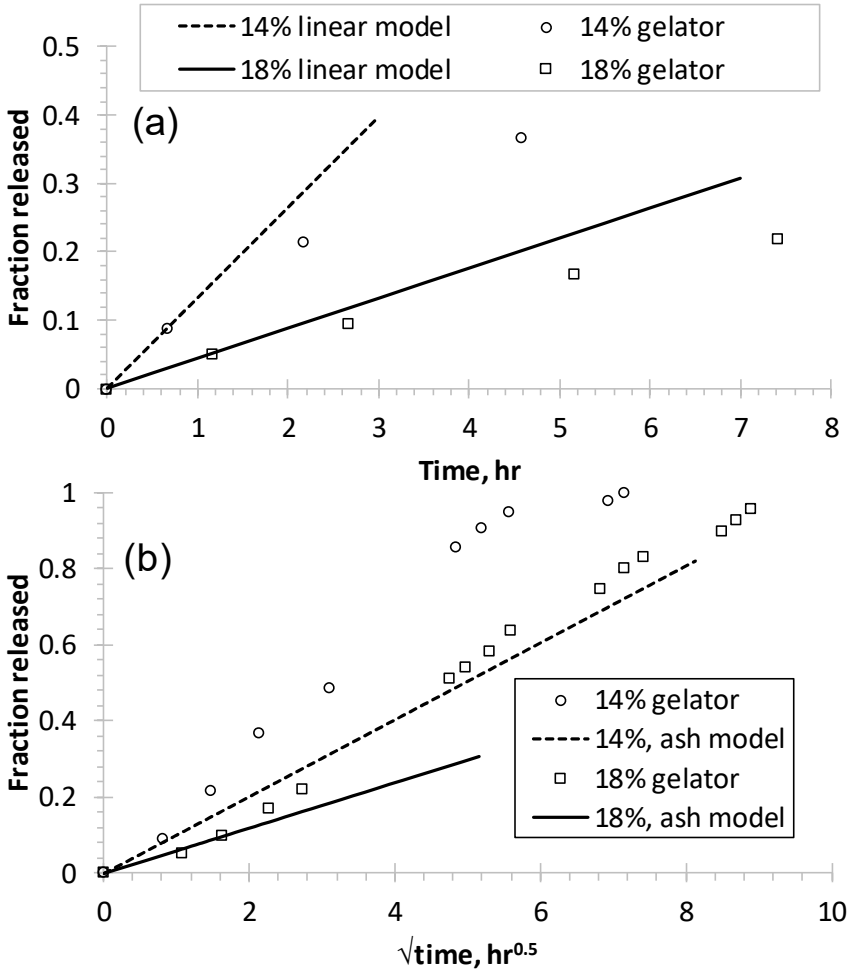

Figure 4-14: The fractional release of solvent blue 35 from D50 SMEDS (open symbols) and D70 SMEDS (filled symbols) in organogels with total gelator concentration (β-sitosterol + γ-oryzanol at 1:1 mass ratio) of 14 wt.% (circles) and 18 wt% (squares). The system remained at 37°C throughout the experiment and the vials.

Using Eq. 4-3, the values of D_{app} fitted using the early time release, and the parameters previously introduced, then the release profile of SMEDS can be predicted. These predictions are shown in Figure 4-14b, where the predicted profiles match the experimental data at the early stages of release, but under-predict the release at later times. There are several potential explanations for the under-prediction, the first is that the prediction assumes release only from one side, but it has been observed that over time the gel detaches from the aluminum pan, exposing greater surface area.

The second explanation is that, over time, the skeleton of the gel, considered constant in the ash model, is eroded during the release process, thus the length L in Eq. 4-3 becomes smaller as the release progresses. These observations suggest that although diffusion is an important part describing the release profile, the erosion of the organogel matrix also plays a role in the process.

Through the discussions above one concludes that although the SMEDS formulation is a lipid-based delivery system, and the gelled SMEDS is an organogel, the self-emulsification mechanism requires for water to diffuse into the gel to initiate the release process. This water-mediated diffusion and release is similar to that experienced by hydrogels, through the processes of matrix swelling, diffusion and erosion [51]. Lee developed analytical solutions for combined diffusion and erosion, that for situations where the amount dosed could be completely dissolved in the receiver solution (the condition of this work), the following fractional release expression applies [52]:

$$X_B = \sqrt{\frac{4}{3}\tau} \cdot + \left(\frac{Ba}{D_{app}}\right)\tau \qquad \textbf{4-4}$$

where τ is a dimensionless time, calculated as $\tau = D_{app} \cdot t/a^2$, where D_{app} and the release time "t" were introduced earlier, "a" is the half thickness of the planar membrane (disk in this case), and "B" is the erosion rate, having units of velocity.

The evaluation of the fractional release with Eq. 4-4 is presented in Figure 4-15. The values of B and D_{app} were fitted for D50 systems prepared with 14% and 18% gelator. For the 14% gelator, D_{app} ~ 1.5E-8 cm^2/s, and B~ 1.2E-7 cm/s (R^2=0.996). For the system of 18% gelator, D_{app} ~ 6.0E-9 cm^2/s, and B~ 4.6E-8 cm/s (R^2=0.982). The values of D_{app} obtained with the combined diffusion and erosion model were 40% smaller than the ones obtained with the linear diffusion model used at early release time, which is consistent with the idea that part of the release experienced, even at early time, would have been associated with erosion. The relative importance of erosion over

diffusion is assessed via the parameter $B \cdot a/D_{app}$. For the 14% organogel system, that value was $B \cdot a/D_{app}=0.47$, and for the 18% organogel system was $B \cdot a/D_{app}=0.46$. The fact that $B \cdot a/D_{app}$ was almost the same for both gelator concentrations explains why the two curves overlap in Figure 4-15, and it also suggests that increasing the gelator concentrations reduces, to the same extent, the erosion rate and apparent diffusivity. The connection between gelator concentration and erosion rate can be explained by the fact that more gelator means more fibrils in the gel, increasing its strength and resistance to erosion. The connection between gelator concentration and the diffusivity of water in the gel could be explained if the viscosity of the gel increases with gelator concentration. This last statement can be evaluated considering that the viscous losses are G"~140 kPa for 14 wt.% D50 SMEDS and G"~320 kPa for 18 wt.% D50 SMEDS. The apparent viscosity of the gel can be estimated as $G"/\omega$, where ω is the angular velocity (10 rad/s). In other words, the viscosity of the 14 and 18 wt.% systems are 14 and 32 kPa·s, respectively. The diffusivities predicted with these viscosities and the Wilke-Chang equation (assuming $M_B \sim 500$ g/mol) are very small, 6.2 E-12, and 2.7E-12 cm^2/s for 14 and 18 wt% gelator, respectively. Although these diffusivities are substantially smaller than D_{app}, it is important to keep in mind that as the water dilutes the SMEDS in the gel, the viscosity should reduce and the diffusivity increase. Throughout this dilution process the diffusivity obtained with 18wt% gelator is expected to be smaller than that obtained with the 14 wt% system.

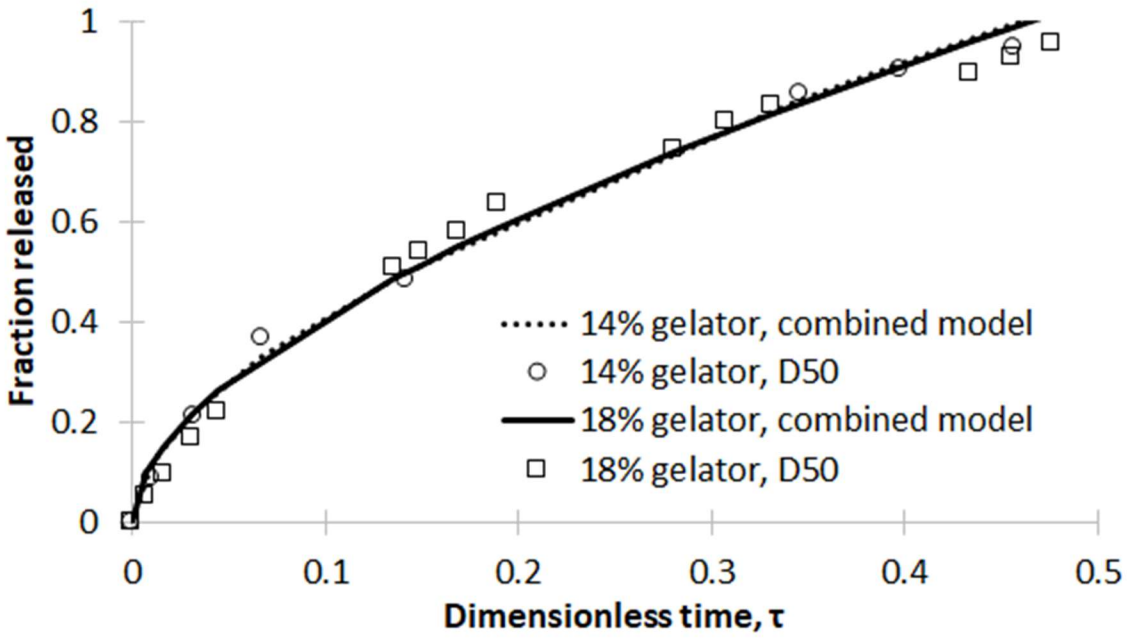

Figure 4-15: The fractional release of solvent blue 35 from D50 SMEDS in organogels with total gelator concentration (β-sitosterol + γ-oryzanol at 1:1 mass ratio) of 14 wt.% (circles) and 18 wt% (squares) as a function of dimensionless time, τ, used in Eq. 4-4.

Figure 4-16 schematically shows the proposed mechanism for the release of the gelled SMEDS upon exposure to water. The schematic of Figure 4-16 presents three main compartments, the bulk aqueous phase, the "hydrated" region, and the "gelled SMEDS" region. The self-emulsification process begins with water diffusing through the "hydrated region" where sterol hydrates are formed and into the gelled SMEDS region where the SMEDS is diluted until it contains about 30 wt% water where a separate liquid phase is formed. This separate, but still concentrated 70 wt% SMEDS, then from drops and streamers that leave the gel through the "hydrated region". Once this concentrated SMEDS is in the bulk aqueous phase, the SEMDS undergoes further dilution to dilution ratios greater than 10 where micelles are formed in the bulk aqueous phase.

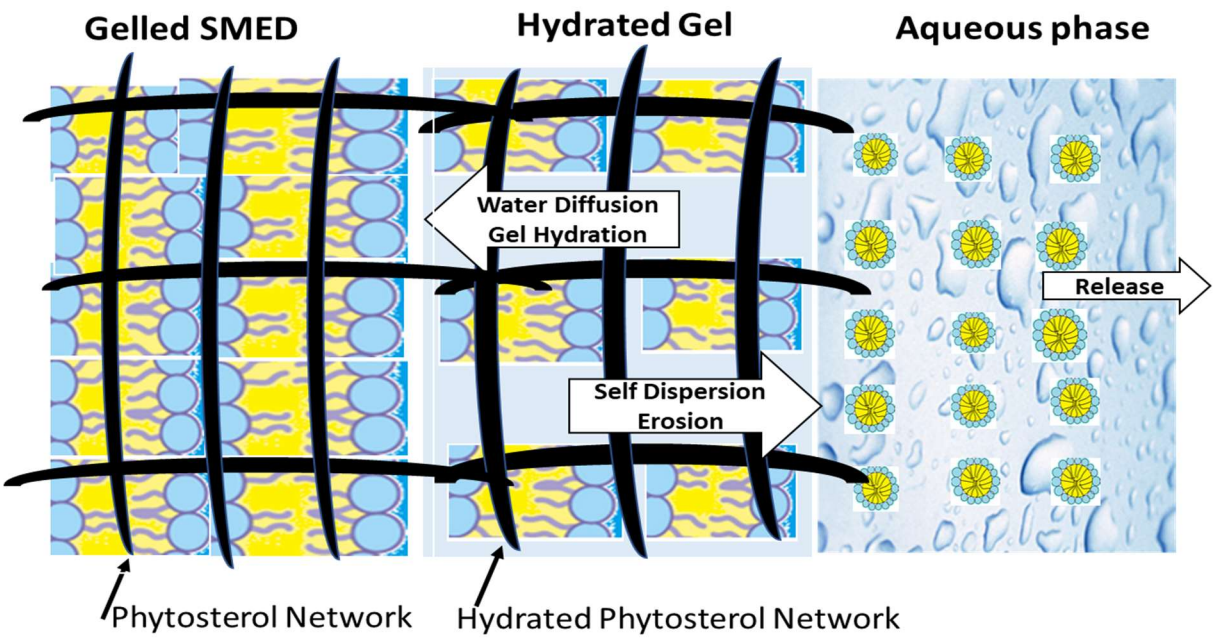

Figure 4-16: Schematic presentation of the G-SMEDS-Water interactions. Structures are not drawn to scale.

Release study of gelled SMEDS loaded with ibuprofen

A similar study, to that presented in Figure 4-13 for solvent blue 35, was carried out with the 18% total sterols gelled SMEDS, in which the SMEDS contained 4 wt.% ibuprofen (3.28 wt.% drug in the gel). To procedure for the release study was identical for the gels loaded with the blue dye except that the diluting medium was distilled water. The fractional release of ibuprofen as a function of time is presented in Figure 4-17. According to Figure 4-17, in this case we one can also obtain a gradual release of the drug over the course of, at least, 3 days. Another similar feature between Figures 4-13 and 4-17 is the presence of an initial fast release over the course of the first 10 hours, followed by a more gradual release over the next three days.

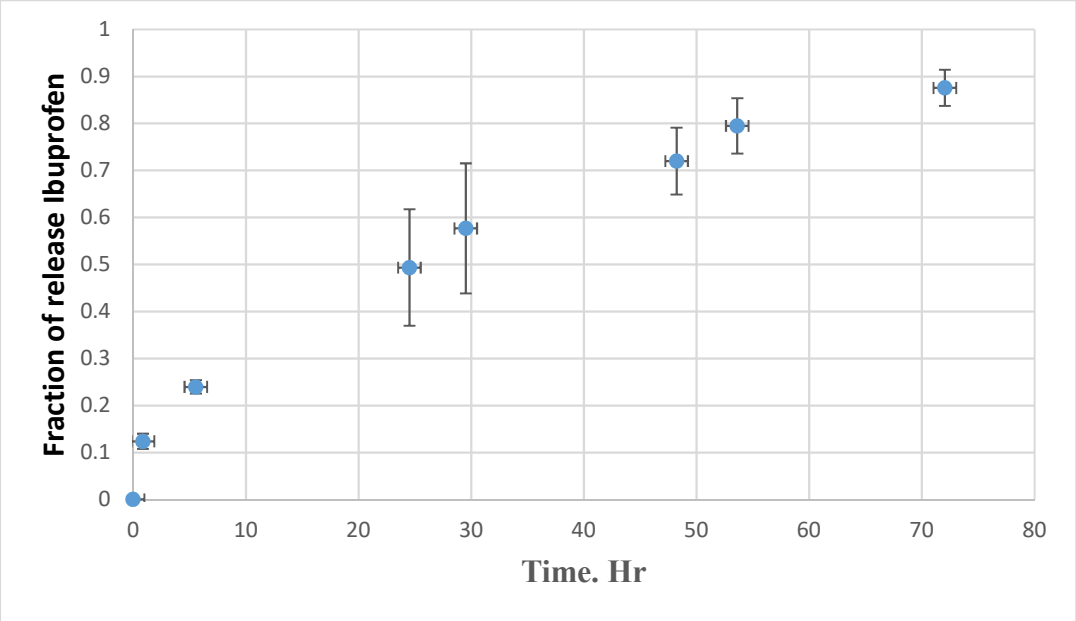

Figure 4-17: Fractional release of ibuprofen from D80, 90-5-5 SMEDS in organogels with total gelator concentration (β-sitosterol + γ-oryzanol at 1:1 mass ratio) of 18 wt.% . The system remained at 37°C throughout the experiment and the vials.

To further interpret the release profile of Figure 4-17, the fractional release of ibuprofen was plotted against the normalized time coordinate of the diffusion-erosion model (Equation 4-4), in Figure 4-18. To obtain the normalized time, and the predicted release, the D_{app} and B values obtained for the 18% gelator obtained when fitting the release of solvent blue were used. Although the SMEDS formulation for ibuprofen and the dilution medium in that experiment were different than those used for solvent blue, the predicted release line obtained with the 18% gelator parameters fitted for solvent blue release produced a very good estimation of the experimental release observed in Figure 4-18. This further supports the idea that the quantity of organogelator and its interaction with SMEDS leading to high G" are the main reasons behind the extended release behavior observed with the gelled SMEDS systems. It also suggests that this approach could be extended to various active pharmaceutical or nutraceutical ingredients.

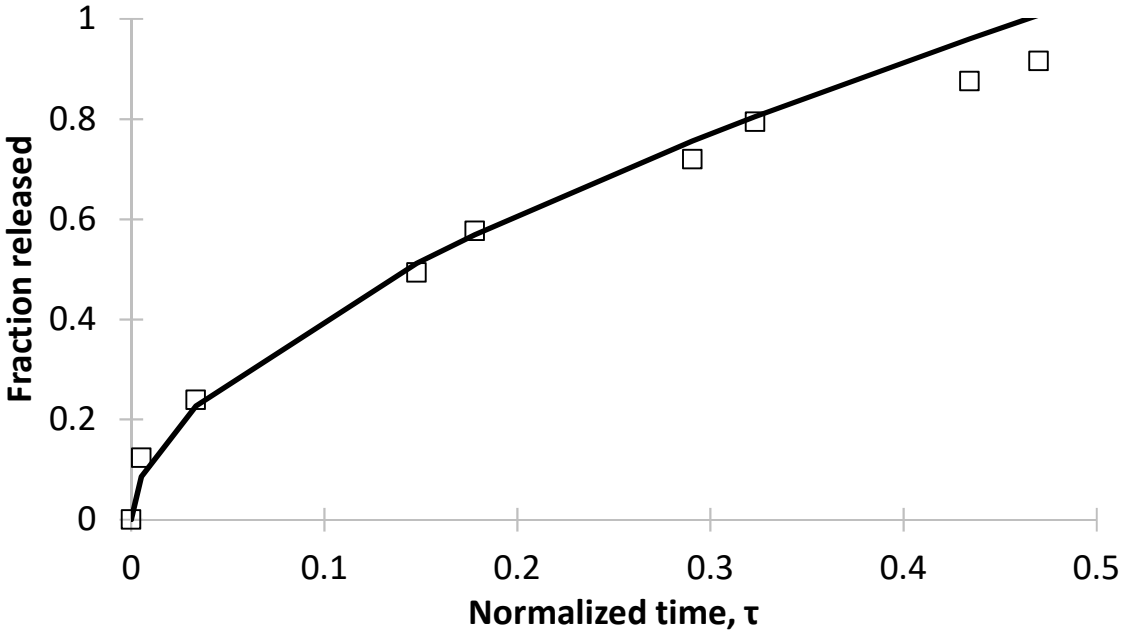

Figure 4-18: The fractional release of ibuprofen from D80, 90-5-5 SMEDS in organogels with total gelator concentration (β-sitosterol + γ-oryzanol at 1:1 mass ratio) of 18 wt.% as a function of dimensionless time, τ, used in Eq. 4-4.

While the considerations above were offered as a way of illustrating the potential release mechanisms from gelled SMEDS, there are numerous questions that need to be answered in future studies. For example, a more detailed investigation of the transport mechanism, an exploration into why G" is so large in gelled SMEDS and how one could manage these values to obtain other release profiles. Also, why do SMEDS induced the formation of spherulites while other oils tend to form fibrils in sterol organogels?. The application of these gelled SMEDS is yet another matter. Release profiles of days are suitable for topical, ophthalmic, buccal, vaginal and possibly subcutaneous release. For oral release, the gels should be incorporated into small particles, protected with enteric coatings to protect them from the stomach's fluids, and allow them to release in the intestine.

4.5. Conclusion

Microemulsion-based systems such as self microemulsifying delivery systems (SMEDS) enhance the solubility and bioavailability of poorly-soluble active ingredients; however, they show a burst release profile due to instant dissolution of the oil + surfactant mixture that results in the spontaneous formation of microemulsion droplets. In this work, an integrated SMEDS and organogel system was developed that allows the organogel to self-disperse while producing a slow release microemulsion. A Minimum 12% of total sterol concentration (β-sitosterol+ γ-oryzanol) is required to turn liquid SMEDS into gelled SMEDS. The concentration of the gelator played an important role in the physicochemical properties and release kinetics of the gelled SMEDS. Gelling time, gel elasticity (G'), gel viscous losses (G"), gel firmness (rupture point), gel melting point and exothermic profile of the gel during heating directly correlates to the gelator concentration. Therefore, the gel concentration was used as tuning tool to control the rate of gel dispersion. Upon exposure to the aqueous phase, water starts to diffuse into the gel and facilitates the self-emulsification of the SMEDS. The emulsified portion of the gel leaves the interface and enters the aqueous phase. The release data and video-microscopy studies suggest that water diffusion is the factor limiting the release rate. After considering diffusion only and combined diffusion + erosion models it was determined that while the release profile is primarily diffusion-controlled, there is also a substantial portion of the release caused by the erosion of the gel.

4.6. References

[1] Porter CJH, Trevaskis NL, Charman WN. Lipids and lipid-based formulations: optimizing the oral delivery of lipophilic drugs. Nat Rev Drug Discov. 2007 Mar;6(3):231–48

[2] Garti N, Avrahami M, Aserin A. Improved solubilization of Celecoxib in U-type nonionic microemulsions and their structural transitions with progressive aqueous dilution. J Colloid Interface Sci. 2006 Jul 1;299(1):352–65.

[3] FDA - Center for Drug Evaluation and Research (CDER). Guidance for Industry, Bioavailability and Bioequivalence Studies for Orally Administered Drug Products. 2003.

[4] Schulz M, Schmoldt A. Therapeutic and toxic blood concentrations of more than 800 drugs and other xenobiotics. Pharmazie. 2003;58(7):447–74.

[5] Mehlisch DR, Sykes J. Ibuprofen blood plasma levels and onset of analgesia. Int J Clin Pract Clin Pract. 2013;67(Suppl. 178):3–8.

[6] Acosta E. Bioavailability of nanoparticles in nutrient and nutraceutical delivery. Curr Opin Colloid Interface Sci. 2009 Feb;14(1):3–15

[7] Yuan JS, Ansari M, Samaan M, Acosta EJ. Linker-based lecithin microemulsions for transdermal delivery of lidocaine. Int J Pharm. 2008 Feb 12;349(1–2):130–43

[8] Yuan JS, Acosta EJ. Extended release of lidocaine from linker-based lecithin microemulsions. Int J Pharm. 2009 Feb 23;368(1–2):63–71

[9] Yuan JS, Yip A, Nguyen N, Chu J, Wen X-Y, Acosta EJ. Effect of surfactant concentration on transdermal lidocaine delivery with linker microemulsions. Int J Pharm. 2010 Jun 15;392(1–2):274–84.

[10] Sansom LN. Oral extended-release products. Aust Prescr. 1999 Aug 1;22(4):88–90.

[11] Mishra MK. Handbook of encapsulation and controlled release. CRC press; 2015. 1512 p.

[12] Karsa DR, Stephenson RA. Encapsulation and controlled release. Woodhead; 2005. 187 p.

[13] Teng Z, Luo Y, Wang Q. Carboxymethyl chitosan-soy protein complex nanoparticles for the encapsulation and controlled release of vitamin D3. Food Chem. 2013;141(1):524–32.

[14] Luo Y, Teng Z, Wang Q. Development of zein nanoparticles coated with carboxymethyl chitosan for encapsulation and controlled release of vitamin D3. J Agric Food Chem. 2012;60(3):836–43

[15] Clifford NW, Iyer KS, Raston CL. Encapsulation and controlled release of nutraceuticals using mesoporous silica capsules. J Mater Chem. 2008;18(2):162.

[16] Tan A, Rao S, Prestidge C a. Transforming lipid-based oral drug delivery systems into solid dosage forms: an overview of solid carriers, physicochemical properties, and biopharmaceutical performance. Pharm Res. 2013 Dec;30(12):2993–3017

[17] Vintiloiu A, Leroux J-C. Organogels and their use in drug delivery--a review. J Control Release. 2008 Feb 11;125(3):179–92.

[18] Murdan S, Gregoriadis G, Florence a T. Interaction of a nonionic surfactant-based organogel with aqueous media. Int J Pharm. 1999 Apr 15;180(2):211–4.

[19] Murdan, S., Gregoriadis, G., Florence AT. Non-ionic surfactant based organogels incorporating niosomes. Pharma Sci. 1996;6(1):44–8.

[20] Bot A, Veldhuizen YSJ, den Adel R, Roijers EC. Non-TAG structuring of edible oils and emulsions. Food Hydrocoll. 2009 Jun;23(4):1184–9.

[21] Kumar, R., Katare OP. Lecithin organogels as a potential phospholipid-structured system for topical drug delivery: A review. AAPS PharmSciTech. 2005;6(2):23.

[22] Lim, P.F.C., et al. Limonene GP1/PG organogel as a vehicle in transdermal delivery of haloperidol. Int J Pharm. 2006;311(1–2):157–64

[23] Sahoo S, Kumar N, Bhattacharya C, Sagiri SS, Jain K, Pal K, et al. Organogels: Properties and Applications in Drug Delivery. Des Monomers Polym. 2011 Mar 1;14(2):95–108

[24] Murdan S. Organogels in drug delivery. Expert Opin Drug Deliv. 2005 May;2(3):489–505.

[25] Nguyen, D.-V., Li, F., Li, H., Wong, B.S., Low, C.Y., Liu, X.-Y., Kang L. Drug permeation through skin is inversely correlated with carrier gel rigidity. Mol Pharm. 2015;12(2):444–52.

[26] Pradhan, S., Sagiri, S.S., Singh, V.K., Pal, K., Ray, S.S., Pradhan D. Palm oil-based organogels and microemulsions for delivery of antimicrobial drugs. J Appl Polym Sci. 2014;131(6).

[27] Bot A, Agterof WGM. Structuring of Edible Oils by Mixtures of γ -Oryzanol with β -Sitosterol or Related Phytosterols. J Am Oil Chem Soc. 2006;83(6):513–21.

[28] Bot A, Adel R, Roijers EC. Fibrils of γ-Oryzanol + β-Sitosterol in Edible Oil Organogels. J Am Oil Chem Soc. 2008 Oct 21;85(12):1127–34.

[29] Bot A, Adel R, Roijers EC, Regkos C. Effect of Sterol Type on Structure of Tubules in Sterol + γ-Oryzanol-Based Organogels. Food Biophys. 2009 Aug 4;4(4):266–72.

[30] Thompson GR, Grundy SM. History and development of plant sterol and stanol esters for cholesterol-lowering purposes. Am J Cardiol. 2005 Jul 4;96(1A):3D–9D.

[31] Chung O. Sterol-Based Organogel Drug Delivery Systems, MASc. thesis. University of Toronto; 2012

[32] Bonnet J, Suissa G, Raynal M, Bouteiller L, Bonnet J, Suissa G, et al. Organogel formation rationalized by Hansen solubility parameters. Soft Matter. 2014;10:3154–60.

[33] Kreye, F., Siepmann, F., Willart, J.F., Descamps, M., Siepmann J. Drug release mechanisms of cast lipid implants. Eur J Pharm Biopharm. 2011;78(3):394–400.

[34] Guse, C., Koennings, S., Kreye, F., Siepmann, F., Goepferich, A., Siepmann J. Drug release from lipid-based implants: Elucidation of the underlying mass transport mechanisms. Int J Pharm. 2006;314(2):137–44

[35] Dufresne, M.-H., Marouf, E., Kränzlin, Y., Gauthier, M.A., Leroux J-C. Lipase is essential for the study of in vitro release kinetics from organogels. Mol Pharm. 2012;9(6):1803–11.

[36] Hoffma SB, Yoder AR, Trepanier LA. Bioavailability of transdermal methimazole in a pluronic lecithin organogel (PLO) in healthy cats. J Vet Pharmacol Ther. 2002;25:189–93.

[37] Alsaab H, Bonam SP, Bahl D, Chowdhury P, Alexander K, Boddu SHS. Organogels in Drug Delivery : A Special Emphasis on Pluronic Lecithin Organogels. J Pharm Pharm Sci. 2016;19(2):252–73

[38] Yuan J. Linker-based lecithin microemulsions as transdermal drug delivery systems, Doctoral dissertations. University of Toronto; 2009.

[39] Nouraei M, Acosta EJ. Predicting solubilisation features of ternary phase diagrams of fully dilutable lecithin linker microemulsions. J Colloid Interface Sci. 2017;495:178–90.

[40] Marques M. Dissolution Media Simulating Fasted and Fed States. Dissolution Technol. 2004;11(2):16.

[41] Zhang Y, Huo M, Zhou J, Zou A, Li W, Yao C, et al. DDSolver: An Add-In Program for Modeling and Comparison of Drug Dissolution Profiles.

[42] Bot A, Adel R den, Regkos C, Sawalha H, Venema P, Flöter E. Structuring in β-sitosterol+γ-oryzanol-based emulsion gels during various stages of a temperature cycle. Food Hydrocoll. 2011 Jun;25(4):639–46.

[43] Adel R Den, Heussen PCM, Bot A. Effect of water on self-assembled tubules in β-sitosterol + γ-oryzanol-based organogels. J Phys Conf Ser. 2010 Oct 1;247:12025.

[44] Han, L.-J., Li, L., Zhao, L., Li, B., Liu, G.-Q., Liu, X.-Q., Wang X-D. Rheological properties of organogels developed by sitosterol and lecithin. Food Res Int. 2013;53(1):42–8.

[45] Wang, R., Liu, X.-Y., Xiong, J., Li J. Real-time observation of fiber network formation in molecular organogel: Supersaturation-dependent microstructure and its related rheological property. J Phys Chem B. 2006;110(14):7275–80.

[46] Löfman, M., Lahtinen, M., Pettersson, M., Sievänen E. Insights into localized manipulation of organogel-related microcrystalline spherulite formation. Colloids Surfaces A Physicochem Eng Asp. 2015;474:18–28.

[47] Szekeres E, Acosta E, Sabatini DA, Harwell JH. Modeling solubilization of oil mixtures in anionic microemulsions: II. Mixtures of polar and non-polar oils. J Colloid Interface Sci. 2006;294(1):222–33.

[48] López-Montilla, J.C., Herrera-Morales, P.E., Pandey, S., Shah DO. Spontaneous emulsification: Mechanisms, physicochemical aspects, modeling, and applications. J Dispers Sci Technol. 2002;23(1–3):219–68

[49] Lees, F.P., Sarram P. Diffusion Coefficient of Water in Some Organic Liquids. J Chem Eng Data. 1971;16(1):41–4.

[50] Levenspiel O. Chemical Reaction Engineering. 3rd Editio. New York: John Wiley & Sons, Ltd; 1999.

[51] Qiuxia, Y, and P Lee, 'Rational Design of Oral Modified-Release Drug Delivery Systems', in *Drug Delivery Systems* (Elsevier, 2013), pp. 1024–27

[52] Lee, P.I.. Diffusional release of a solute from a polymeric matrix - approximate analytical solutions. J. Membrane Sci. 1980;7 (3):255-275.

Chapter 5. Conclusions and Future Works

5.1. Conclusions

Fully dilutable Microemulsion-based systems, when used as delivery systems, show promising results for enhancing the solubilization and delivery of hydrophobic compounds. However, there are numerous gaps/challenges, as indicated in chapter 1, which can be grouped into two main types: design challenges and application challenges. The work on design and formulation challenges was split into three stages:

- Introducing an alternative approach to replace PEGylated surfactants and short chain alcohol cosurfactants to formulate food grade SMEDS
- Understanding and predicting the phase behavior of fully dilutable SOW systems
- Quantifying the shift in hydrophilicity/lipophilicity upon addition of polar oil (such as active pharmaceutical ingredient).

Having reviewed various ternary phase diagrams introduced in the literature identified as SEDS/SMEDS system, it was determined that most of the formulations are only partially dilutable and only a handful of them show complete dilutability. In terms of excipients, the common ingredients in almost all dilutable formulations are PEGylated compounds (as surfactant/cosurfactant), and ethanol as cosolvent. In chapter 2, it is shown that lecithin - in combination with hydrophilic and lipophilic linkers - enhances the solubilization capacity of the oil and can form fully dilutable systems. The linkers are plant-derived, biologically compatible, and in several cases food grade ingredients. The selected linkers proved to be appropriate additives to balance the hydrophilicity/lipophilicity of the surfactant/Oil/Water systems. In particular, polyglycerol esters of medium chain fatty acids enhanced the solubilisation capacity of SMEDS and produced a path of full dilutability. The analysis of the changes in particle size, viscosity and conductivity revealed a smooth phase transition from water-free oil/surfactant mixture *(SMEDS)*

to W/O μE → bicontinuous μE → O/W μE, without phase separation as the dilution with aqueous phase progressed. While lecithin linker microemulsions are a promising approach in developing green microemulsions, some challenges persist. There is a limited number of marketed polyglycerol compounds that could be used as hydrophilic linkers. A technical issue with them is the ample difference in their hydrophilic lipophilic nature for similar products among different brands. As exemplified in chapter 3, there was a substantial difference in characteristic curvature (Cc) of three hexaglycerol caprylates (-3, -7.1 and 2) obtained from three sources. This makes formulating linker-based microemulsions a challenging task.

For modeling the phase behavior of complex systems such as lecithin linker SMEDS, a modified version of HLD–NAC framework –namely surfactant continuum NAC- was devised to predict the phase behaviour of SOW systems. Reviewing the literature revealed that the majority of the phase diagrams are constructed through aqueous titration (spontaneous emulsification) method in which aliquots of each surfactant and cosurfactant mixture are mixed and then titrated with the aqueous phase. The phase behavior of the system at each water dilution ratio during titration is observed and recorded. This method does not represent the true phase behavior because only the immediate response is observed and reported and not the equilibrated phase behavior. Mapping a detailed and accurate experimental ternary phase diagram is a resource-intensive process and involves preparing more than one hundred compositions of water/oil/surfactant and observing the phase behavior after equilibration time (1- 2 weeks or even longer in certain cases). This process needs to be repeated for each specific set of oils/surfactant/cosurfactant/linkers formulation. The proposed NAC framework can be used to determine the optimum oil to surfactant ratio(s) that leads full dilutability. The surfactant continuum NAC model can predict the solubilization boundaries and may be used as a guideline to construct virtual ternary phase diagrams. Comparing the experimentally constructed ternary phase diagrams and the predicted ones showed that the

HLD-NAC surfactant continuum approach provides a reasonable estimation of the boundaries of the two-phase region, beyond which a fully dilutable single-phase region can exist. Using this approach, one can calculate the minimum surfactant concentration for fully dilutable microemulsion. The surfactant continuum NAC model showed improvements over the simple NAC model, but some inconsistencies still persist near the apex of the multiphase region, which suggests that not all the surfactant belongs to the continuous phase. Furthermore, the HLD-NAC model is totally silent on predicting the phase behavior of surfactant-rich region of ternary phase diagram where liquid crystals are formed.

A stepwise approach was introduced to calculate the model parameters for oil (EACN) and non-ionic surfactants (Cc) and NAC parameter (L) from simple scan results. However, it was noticed that the protocols for measuring these parameters are not harmonized within the scientific community and our results were in some cases different from other findings. The heart of HLD approach is running a phase scan-typically a salinity scan- and identifying the optimum salinity (S^*) during phase transitions (type *II* μE→type *III* μE →type *I* μE). Therefore, the reliability of calculated values depends on identifying the correct optimum salinity. This is more crucial for ionic surfactants since the log of S^* is used and small changes can lead to substantial differences. The application of proposed HLD-NAC approach can be extended beyond the drug delivery systems and it can successfully be used in other applications such as enhanced oil recovery (EOR) with reasonable accuracy and only a limited number of experiments and inputs are needed to minimize the experimental efforts.

Chapter 3 - part 1- discusses how adding an additive to an oil/surfactant system significantly alters the phase behavior of the system in two ways: changing the physical properties of the dilution and changing the dilution profile. For SMEDS, it is critical that the phase behavior can be substantially

different formulation remains dilutable after loading the drug. However, the experimental data shows that the phase behavior can be substantially different, especially if the active ingredient is a polar oil. To manage this issue properly, one needs to quantify the changes in the hydrophilicity/lipophilicity of the system. Currently there is not a comprehensive model to calculate the net interaction of the formulation-active ingredient, hence the routine approach to restore a formulation loaded with active ingredient is using numerous trials to re-optimize the formulation. In Chapter 3, it was shown that the HLD framework can be used as a guide not only in the quantification of the phase behavior changes, but also to reformulate the system. In this approach, the shifts in optimum salinity due to the addition of a new component is measured, followed by an assessment of the shift in HLD as an indicator of the magnitude of the impact of the additive. The sign and extent of ΔHLD can direct the formulator to identify proper strategies to restore the system. From a HLD point of view, the change could be arisen from changing either oil or surfactant properties (EACN, Cc). Therefore, to compensate the impact of the drug; either an oil with appropriate EACN or a surfactant with suitable Cc is required. In Chapter 3, a mathematical methodology was introduced to calculate ΔHLD and the required change in Cc to restore the formulation. The HLD-guided approach clearly illustrates the connection between the HLD and ternary phase diagrams and can save a great amount of time in trials to restore the formulation. This new application of HLD is not limited to drug delivery systems and can be extended to quantify any polar oil-formulation interactions and to estimate the EACN of unknown polar compounds. However, the main assumption in the current HLD approach is considering the additive as an oil. Some polar compounds may have dual functions (oil as well as a surfactant) and therefore this assumption may need to be revised and/or validated.

The work on application challenges and extending the SMEDS release profile took three steps:

- Evaluating the biological performance of lecithin linker system
- Modifying the SMEDS release profile via developing a gelled SMEDS with controlled release profile

The second section of chapter 3 and Appendix A are dedicated to evaluating the biological performance of lecithin linker SMEDS in rat studies. The formulation showed a high loading capacity (>10%) for ibuprofen, a hydrophobic NSAID. A 25 mg/kg dose of the drug in aqueous suspension and in loaded SMEDS were orally administered and the absorption / elimination kinetics was monitored. The results showed a 3.5-fold increase in bioavailability of the formulated drug in comparison to the control. This suggests that lecithin linker SMEDS is a promising strategy to enhance the absorption and bioavailability of poorly soluble active ingredients.

Since the lecithin linker formulation is in its early stages of development, there was no previous data on the safety of the lecithin linker upon consumption. To investigate the side effects of the formulation on extreme conditions, Sprague-Dawley rats were fed a diet enriched with blank SMEDS and loaded SMEDS for six weeks. The necropsy data was collected and as it is shown in appendix A, no significant differences were identified between the control group (regular diet) and enrich diet.

In chapter 4, a novel approach to reduce the rate of self-micro emulsification and generate controlled release microemulsions was introduced. While SMEDS are excellent in enhancing drug dissolution and improving the absorption, they produce an immediate release profile. In some applications, a controlled release profile is desired. Conventional organogels (OG) are made with oil and gelator to produce a slow release profile. In this work, we consolidated the two approaches (SMEDS and OG) to form a novel gelled SMEDS, hypothesizing that this material integrates the

slow release of organogel and self-emulsification of SMEDS. Two phytosterols (β-sitosterol and γ-oryzanol) at equal weight ratio were used as LMWG and dissolved in hot SMEDS as the bulk oil phase. Texture analysis, calorimetry and rheological studies showed the link between gelator concentration and gel strength. Therefore, it was hypothesized that the gelator concentration can be used to influence the release rate. Using a lipophilic dye as a marker, it as shown that the release profile is largely influenced by gelator concentration. The time-release results showed that gelled SMEDS are released in 2 to 5 days, depending on gelator concentration. This suggests that this system is useful for subcutaneous applications and no bulk of gel remains at the site. Nevertheless, it is worth noting that the results are likely dependent of test conditions such as cooling rate, shear rate, age and more importantly the amount and geometry of the tested gel piece. This makes the comparison between different works challenging.

In summary, this work has addressed some of the common challenges in the design and use of microemulsion-based delivery systems for pharmaceutical and nutraceuticals and the results suggest that the lecithin linker systems can be considered as a new opportunity to improve the bioavailability of poorly soluble bioactive compounds. However, more works need to be done as will be discussed below.

5.2. Future Works

In this work, it was demonstrated that lecithin linker SMEDS can generate fully dilutable microemulsions upon exposure to simulated intestinal fluids. Ethyl caprate showed a solubilization capacity for lecithin and active ingredients. Though its usage is approved as a food additive (flavouring agent), it has a sharp note and has limitations in the amounts that can be used. Replacing ethyl caprate with a tasteless/odorless oil such as ethyl oleate can facilitate the

application of lecithin linker microemulsions in food systems. Recent studies on using ethyl oleate as the oil have shown it forms a large microemulsion area in the ternary phase diagram and also increases drug solubility and lymphatic transportation [1].

In this work, ibuprofen was used as a model API, however the results could be extended to other lipophilic drugs, micronutrients and nutraceuticals. SMEDS provides an opportunity to improve the bioavailability of fat-soluble vitamins (A, D, E, K) and oil-soluble nutraceuticals such as carotenoids (beta-carotene, astaxanthin, lycopene), polyunsaturated fatty acids (PUFA) such as health promoting omega 3-6-9 oils, Coenzyme Q10, and phytosterols; and nonsteroidal anti-inflammatory drugs (NSAID) such as ibuprofen. Currently, there are no SMEDS formulations for these bioactive compounds. Table 5-1 below introduces an assessment of the percentage of the recommended daily intake (RDI) of vitamins, the recommended daily allowance (RDA) of nutraceuticals and the typical dose for ibuprofen obtained when ingesting 1 gram of SMEDS. The 1 gram of SMEDS threshold was set considering this is typically the largest size in gel-type capsules used in drugs and nutraceuticals. When considering the use of SMEDS in foods, this work has shown that introducing SMEDS in 1 to 5% in dry foods, even when eaten daily for 6 weeks, did not produce physiological changes. Considering, for example, the introduction of SMEDS in fortified rice, an average daily consumption of 100 grams (in some countries could be substantially higher), then a 1% loading of SMEDS would correspond to 1 gram of SMEDS.

As shown in Table 5-1, a 1 g dose of SMEDS loaded at the maximum solubility of the active- provides considerable percentage of the RDI or recommended / required does in a highly bioavailable state. The data suggest that the SMEDS is most effective for active ingredients with either higher solubility or lower recommended / required amount. For specific case of ibuprofen,

one might need to consider the increase bioavailability over ibuprofen alone. Considering a 3.5 times higher SMEDS bioavailability, a 200 mg SMEDS dose ~ 700 mg drug-only dose.

Table 5-1. Percentage of the recommended daily intake (%RDI, for vitamins only) or allowance (% RDA, for nutraceuticals) or typical dose (% dose, drugs) provided with1 g SMEDS

RDI, RDA or dose		unit	Solubility in SMEDS (%)	Amount (mg) in 1 g SMEDS	% to RDA
Vitamins					
Vitamin A	1	mg	0.3	3	300%
Vitamin D	5	µg	5	50	1'000'000%
Vitamin E	10	mg	10	100	1'000%
Vitamin K	80	µg [2]	5	50	62'500%
Nutraceuticals					
Phytosterols	1.3	g [3]	25	250	19%
CoQ10	100	mg	10 [4,5]	100	100%
Omega 3 oil	1000*	mg	70	700	70%
Drug					
Ibuprofen	200	mg	10	100	50%

There is no set recommended dose for CoQ10 and ω-3 oil. The dose for ibuprofen is based on a single dose. *Based on the American Heart Association recommendation

The concept of fully dilutable microemulsions could be extended beyond drug delivery systems. Examining the potential of different formulations can create new opportunities for the use of dilutable microemulsions in the agri-food sector, in the flavor and fragrance industry and in oil spill applications. Microemulsions can be considered as nano-reactors and may be used in other industries. One application of interest is extracting lipid compounds from plant tissues. Some early

works on using lecithin linker microemulsions have shown to be very efficient in extracting oil-soluble components from plant material, including algae, fruit peels and vegetables. The extract can then be processed, without additional separation, to produce a variety of liquid, gel and powder forms that can be used for food fortification, targeted-delivery of nutraceuticals, and even delivery of flavoring agents or fragrances at room temperature and pressure. Extraction of beta carotenoids from carrot pulp and microalgae have also been shown to have superior recovery to that of hexane extraction [6]. Another application for fully dilutable microemulsions is cleaning oil spills. An oil spill is the release of a liquid petroleum hydrocarbon into the environment, especially the marine ecosystem, and typically causes widespread ocean and coastal pollution. Microemulsions can help disperse the oil and a food grade microemulsion may even enhance the biodegradation.

In terms of formulating SMEDS, the hydrophilic likers play an important role in solubilization capacity of the system. There is a need to find more choices for hydrophilic linkers with high negative values. In this work, we used a hexa-glycerol ester of Caprylic acid (C8) with a Cc of -7. Polyglycerols esters of medium chain fatty acids (C7-C10) seems to be the appropriate choices. Other polyglycerols (hepta-, deca-glycerols) with C7, C9 and C10 fatty acids need to be examined to determine their Cc. Using hydrophilic linkers with large negative Cc values may decrease the required amount of hydrophilic linker, and could increase the drug loading capacity in the formulation. However, the issue with these compounds is the variety in physical properties of the same chemical compound. As reported in Chapter 3, the two hydrophilic linkers used in this work - Dermofeel® 6CY and Caprol® 6GC8 - had the same alkyl chain and number of glycerols, but their characteristic curvature (Cc) was very different. This ample difference in Cc values illustrates the impact of the manufacturing process, particularly in the location of the monomers during the polymerization of multifunctional monomers like glycerol.

The Cc of the surfactants and the EACN of the oils influence the phase behavior. However, there is not a universal methodology to measure Cc and EACN. For example, in this work salinity scan was used to determine the Cc and EACN values while there are reports that use temperature scan to measure EACN [7]. Even with our method, the current protocols could have up to 20% uncertainty in the reported values. Improving/ standardizing the protocols for calculating reliable and reproducible Cc and EACN with higher accuracy is recommended.

While the there was a strong correlation between experimental data and HLD-NAC predicted values for phase volumes, future work on optimizing the HLD-NAC model should focus on quantifying the partitioning of surfactants and linkers in the continuous phase and at the interface. The use of the surfactant-continuum HLD-NAC to other SOW systems applications – such as enhanced oil recovery- should also be explored.

In chapter 3 it was shown that addition of a new component such as a drug – even in small amounts - alters the phase behavior and dilution profile of the SMEDS significantly. HLD framework can quantify the amount of the change and can be applied to restore the hydrophilicity of the system. However, the main assumption in his approach was considering ibuprofen as an oil that causes a change the EACN of the main oil and drug mixture. Considering the chemical structure of the drugs, one can conclude that they can have amphiphilic properties and therefore can have surfactant functionality. Therefore, a Cc could be defined for them as well. In future works, it is needed that for such polar compounds to have both Cc and EACN to be measured and considered in the calculation of the HLD of the system.

In chapter 3, it was shown that SMEDS is a promising approach to improve drug uptake, bioavailability, and increase in circulation time. However, the mechanisms that explain these

improvements are not known [8]. Though some mechanisms are proposed, further work is required to explore these mechanisms and develop improved formulations that take full advantage of them.

In Chapter 4, it was shown that in gelled SMEDS the rate of self-emulsification is substantially slower than that of SMEDS alone. However, the phytosterols used in this work (β-sitosterol and γ-oryzanol) form firm gels at 14% and higher total gelators. This reduces the relative percentage of SMEDS in the organogel and subsequently lowers the drug loading capacity. Alternative low molecular weight gelators (such as surfactant-like compounds) that make gels at lower gelator concentration should be investigated. In preliminary experiments, we found that fatty acids iron salts form a gel at concentrations as low as %1.5. The advantage of these compounds is that other than gelator functionality, they can be considered as an iron delivery system.

The gelled SMEDS gradually self-disperses in the aqueous phase. To better understand, the dissolution kinetics and the mechanism involved in gel erosion, it is recommended to conduct the experiment with USP Dissolution Apparatuses (basket, paddle or cylinder).

In this work a gradual release of the gelled SMEDS was attained in the range of 4 days. Future improvements in the formulation should be explored to extend the release time to weeks or months to create new opportunities in subcutaneous administration [9]. Furthermore, in vivo experiments is suggested to study the biological performance of the gel in oral and subcutaneous routes of delivery.

5.3. References

[1] Xing Q, Song J, You X, Xu D, Wang K, Song J, et al. Microemulsions containing long-chain oil ethyl oleate improve the oral bioavailability of piroxicam by increasing drug solubility and lymphatic transportation simultaneously. Int J Pharm. Elsevier B.V.; 2016;511(2):709–18.

[2] CFIA. Guidance Document Repository , Recommended Daily Intakes [Internet]. Available from: http://www.inspection.gc.ca

[3] FDA. 21 CFR Part 101 Food Labeling; Health Claim; Phytosterols and Risk of Coronary Heart Disease; Proposed Rule. 2005.

[4] Kommuru TR, Gurley B, Khan M a, Reddy IK. Self-emulsifying drug delivery systems (SEDDS) of coenzyme Q10: formulation development and bioavailability assessment. Int J Pharm. 2001 Jan 16;212(2):233–46.

[5] Balakrishnan P, Lee BJ, Oh DH, Kim JO, Lee YI, Kim DD, et al. Enhanced oral bioavailability of Coenzyme Q10 by self-emulsifying drug delivery systems. Int J Pharm. 2009;374(1–2):66–72.

[6] Chan J. Extracting Lipid and Carotenoids from Microalgae with Lecithin- Linker Microemulsions. University of Toronto; 2012.

[7] Tchakalova V, Fieber W. Classification of fragrances and fragrance mixtures based on interfacial solubilization. J Surfactants Deterg. 2012;15(2):167–77.

[8] Hauss DJ. Oral lipid-based formulations. Adv Drug Deliv Rev. 2007 Jul 30;59(7):667–76.

[9] Vintiloiu A, Leroux J-C. Organogels and their use in drug delivery--a review. J Control Release. 2008 Feb 11;125(3):179–92.

Appendix A. Safety/Toxicological studies on rats fed with β-carotene loaded SMEDS

The objective of this study was to examine the safety of lecithin linker SMEDS when the body is exposed to a high dose of the formulation for a long period of time.

A.1. Methods

Diet enrichment with loaded SMEDS

Water was added (30% w/w) to the regular diet to form a paste. SMEDS was then added to the paste (1% or 5%) and thoroughly mixed to make a homogenized diet. Then it was spread on a flat surface and cut into grids while they were moist. They were air dried at room temperature to form dry cubic pellets.

Animal treatments

Male Sprague-Dawley rats (350 ± 20 g), supplied by Charles River Laboratories Canada, were acclimatized for a week at the Division of Comparative Medicine (DCM) lab in a temperature-controlled environment in individually ventilated cages with free access to water and food. Rats were randomly assigned to three groups (n = 6/group) depending on whether they received regular diet (control group), the diet enriched with 1% SMEDS and the diet enriched with 5% SMEDS. The SMEDS was already loaded with 1000 ppm β-carotene. During the 6-week period, the animals were monitored both physically and psychologically. At the end of the period, the rats were euthanized. Blood samples were collected by cardiac puncture and stored at -20 C for further analysis. The tissues (gastrointestinal tract, kidney, liver, eye balls) collected for histopathological

evidence of toxicity. Throughout this period, any animal appeared ill or moribund was euthanized and tissue samples were collected for histopathological analysis. All *in vivo* experiments were conducted in the Division of Comparative Medicine (DCM) vivarium at University of Toronto and procedures were approved by the Faculty of Medicine and Pharmacy Animal Care Committee.

Extracting β-carotene and vitamin A from liver:

One gram of the liver samples was weighed and transferred to centrifuge tube and four mL of distilled water was added. The samples were homogenized for 60 seconds and then ethyl alcohol was added, and the mixture was vortexed for 1 minute. To saponify the fats, 2 mL of KOH 10M was slowly mixed and the tubes were placed in water bath for 30miutes at 65° C. To extract the carotene and vitamin A, 4 mL water, 4 mL ethanol and 10 mL hexane 5 minutes were added and shaken for 5 minutes, followed y 2 minutes centrifuge (4000 rpm). The supernatant organic solvent was transferred to another vial. Hexane was evaporated to dryness under nitrogen gas stream. The extraction repeated two more times and the residues were stored in -80 ºC freezer for HPLC analysis. For HPLC analysis, the samples were dissolve in mobile phase (acetonitrile, 2-propanol and ethyl acetate at 50:35:15 ratio) and filtered by 0.2 syringe filters. The mobile phase flow rate is 0.7 ml/min. Nile red is used as internal standard. The UV detector reads at 350 nm for β-carotene, 450 nm for vitamin A and 620 nm for Nile red.

A.2. Results

The rats were monitored for food consumption and weight gain. The results showed that despite similar initial weight at the beginning of the experiment, the rats in both enriched diets gained more weight than the control group. There was not a significant difference between 1% and 5%

fortified diets. This is despite the lower amount of food consumed during the test period. The results suggest that in the enriched diet groups the conversion ratio of food to body mass is higher.

Figure A-1: The changes in weights of the rats during enriched diet consumption

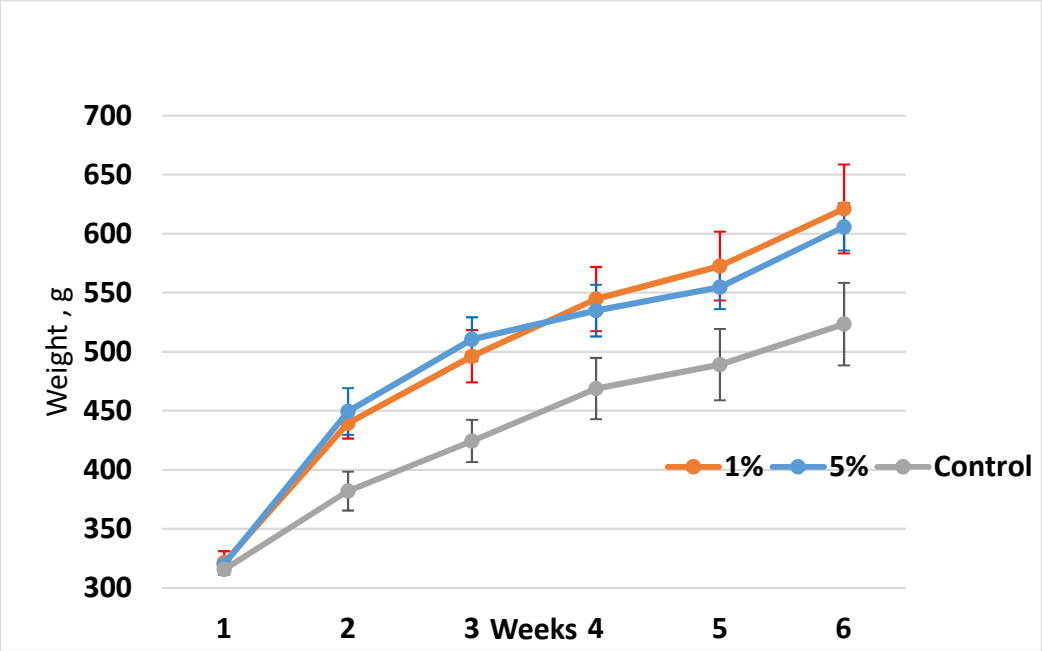

After six weeks, body dimensions (body length, thoracic width and abdominal width) were measured and no significant changes among groups was identified. Kidney, heart, liver, thymus, spleen and salivary glands were removed and their weights were measured. The kidney in 5% group was lighter in weight than the other two groups. Complete blood tests (CBT) were performed. For white blood cells (WBC), lymphocyte (LYM), monocyte (MON) and Neutrophils (NEU) the results for all three groups were in the normal range. The results suggest that special diet had no adverse effect on immune system. The red blood cell (RBC) , hemoglobin (HGB) an hematocrit (HCT) for the control were below the normal ranges while the results for two test groups felled within the normal ranges. The summary of the results are presented in table below:

	Regular Diet		1%		5%	
Test	**Mean**	**Stdev**	**Mean**	**Stdev**	**Mean**	**Stdev**
Body length	27.75	0.63	27.24	0.84	27.40	1.01
Thoratic width	17.87	1.27	17.16	1.25	15.82	1.65
Abdonimal width	20.85	0.92	20.50	1.13	20.42	1.07
Glucose (GLU)	7.85	1.75	8.14	1.61	9.12	3.62
High density lipoprotein (HDL)	1.62	0.27	1.36	0.30	1.42	0.40
Triglycerdides (TRI)	1.34	0.27	1.78	0.51	1.68	0.52
Body Weight	610.67	31.51	621.00	37.74	605.80	19.98
Liver weight	24.33	2.45	24.54	3.26	24.57	1.71
Thymus Weight	1.04	0.24	0.83	0.18	1.30	0.17
Heart Weight	1.90	0.22	1.84	0.10	1.76	0.10
Speelen Weight	0.98	0.15	0.99	0.08	1.03	0.09
Kidney Weight	3.77	0.40	3.62	0.40	3.32	0.20
Salivary glands Weight	0.81	0.12	0.86	0.17	0.93	0.08
White Blood Cells (WBC)	8.90	1.74	9.89	5.35	10.45	2.09
Lymphocyte (LYM)	6.83	1.22	7.73	3.81	8.46	2.42
Monocyte (MON)	0.49	0.49	0.74	0.60	0.71	0.28
Neutrophils (NEU)	1.55	1.53	1.42	1.01	1.28	0.38
LYM%	78.40	12.83	79.64	4.24	79.96	7.27
MON%	5.25	4.20	6.80	1.86	7.36	2.95
NEU%	16.37	14.22	13.54	2.48	13.10	5.52
Red Bood Cell (RBC)	4.83	1.48	5.42	1.18	6.38	0.71
Hemoglobin (HGB)	9.55	2.50	10.92	2.67	12.60	1.21
Hematocrit (HCT)	26.46	6.70	30.83	6.72	36.11	4.60
Mean volume of erythrocytes (MCV)	55.50	2.26	56.80	1.79	56.60	1.52
Mean content of hemoglobin (MCH)	19.95	0.96	20.06	0.76	19.82	0.72
Mean concentration of hemoglobin in erythrocytes (MCHC)	36.00	1.04	35.26	1.08	34.98	1.51
Relative distribution width of RBC by volume, coefficient of variation (RDWc)	15.78	0.75	16.70	0.41	16.06	0.70
Relative distribution width of RBCby volume, standard deviation RDWs	33.47	2.06	36.56	0.84	34.54	1.95
Absolute content of platelets (PLT)	305.33	116.68	345.20	162.67	353.60	64.11
Mean platelet volume (MPV)	7.50	0.41	7.42	0.36	7.72	0.10
Platelet crit (PCT)	0.22	0.09	0.26	0.13	0.27	0.05
Platelet distribution width (PDWc)	31.55	1.06	31.22	0.83	32.12	0.28
PDWs	8.27	0.76	7.88	0.48	8.42	0.17
PrVW	364/366		365/367		367/370	
PrVR	349/350		350/351		351/352	
PrVE	0/0		0/0		0/0	
WBC Lysis	0.700		0.700		0.700	
Lyse 2	0.000		0.000		0.000	
Food weight/Body weight	0.68	0.068	0.55	0.086	0.64	0.008
Body Mass Index (BMI)	0.79	0.03	0.84	0.05	0.81	0.04

Appendix B. Synthesizing and characterizing oil-soluble iron compounds

B.1. Methods

1-Two separate solutions of iron source and organic acid sodium salts (table below) were made, one providing an iron source and the other using an organic sodium salt.

Table: Iron sources and Organic sources

Iron Sources		Organic Sources	
Ferric chloride hexahydrate $FeCl_3 . 6H_2O$	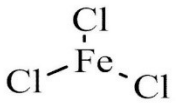	Sodium octanoate	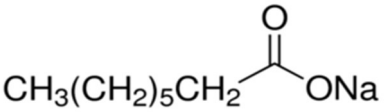
Ferrous ammonium Sulfate hexahydrate $(NH_4)_2Fe(SO_4)_2 \cdot 6H_2O$.	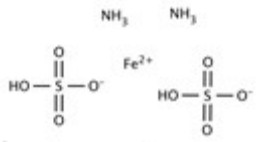	Sodium acetate	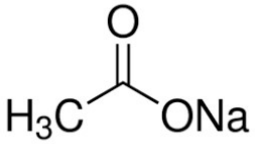
Ferrous sulfate heptahydrate $FeSO_4 \cdot 7H_2O$	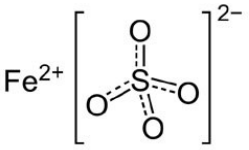	Sodium citrate	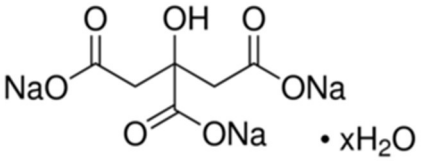

2-Solutions were made so there were equivalent stoichiometric molar concentrations.

3-Equivalent volumes of each solution were added to a jar and shook to react.

4-Precipitates separated, and leftover solution was discarded.

5-Water was added, and jar was shaken to wash the product, this was repeated twice more. vacuum filtration was used when the liquid was difficult to pour off without losing product.

6-Cleaned product was left to air dry overnight.

Reactions

For Ferric chloride the molar concentration of the organic solution was three times the molar concentration of the iron solution.

$$FeCl_3 + 3CH_3(CH_2)_6COONa \rightarrow Fe(CH_3(CH_2)_6COO)_3 + 3NaCl$$

And for ferrous sulfate and ferrous ammonium sulfate, the molar concentration of the organic solution was twice the molar concentration of the iron solution.

$$Fe(SO_4)_2 + 2CH_3(CH_2)_6COONa \rightarrow Fe(CH_3(CH_2)_6COO)_2 + 2\ NaSO_4$$

Solubility tests

The products were tested to observe their behaviour in various solvents (water, hexane, ethyl caprate (EC), canola oil, and EC+ Peceol mixture).

Loading organic iron into SMEDS

The produced organic iron was to be loaded into the SMEDS formulation the iron (III) variation specifically. Attempted to add the organic iron to prepared SMEDS and mix by vortex and heating.

B.2. Results

Only the caprylate salts were hydrophobic and were precipitated. The acetate and citrate iron salts were water-soluble

	Caprylate	**Acetate**	**Citrate**
$FeSO_4$	• Light reddish-brown Precipitate 	• Red particles appear on bottom after some time. 	• Pale yellow-green solution. 
$(NH_4)_2Fe(SO_4)_2 \cdot$	• Dark reddish-brown Precipitate 	• Green suspension in clear liquid. 	• Small particles. 
$FeCl_3$	• Pale red Precipitate 	• Dark red layer at bottom. 	• Green solution. 

Solubility

The solubility of ferric caprylate in oils were higher than ferrous caprylate salts

	Water	**EC**	**Hexane**	**EC+ Peceol**
Iron(II) Caprylate	 insoluble	 Insoluble	 slightly soluble	slightly soluble
Iron (III) Caprylate	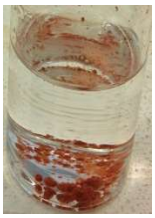 insoluble	 Soluble	 Fairly soluble	 soluble

The effect of HLD on solubility of iron caprylates at 2, 3, 4, and 5%

The solubility of ferric caprylate in oils was inversely correlated with its HLB

Oil	HLB	2% 3% 4% 5%
Propylene Glycol Dicaprylate (Labrafac PG)	2	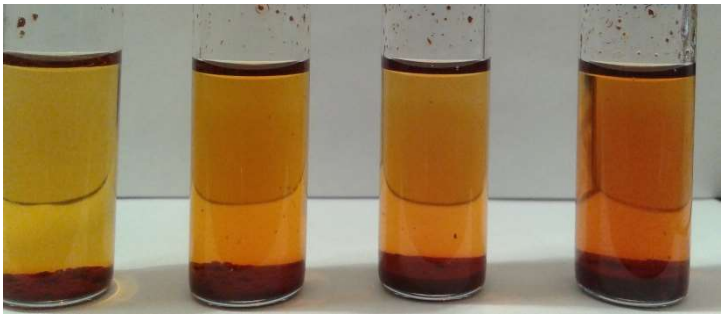
Propylene Glycol Monocaprylate(type II) (Capryol 90)	6	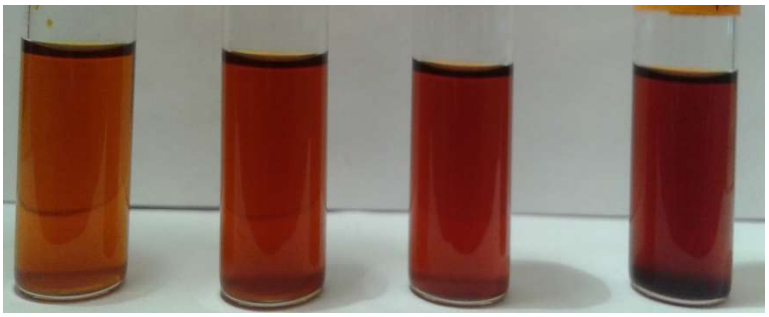
Caprylocaproyl macrogol-8 glycerides (Labrasol)	14	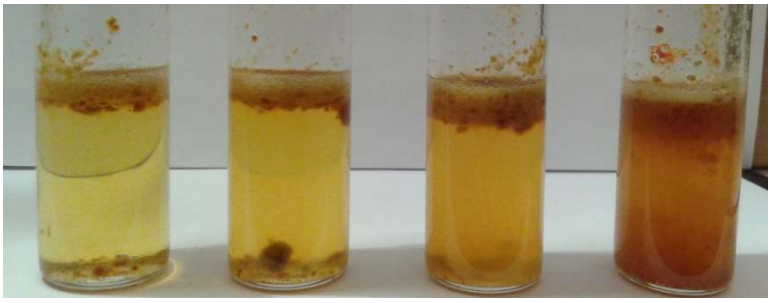
Oleic acid	1	

Polyglyceryl-3-polyricinoleate (Dermofeel PR)	9	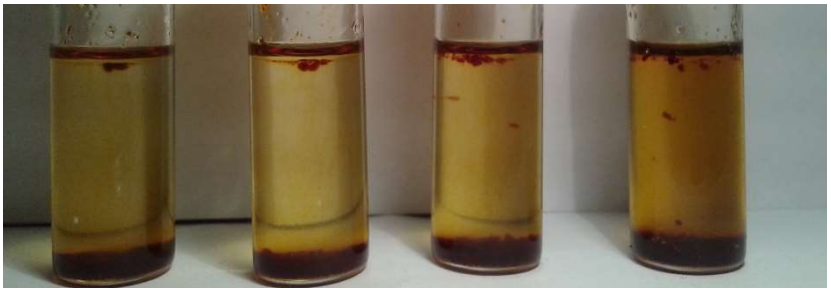
Polyglycerol-6-caprylate (Dermofeel G6YC)	11.5	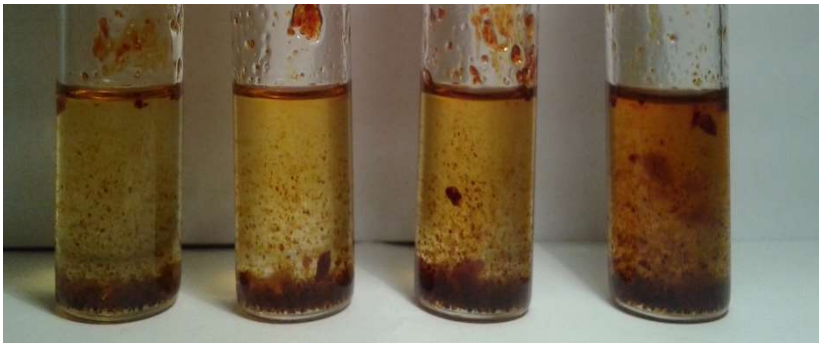

Gelation properties

The concentration and gelling properties of iron(III) caprylate depends on oil type (Canola oil, Peceol, 10:10:80 SMEDS and 15:15:70 SMEDS). The galling properties is correlated to oil polarity. For example, in edible oils, which mainly consists of triglycerides, no gelation occurred but in surfactant-rich formulations such as SMEDS, they turn the liquid formulation into a gel state.

Iron (III) Caprylate made the SMEDS gel at ~5%. Due to the gelling and high viscosity of higher concentrations, the loaded SMEDS was only made with 1.5% Iron (III) Caprylate concentration.

Ferric caprylate w/w%	1%	2%	3%	4%	5%	10%
Canola oil	Liquid, Oversaturate					
Peceol	Liquid, Oversaturate				Viscous	Gel
SMEDS 10:10:80	Viscous Soluble		Very viscous	Very viscous Oversaturate	Gel	
SMEDS 15:15:70	Viscous Soluble	Viscous Soluble	Viscous Oversaturate	Very viscous	Gel	

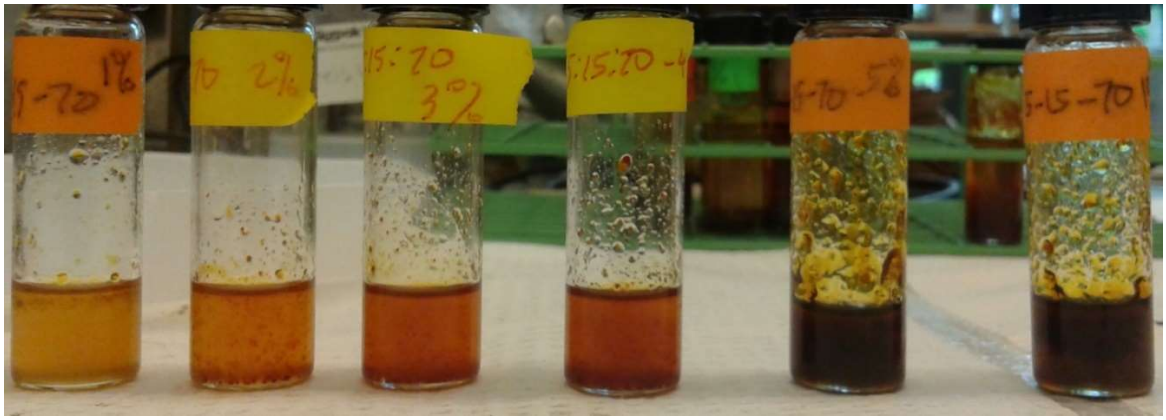

Obtaining an iron compound with different tail

To improve the loading capacity and increase the ratio of iron to the fatty acid salt in ferric and capryalte, 1 or 2 caprylate were replaces by acetate to synthesize ferric di-acetate caprylate and ferric di-caprylate acetate and ferrous caprylate acetate.

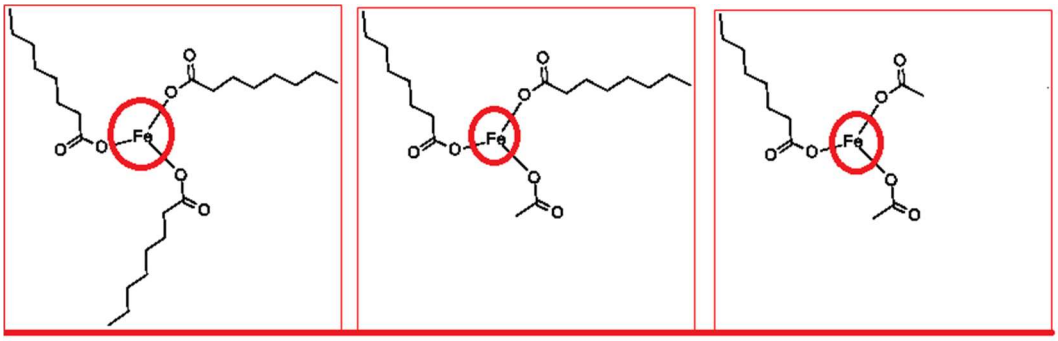

Ratio of Acetate:Caprylate when interacted $FeCl_3$	Observation	AA tested % Iron Content	Calculated % Iron Content
2:1	Red precipitate	20.46	17.6
1:2	Red precipitate	13.295	13.9
0:3	Red precipitate	12.565	11.5